COMPETENCE OF MUSCLE STEM CELL EXPANSION AND SELF-RENEWAL IS INSTRUCTED BY A CREB-MPP7-AMOT-YAP AXIS

by
Lydia Li

A dissertation submitted to The Johns Hopkins University in conformity with the requirements for the degree of Doctor of Philosophy

Baltimore, Maryland
August 2016

ABSTRACT

Healthy skeletal muscle has a robust ability to respond to tissue damage. Restoration of functional tissue depends on cellular expansion of muscle stem cells, a.k.a. satellite cells (SCs). During resting conditions, healthy muscle fibers have minimal turnover and SCs are mitotically quiescent. However SCs exist in a reversible quiescent state. Tissue damage prompts quiescent SCs to enter the cell cycle to produce progenitors that will differentiate to form new muscle fibers (myofibers) while a portion will self-renew to preserve the stem cell population. The notion that growth factor deprivation during rest is responsible for quiescence led to the widely held belief that quiescence is a passive state. But more recently, researchers have characterized molecules that maintain quiescence by inhibiting proliferation, leading the field to reconsider this notion and recognize maintenance of quiescence as an active state. However the mechanism by which SCs maintain proliferative potential during dormancy has not been studied.

Here, I have identified a CREB-Mpp7-AMOT axis that directs proliferative competence during quiescence. Using a tamoxifen-inducible, Pax7-lineage specific driver to inactivate CREB in SCs, I found that CREB inhibition does not cause a break in quiescence. However, upon muscle damage, SCs without CREB activity showed defective regeneration, attenuated proliferation, accelerated differentiation, and lack of SC self-renewal. Using RNA-seq based transcriptome comparison and ChIP, I determined that *Mpp7* is a CREB target in SCs during quiescence. Using siRNA and

overexpression, I found that Mpp7 is necessary and sufficient to maintain proliferation and self-renewal. Additionally, I found that Mpp7, a scaffolding protein, promotes the polarized localization of AMOT protein and nuclear accumulation of YAP. In summary, I discovered that CREB regulates Mpp7 expression thereby mediating a Mpp7-AMOT protein complex to promote YAP activity upon activation. Lack of CREB activity does not affect quiescence per se, but severely attenuates activation during an injury response. My work delineates a novel protein network that maintains SC activation competence during quiescence for stem cell function.

Advisor: Chen-Ming Fan, Ph.D.

Second Reader: Haiqing Zhao, Ph.D.

Committee Members: Trina Schroer, Ph.D.

Allan Spradling, Ph.D.

Yixian Zheng, Ph.D.

PREFACE

My research accomplishments and the completion of my degree have been made possible by the invaluable support of the mentors and colleagues around me. I would like to express sincere appreciation for my advisor Dr. Chen-Ming Fan who has provided countless hours of direction through scientific insight, experimental design and critical analysis. Dr. Chen-Ming Fan's valuable advice has enhanced my research and his encouragement has provided me inspiration to pursue my career goals. I would also like to acknowledge my thesis committee, consisting of Drs. Allan Spradling, Trina Schroer, and Yixian Zheng, who have given me an immense amount of quality feedback on my project and helped me to contextualize my work on a broad scale. I would like to thank Drs. Fred Tan and Nicholas Ingolia for assistance designing the analysis strategy for the bioinformatics portion of my work. Previous lab members Drs. Christoph Lepper and Peter Lopez were critical during the initial stages my project by providing training on experimental techniques and engaging in thoughtful discussions of current literature. And current lab member Dr. SiewHui Low has shared her expertise of research concepts and techniques that have allowed me to move past road blocks in my project. Additionally, Dr. Matthew Sieber has provided meaningful guidance as I pursue a career in academia. Lastly, I would like to thank my family and friends for their incredible support.

TABLE OF CONTENTS

LIST OF TABLES

LIST OF FIGURES

LIST OF ABBREVIATIONS

A-CREB	=	acidic CREB (d.n. version of CREB)
AMOT	=	Angiomotin
AMOTL1	=	Angiomotin Like 1
AMOTL2	=	Angiomotin Like 2
ATF1	=	Activating Transcription Factor 1
bZIP	=	leucine zipper
ChIP	=	chromatin immunoprecipitation
CRE	=	cAMP responsive element
Cre-ERT2	=	Cre recombinase - estrogen receptor T2
CREB	=	cAMP responsive element binding protein 1
CREM	=	cAMP responsive element modulator
CTX	=	cardiotoxin
EDL	=	extensor digitorum longus
FACS	=	fluorescence activated cell sorting
KEGG	=	Kyoto Encyclopedia of Genes and Genomes
miRNAs	=	micro RNAs
Mpp7	=	MAGUK p55 subfamily member 7
MyoD	=	Myogenic Differentiation 1
nGFP	=	nuclear green fluorescence protein
Pax7	=	Paired Box 7

pCREB	=	phospho-CREB (serine 133)
qPCR	=	quantitative polymerase chain reaction
RNA-seq	=	RNA sequencing
SC	=	satellite cell
$SC(s)_{A\text{-}CREB}$	=	A-CREB expressing satellite cell(s)
siRNA	=	small interfering RNA
TA	=	tibialis anterior
TAM	=	tamoxifen
TAZ	=	Tafazzin
TEAD	=	TEA Domain
YAP	=	Yes-associated protein 1
YFP	=	yellow fluorescence protein

CHAPTER 1: INTRODUCTION TO MUSCLE STEM CELL MEDIATED REGENERATION

Muscle stem cells

Skeletal muscle enables locomotion of vertebrates. The basic cellular unit of skeletal muscle consists of the myofiber containing the actin-myosin contractile unit that enables force generation. Intimately associated with myofibers are SCs, named such based on the early observation by electron microscopy of their position sandwiched between the basal lamina and cell membrane of the myofibers (Mauro, 1961). Because of their close juxtaposition with the myofiber, SCs were hypothesized to be involved in muscle growth and regeneration (Mauro, 1961). Subsequent experiments using radiolabeled thymidine to trace newly synthesized DNA showed that SCs were proliferative and contributed to newly formed myofibers (Moss and Leblond, 1970, 1971; Reznik, 1969). Culturing isolated myofibers and associated SCs revealed the ability for SCs to migrate away from the myofiber, proliferate, and differentiate fully to form multi-nucleated myofibers (Bischoff, 1975; Konigsberg et al., 1975). Thirty years later, techniques to characterize SCs, such as label retention and transplantation, has been key to showing that SC is a bona fide muscle stem cell *in vivo* (Collins et al., 2005; Shinin et al., 2006).

The functional role of SCs has led to the interest in identifying the molecular properties of these cells. During embryonic myogenesis, a progenitor population arises from the central dermamyotome, expresses Pax3 and Pax7, and are maintained throughout the developing skeletal muscle (Fan and Tessier-Lavigne, 1994; Gros et al., 2005; Relaix et al., 2005). These cells will settle in to the SC position during late fetal development, mirroring their location in the adult muscle (Relaix et al., 2005). Using Pax7 as drivers for conditional expression of reporter constructs, it was shown that these

embryonic precursors do indeed mature into the adult SC (Hutcheson et al., 2009; Keller et al., 2004; Lepper and Fan, 2010). Previously limited to germline mutants, the advent of lineage-specific conditional-activation of Cre by the Cre-loxP system allows for SC specific deletion of genes. This enables the study of gene function of germline lethal genes as well as SC specific manipulations using the canonical biomarker Pax7 to drive specified gene deletions.

Skeletal muscle regeneration

A central property of stem cells is the capacity to generate daughter cells that self-renew and differentiate into specialized cell types (Weissman, 2000). Mammalian stem cells of rapidly regenerating tissues such as the hair follicle, intestinal crypt, and blood are predominantly quiescent while a subset are actively cycling for ongoing tissue restoration (Li and Clevers, 2010). Skeletal muscle, during normal physiology, has low turnover and fittingly, resident muscle stem cells rarely become activated. SCs are normally quiescent (Schultz et al., 1978), however, upon tissue damage, have robust capacity to mount a proliferative program to provide the necessary cellular source for generating new myofibers (Brack and Rando, 2012). In response to injury, damaged myofibers undergo a degenerative phase in coordination with SC activation to replace lost tissue. Proliferating SCs generate mono-nucleated muscle progenitors, termed myoblasts, which undergo fusion to form multi-nucleated myofibers. Myogenic progression of SC derived myoblasts are marked by overlapping but distinct expression of muscle lineage specific genes that designate quiescence: Pax7 (Seale et al., 2000); activation: Myf5 (Davis et al., 1987) and MyoD (Cornelison and Wold, 1997; Davis et

al., 1987); differentiation: Myogenin (Mgn) (Wright et al., 1989) and Mrf4 (Rhodes and Konieczny, 1989); and terminal differentiation: myosin heavy chain (MHC) (Bader et al., 1982). Alterations in the timing and level of expression of these markers indicate an abnormal myogenic program.

In addition to SC derived myogenic lineage, muscle-derived pluripotent stem cells have been suggested to contribute to muscle growth. Bone marrow cells and muscle derived, hematopoietic stem cell marker Sca-1^+ cells were able to form myocytes and SCs after intramuscular transplantation (Asakura et al., 2002; Gussoni et al., 1999; LaBarge and Blau, 2002). Muscle resident $PW1^+$/$Pax7^-$ and $CD45^+$ interstitial cells have also been shown the contribute to the muscle regeneration *in vivo* (Mitchell et al., 2010; Polesskaya et al., 2003). Similarly mesoangioblasts and pericytes have the capacity to contribute to newly formed myofibers during regeneration (Dellavalle et al., 2007; Sambasivan et al., 2011). Nevertheless, ablation of the SC population results in complete absence of muscle regeneration, providing evidence that SCs are the major contributor to muscle regeneration under the normal physiological conditions (Lepper et al., 2011; Murphy et al., 2011; Sambasivan et al., 2011).

The ability to reform skeletal muscle after damage is of paramount importance to the quality of life. Traumatic injuries, such as heavy weight lifting, mechanical damage and downhill running, engage the SC to proliferate and form new muscle. Disease states such as muscular dystrophy, cachexia, and aging, are accompanied by reduced ability to regenerate due to SC defects. Therefore, the understanding of the basic biology of SCs can inform translational medicine with the goal of restoring muscle growth and function to dystrophic patients.

SC self-renewal

Stem cells are a long-lived population of cells that enable tissue growth throughout the lifetime of animals. SCs have a remarkable capacity to proliferate to form the necessary cells for muscle regeneration. Transplantation of a single myofiber an its associated 7-22 SCs into immunodeficient dystrophic mice generated 100 new multinucleated myofibers, which is equivalent to over 25,000 differentiated myonuclei (Collins et al., 2005). Additionally, the newly formed tissue contained functional SCs that could complete another round of regeneration (Collins et al., 2005). A similar study used single SC transplantations, tracked by luciferase reporter activity, showed that SCS are capable of 14-17 doublings *in vivo* and supplies newly formed myofibers and self-renewed Pax7 expressing SCs (Sacco et al., 2008). These transplantation studies provided key evidence that SCs are able to give rise to differentiate progeny and self-renew.

The mechanism of SC self-renewal has been explored in several studies. SCs are positioned in a polarized environment when they establish quiescence with the apical side juxtaposed to the myofiber and basal side adherent to the basal lamina of the myofiber. Culturing single myofibers and their associated SCs allows for determination of the molecular fates of dividing SCs and their mitotic division plane orientation. SCs showed asymmetric expression of a Myf5 reporter during cell divisions when their division planes were perpendicular to the long axis to the myofiber (Kuang et al., 2008). SC divisions that are oriented parallel to the long axis of the cultured myofiber, planar divisions, are regulated by Wnt signaling and promote symmetric SC expansion (Le

Grand et al., 2009). Interestingly, intravital imaging showed that SCs exclusively contacted the myofiber basement membranes during divisions suggesting that in physiological conditions, only planar divisions occur (Webster et al., 2016). Regardless, the molecular cues form the myofiber are important for self-renewal since Collagen VI, a component of the myofiber niche, is important for SC activation and self-renewal (Urciuolo et al., 2013). All together these studies point to an important role for positional cues coming from tissue architecture to direct SC self-renewal during regeneration.

The molecular components of self-renewal have been explored. A downstream target of RTK signaling, Sprouty1, is enriched during regeneration at the phase corresponding to reestablishment of quiescence and required for restoring the SC pool after injury. Constitutive Notch signaling in SCs promotes the $Pax7^{+}$ fraction while reducing proliferation, thereby representing quiescent SCs in culture conditions (Wen et al., 2012). The polarity protein Mark2 (Par1b) is basally localized in activated SCs and regulates asymmetric division to promote the self-renewing population (Dumont et al., 2015). The cell autonomous molecular properties of SCs have only begun to be explored.

Quiescence and Activation of SCs

SCs show low turnover during normal conditions and are typically quiescent. However reversible quiescence is critical for SCs to both provide cellular supply after injury and to reestablish quiescence when proliferative needs are met. The self-renewed satellite cells form the source of SCs for future rounds of repair. The loss of the ability to maintain a quiescent state, would therefore lead to unrestricted cellular proliferation or the depletion of the SC population due to cellular death or differentiation. The tight regulation of

quiescence and activation are therefore key to the maintenance of SCs throughout the lifetime of the organism.

Quiescence is an active process that requires proper maintenance at the level of transcription, post-transcriptional regulation, and chromatin structure. Suv4-20h1 dependent facultative heterochromatin restricts aberrant MyoD expression and cell cycle entry during quiescence to prevent aberrant activation during homeostasis (Boonsanay et al., 2016). Inhibition of miR-31 by antagomiR tail vein treatment leads to increased $Pax7^{+}$ cells and cell cycle entry which leads to more myonuclei and larger myofibers in the absence of injury (Crist et al., 2012). Calcitonin receptor restricts aberrant cell cycle entry of SCs and prevents emergence from the niche (Yamaguchi et al., 2015). Notch signaling component, RBP-J, prevents aberrant activation and progressive loss of the SC pool due to differentiation during quiescence (Bjornson et al., 2012; Mourikis et al., 2012). These key factors are important during quiescence to restrict the improper activation or differentiation of SCs in the absence of injury.

The maintenance of quiescence is important during the resting phase to preserve the cellular pool. Upon injury, every SC that will give rise to a future SC will undergo at least one round of division (Troy et al., 2012). Therefore, SCs quiescence must be reestablished from a proliferative population during regeneration. Sprouty, which is important for renewing the Pax7 population during regeneration, also is essential for homeostasis of the replenished SC pool after injury (Shea et al., 2010). The forkhead transcription factor FOXO3 promotes self-renewal during regeneration by enhancing Notch-mediate return to quiescent and differentiation inhibition (Gopinath et al., 2014).

Reestablishing the SC population requires the restriction of proliferation and maintenance of an undifferentiated state within a population of transit amplifying myoblasts.

Some of the key factors are important for maintaining quiescence during rest, regaining quiescence after activation, and promoting myoblast expansion are beginning to be revealed. Growth factors are potent promoters of proliferation during regeneration. Insulin-like growth factor (IGF), hepatocyte growth factor (HGF), and fibroblast growth factor (FGF) fare released by myofibers and are required to stimulate myogenic proliferation during regeneration (Chakravarthy et al., 2000; Floss et al., 1997; Tatsumi et al., 1998). Interleukin-6 (IL-6) is secreted by myoblasts and macrophages during injury to promote removal of necrotic tissue and synchronize proliferating myoblasts (Cantini et al., 1995). The robust proliferation of myoblasts is mediated by widely expressed growth factors.

While the factors that mediate quiescence and activation have been uncovered, the potential for proliferation during the quiescent state has not been studied. Whether and how a proliferative competent state co-exists with SC quiescence to permit cell cycle entry upon muscle injury is unknown. Based on the rapid response of SCs to stimulus and the repressive role of quiescent factors implies that activation potential is present in the SC. The outstanding question of how SCs are poised to activate yet remain quiescent is investigated in this study.

CHAPTER 2: CREB IS ACTIVATED IN SCS AND MYOGENIC PROGENITORS

INTRODUCTION

CREB mediated transcriptional control

The cAMP-response element binding (CREB) protein family of activators, consisting of CREB, ATF1 and CREM, is important for the execution of various transcriptional programs. The leucine zipper (bZIP) domain and basic region impart selective dimerization and DNA binding, respectively, to all members of CREB transcription factors. CREB regulates transcription of certain genes by binding to conserved promoter elements, cAMP response elements (CRE), as homodimers or heterodimers between CREB family members (Montminy and Bilezikjian, 1987; Short et al., 1986). A dominant-negative inhibitor of CREB, termed A-CREB, was constructed by fusing an acidic extension onto the CREB bZIP dimerization domain. Upon dimerization with A-CREB, CREB proteins are prevented from binding DNA to affect transcription (Ahn et al., 1998). In addition to its DNA binding domain, CREB contains a Ser133 phosphorylation site for PKA, which is stimulated by adenylyl cyclase (AC) via cAMP (Gonzalez and Montminy, 1989). Phospho-Ser-133-CREB interacts with p300/CBP, a histone-acetyltransferase (Bannister and Kouzarides, 1996; Ogryzko et al., 1996) that recruits RNA polymerase II (Nakajima et al., 1997), to promote expression of downstream genes.

CREB signaling in myogenesis and muscle

Previous work by our lab and others has shown that the CREB transcription factor family controls gene expression for proper muscle development, repair, and survival. Our

previous study of CREB function during myogenesis found that adenoviral mediated expression of A-CREB, abolished myogenic gene induction in cultured embryos (Chen et al., 2005). In cultured myoblasts, crushed muscle extracts increased pCREB levels and canonical CREB target gene induction (Stewart et al., 2011). Mice expressing an activation-sensitive form of CREB (CREB-YP) showed increased general cell proliferation after muscle injury (Stewart et al., 2011). Given that CREB activity also prevents muscle fiber death directly and promotes muscle repair indirectly via M2 macrophages (Berdeaux et al., 2007; Ruffell et al., 2009), the general proliferation increase in CREB-YP injured muscle likely has multiple origins. Furthermore, the SCs of CREB-YP mice were not examined nor were regeneration outcomes. As extensive as these collective studies are, the role of CREB activity in adult SCs is unknown.

RESULTS

Differential CREB activity is detected during myogenic progression of SCs

To gain insight into whether CREB activity might operate during adult myogenesis, I conducted a thorough characterization of CREB activity in adult SC and its descendants during myogenic progression by immunofluorescence detection of pCREB. In uninjured tibialis anterior (TA) muscle, pCREB was detected in 97% of SCs (stained positive for the definitive marker Pax7, $Pax7^{+}$; Figure 1), suggesting an active role for CREB during quiescence.

I next examined how pCREB pattern might change after SC activation. For this, I assessed pCREB levels in SCs associated with myofibers at various time points in culture. For identification of SC lineage, we isolated myofibers with YFP marked SCs from tamoxifen (TAM) treated $Pax7^{CE/+};Rosa26^{YFP/YFP}$ mice (Figure 2). Immediately upon isolation pCREB was detected in 98% of YFP marked SCs (time 0, T0; Figure 3B), in agreement with *in vivo* pCREB levels of quiescent SCs in uninjured muscles (Figure 1). SCs displayed changed levels of pCREB over 2 days (Figure 3A,B). Using average pCREB fluorescence signal intensity of associated myonuclei as a reference, I observed the SC fraction with high pCREB (>1.5X of myonuclear signal) gradually declined, whereas fractions with low or virtually non-detectable/negative pCREB (1.5-0.5X or <0.5X of myonuclear signal, respectively) increased (Figure 3B).

I also assessed pCREB levels in SC-derived primary myoblasts. Unsynchronized differentiation of this population allowed assessment of pCREB levels in $Pax7^{+}$, $MyoD^{+}$, Mgn^{+}, or MHC^{+}, each representing a progressively more differentiated state. $Pax7^{+}$ and $MyoD^{+}$ cells were mainly positive for pCREB signal, while only small fractions of Mgn^{+}

and MHC^+ cells had high levels of pCREB (Figure 4A,B). These data extend the prior report showing enhanced pCREB levels in myoblasts after exposure to crush muscle extract (Stewart et al., 2011) by demonstrating that CREB activity is present in quiescent SCs, declines after activation, and is low in differentiating myogenic cells.

DISCUSSION

Characterization of temporal pCREB levels reveals differential CREB activity during quiescence and early activation. Prior observations (Stewart et al., 2011) found that pCREB was present in proliferating myoblasts, however my study of the kinetics of CREB activity during early activation revealed CREB activity during quiescence as well as activated cells. Additionally, I found that pCREB activity was enriched in undifferentiated myoblasts compared to terminally differentiated myoblasts. This could be assessed through co-staining of terminal differentiation markers Mgn and MHC (Figure 3A,B) or by comparing the fluorescence intensity of the SC/myoblast to its neighboring myonuclei. The lack of CREB activity in terminally differentiated myoblasts/myotubes is a bit counterintuitive considering the requirement of CREB activity in maintaining mature myofibers (Berdeaux et al., 2007). However, the study by Berdeaux et al. tested the role of CREB in maturated muscle fibers. The study utilized a promoter skeletal muscle actin was used to drive A-CREB in adult myotubes that contain hundreds of myonuclei and have structural requirements that may not be required for newly differentiated cells in culture. In summary these data suggest a novel role for CREB during the quiescent state as well as during early activation.

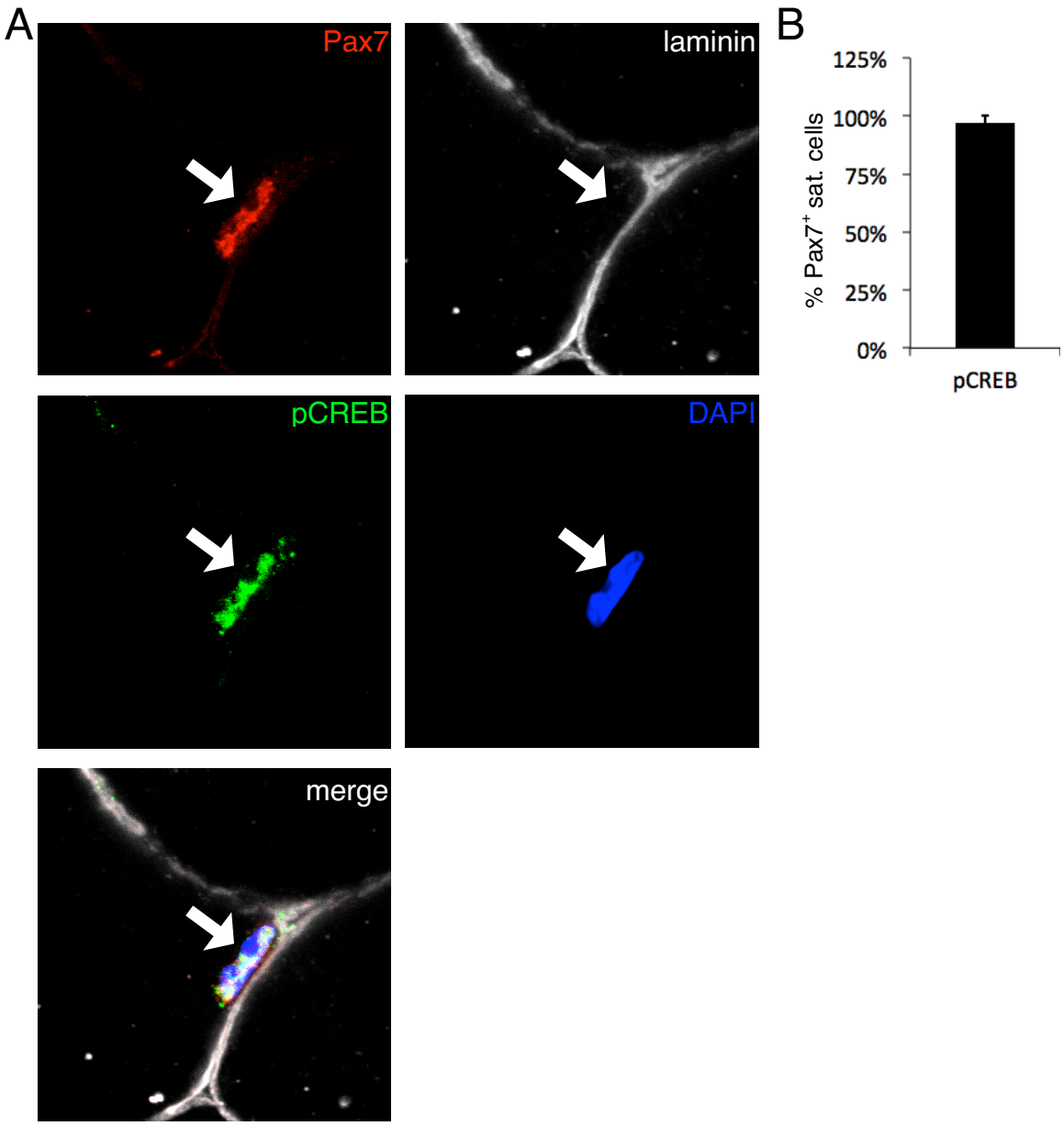

Figure 1. CREB is activated in quiescent SCs (A) TA muscle sections of 2 month old CD1 wild-type mice. SCs ($Pax7^{+}$) express $pCREB^{+}$. (B) Double positive satellite cells (white arrow) were quantified as a percentage of total $Pax7^{+}$ cells. N=3 mice, n≥50 cells per animal. Data represented as mean +/- 1 standard deviation. Scale bars 10μm

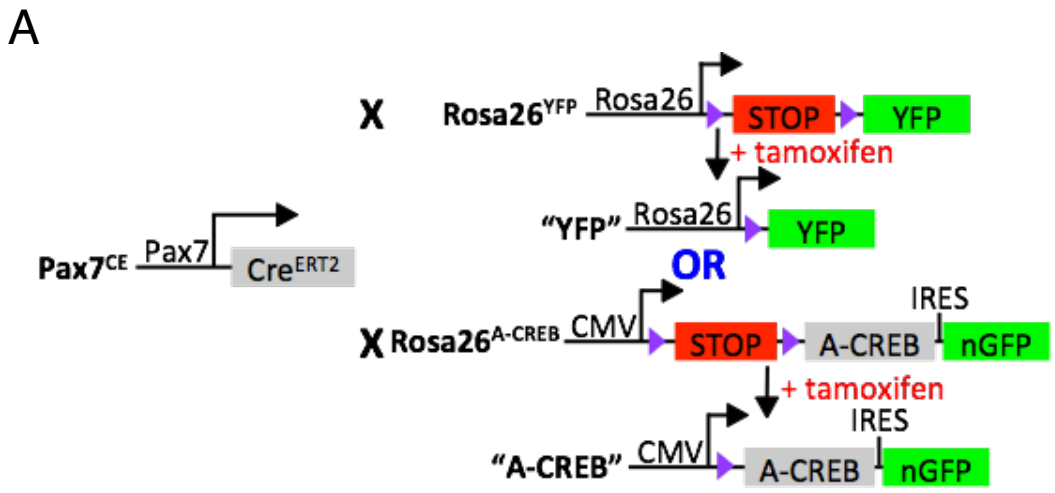

Figure 2. Alleles used for spatial and temporal expression of YFP and A-CREB in the Pax7^{+} lineage (A) Schematic illustrating Pax7^{CE} allele and resultant genotypes upon combining with Rosa26^{YFP} or Rosa26$^{A\text{-}CREB}$ alleles before and after tamoxifen-induced recombination.

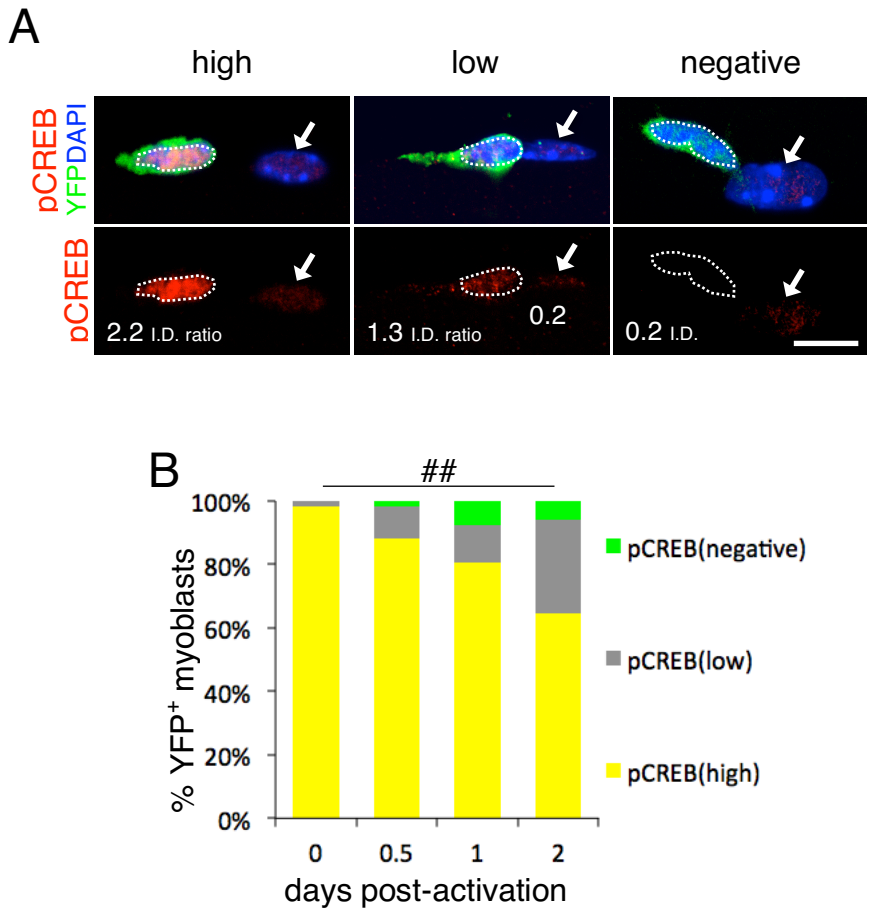

Figure 3. CREB is activated in quiescent SCs and activated myoblasts EDL single fibers and associated SCs of YFP mice were harvested for immediate fixation or cultured in plating medium for 0.5, 1, and 2 days and then fixed for immunostaining. (A) Representative images of pCREB fluorescence intensity (high, low and negative) at 0.5 days after harvest. Dotted line marks myoblast nuclei, white arrow marks myofiber nuclei, number indicates $pCREB^+$ integrated density (I.D.) normalized to myofiber nuclei pCREB I.D. (B) Quantification of pCREB I.D. shows pCREB expression declines over time. n≥150 cells per time point. ##p<0.01, Chi-squared test. Scale bars 10μm.

A

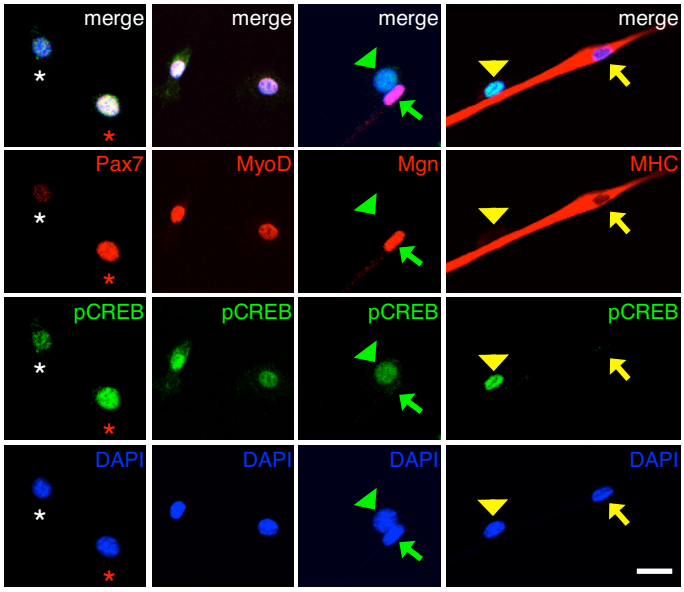
merge
merge
merge
merge
Pax7
MyoD
Mgn
MHC
pCREB
pCREB
pCREB
pCREB
DAPI
DAPI
DAPI
DAPI

B

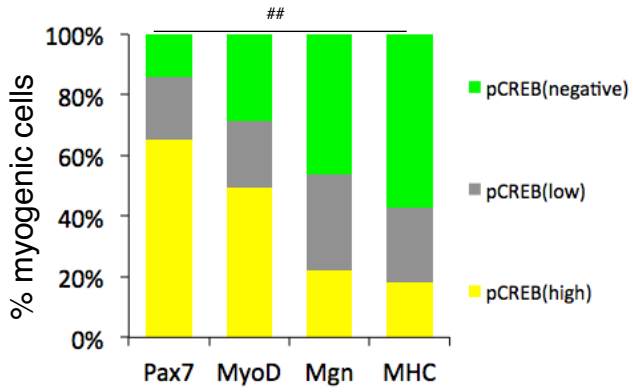
##
100%
80%
60%
40%
20%
0%
% myogenic cells
Pax7
MyoD
Mgn
MHC
pCREB(negative)
pCREB(low)
pCREB(high)

Figure 4. CREB is enriched in Pax7^{+} cells and reduced in differentiated cells (A) Primary CD1 myoblasts cultured in growth media were assessed for coexpression of pCREB and Pax7, MyoD, Mgn or MHC. Pax7^{+} myoblasts express various pCREB levels. Pax7(low)/pCREB(low) (white asterisk) and Pax7(high)/pCREB(high) myoblasts (red asterisk) were observed. Mgn (green arrow) and MHC (yellow arrow) myoblasts showing absence of pCREB expression. Green and yellow arrowheads indicate Mgn and MHC negative cells, respectively, which serve as as internal positive controls for pCREB expression. (B) Coimmunostaining of pCREB with Pax7 and differentiation markers MyoD, Mgn, MHC show a significant negative association between pCREB versus MyoD, Mgn and MHC expression. $n \geq 150$ per marker. ##$p<0.01$, Chi-squared test. Scale bars 40μm.

METHODS

Mice

Three month old, CD1 wild-type or $Pax7^{CE/+}Rosa26^{YFP/YFP}$ were used. Appropriate mating schemes were performed to obtain $Pax7^{CE/+}Rosa26^{YFP/YFP}$ mice. Animal treatment and care conform to the requirements of the Carnegie Institution and NIH guidelines.

Tibialis anterior (TA) cryosections

Animals were sacrificed by cervical dislocation. TA muscle was immediately dissected and fixed in ice cold 4% paraformaldehyde, EM grade catalog #15710, Electron Microscopy solution, diluted in 1XPBS for 10 minutes. After two washes in ice cold 1XPBS, muscle was subjected to two sucrose treatments, 10% sucrose in PBS and 20% sucrose in PBS for 8-12 hours each. Cryoprotected TA muscle was mounted onto cork slices using tragacanth (1:2::tragacanth:water), catalog # G1128, Sigma. Mounted muscle was submerged in liquid nitrogen cooled isopentane bath for 45 seconds and stored at -80 ^{o}C until sectioning. Sections were obtained using Leica cryostat set at -21 ^{o}C using 12 μm increments for collecting sections onto Superfrost glass slides, catalog #12-550-15, Fisherbrand.

Single fiber isolation

For immediate fixation, T0 fibers, extensor digitorum longus (EDL) muscles were digested in 0.6% Collagenase, catalog #C0130, Sigma/1XDMEM, catalog #11995-073, Invitrogen, for 15 minutes in 37^{o}C shaking water bath. Using a fire-polished, horse serum coated, wide aperture glass pipette, single fibers were dissociated from EDL muscle by gentle trituration for 10 minutes and fixed for IF.

For single fiber cultures, EDL muscles were digested in 0.2% Collagenase for 1.5 hours and then transferred to 37^{o}C DMEM. Using a fire-polished wide aperture glass pipette, single fibers were dissociated from EDL muscle by gentle trituration for 1-2 hours and transferred to fresh culture media.

Myoblast isolation

Hindlimb muscle was minced and then digested in 0.2% Collagenase for 1.5 hours and then 0.2% Dispase, catalog #17105-041, Invitrogen, (20 mL enzyme solution per mouse) for 20 minutes. Cells were washed twice by spinning and removing cell debris by vacuum aspiration and resuspended in 1XDMEM for washes. Cell pellet was resuspended in 1XDMEM and filtered through 40μm cell strainer and spun. Cell pellet was resuspended in culture media for transfer to matrigel coated (1:100 dilution in DMEM), catalog #356234, BD Biosciences, tissue culture plates.

Tissue culture

Floating myofibers were cultured on horse serum coated 3.5cm tissue culture dishes in plating media (10% horse serum, 0.5% chicken embryo extract, 1XPENSTREP, 1% Glutamax). Myoblasts were cultured on matrigel, (1:100 dilution in DMEM), catalog #356234, BD Biosciences, coated tissue culture plates in, growth media (20% fetal bovine serum, 5% horse serum, 1% chicken embryo extract, PENSTREP, 1% Glutamax, bFGF).

Antibodies

Primary antibodies were mouse IgG1 anti-Pax7 (1:5), DSHB; rabbit anti-pCREB-ser133 (1:1000), catalog # #9198 (87G3); chicken anti-laminin (1:50), catalog #ABIN573807, Antibodiesonline.com, discontinued; chicken anti-GFP (1:250), catalog #GFP1020, Aves

Labs; rabbit anti-MyoD (1:500), catalog #sc304, Santa Cruz; mouse anti-Mgn IgG1 (1:20), catalog #F5D, DSHB, mouse anti-MHC IgG2b (1:20), catalog #MF20, DHSB. Secondary antibodies (all used at 1:500) were goat anti-mouse IgG1, Alexa Fluor 568, catalog #A21124, Invitrogen; goat anti-rabbit, Alexa Fluor 488, catalog #A11034, Invitrogen; goat anti-chicken, Alexa Fluor 647, catalog # A21449; goat anti-rabbit, Alexa Fluor 568, catalog #A11011, Invitrogen; goat anti-chicken Fluorescein, catalog #F1005, Aves Labs.

Immunostaining

Collected sections were dried at room temperature for 15-30 minutes. PAP pen, catalog #100491-772, was used to delineate create a hydrophobic boundary around sections to contain solutions. Sections were fixed with ice cold 4% paraformaldehyde, EM grade catalog #15710, Electron Microscopy solution, diluted in 1XPBS for 10 minutes and washed twice in PBST (0.05% Triton X-100/1XPBS). Sections were permeabilized in 0.3% Triton X-100/1XPBS for 30 minutes and washed twice in PBST before blocking overnight in 3.2% M.O.M. block/PBST, catalog #BMK-2202, Vector Laboratories at 4^{o}C. After 2 washes in PBST, a second block in normal goat serum (NGS) based blocking buffer (10% normal goat serum, 1%(w/v) blocking powder, catalog #pc2307-1001 FP1020, PerlinElmer Life Sciences, 0.05% Triton X-100, in 1XPBS) was performed for 30 minutes.

Single fibers were fixed in 37^{o}C 2% PFA, EM grade for 10 minutes. PBST washes were performed by removing PFA solution and adding PBST at 1:5 serially three times. Fixed fibers were transferred with horse serum coated fire polished glass pipette

to horse serum glass staining dish and permeabilized using 0.3%Trition X-100/1XPBS for 30 minutes and then washed twice with 1XPBST.

Primary antibody was diluted in NGS-based blocking buffer and applied to sections or fibers overnight at 4^{o}C. After 3 PBST washes, 5 minutes per wash, NGS-based blocking buffer diluted secondary antibody was applied to sections for 30 minutes. DAPI counterstain and 2 additional washes in PBST was performed before mounting in Vectashield mounting medium, catalog #H-1000, Vector Laboratories.

CHAPTER 3: CREB ACTIVITY IS NECESSARY FOR MUSCLE REGENERATION

INTRODUCTION

Choreographed Muscle Regeneration

SCs are the main cellular source for new myofiber formation (Lepper et al., 2011; Murphy et al., 2011; Sambasivan et al., 2011). Muscle repair is a highly regulated process that requires proper activation of SCs for building the cellular source for myofiber formation and SC self-renewal. SCs enter a transit amplification phase in which SCs undergo cell divisions and begin to fuse into new myofibers. Myocytes migrate into an organized linear pattern then fuse to form the multinucleated myofiber (Knudsen et al., 1989; Mintz and Baker, 1967; Yaffe and Feldman, 1965). After fusion, myofibers will begin to grow in size to reestablish the original muscle mass prior to injury (Chargé and Rudnicki, 2004). A portion of proliferating myoblasts will exit the cell cycle, express Pax7, and return to the myofiber niche to serve as a reserve population for future rounds of injury (Fan et al., 2012).

Biological sources for initiation of the muscle regeneration program are disease and injury. Duchenne muscle dystrophy is an X-linked recessive form of muscular dystrophy that is characterized by structurally defective myofibers that undergo cyclic rounds of regeneration and degeneration (Hoffman et al., 1987). Traumatic damage by intense exercise such as weight lifting and eccentric exercise can also induced muscle regeneration (Armstrong et al., 1983; Singh et al., 1999). To generate consistent and robust injuries in controlled experiments, chemical based toxins such as CTX, notexin and barium chloride can be locally injected into skeletal muscle to produce muscle injury. This method is the conventional injury paradigm for studying muscle regeneration.

RESULTS

Genetic strategy to selectively inhibit CREB activity in adult SCs

Forced expression of A-CREB, a potent and selective inhibitor of CREB activity, is routinely used in *in vivo* systems to study CREB function (Ahn et al., 1998b; Herzig et al., 2001; Riccio et al., 1999). Our lab has previously generated a functional mouse allele, *Rosa26*$^{A\text{-}CREB}$, for Cre-dependent A-CREB expression and bicistronic nuclear GFP (nGFP) cell marking (Figure 2A; Lopez and Fan, 2013). After combining this allele with the inducible *Pax7*^{CE} driver (Figure 2A), we could detect nGFP expression in 95% of SCs after tamoxifen administration (Figure 5A,B,C), similar to the cell marking efficiency in *Pax7*^{CE}*;Rosa26*^{YFP} control mice (Figure 5A,B,C). Mice with SC specific A-CREB ($SC_{A\text{-}CREB}$) expression did not show altered Pax7^{+} SC number immediately nor over the long-term (Figure 6A,B). To further investigate the maintenance of the SC population, I tested the expression pattern of β 1-integrin and found no disturbance of basal localized expression in $SCs_{A\text{-}CREB}$ (Figure 7A,B). Additionally, break of quiescence was not detected when following EdU incorporation $SCs_{A\text{-}CREB}$ for 3 weeks (Figure 7A,B), which is one week longer than experiments by other groups that found spontaneous proliferation of mutants (Bjornson et al., 2012; Boonsanay et al., 2016; Cheung et al., 2012; Crist et al., 2012; Mourikis et al., 2012; Yamaguchi et al., 2015). The preservation of Pax7^{+} cell number, localization within the niche, and maintenance of quiescent indicates that CREB activity is not required to maintain the SC population during quiescence.

CREB activity is necessary for SC regenerative capacity

Because $Pax7^+$ and $MyoD^+$ myoblasts showed high pCREB levels, I postulated that CREB might have a role in progenitor expansion after SC activation. I therefore examined muscle regeneration in mice after cardiotoxin (CTX)-induced injury (Figure 8). At 5 and 10 days (d) post-injury, $SC_{A\text{-}CREB}$ mice showed significant reductions in regenerated myofiber number and diameter by histology and MHC immunofluorescence (Figure 9A, 10A,B). At 35 d post-injury, the few regenerative fibers at earlier time points were no longer detectable in $SC_{A\text{-}CREB}$ mice (Figure 11), consistent with CREB's role in maintaining mature myofiber survival (Berdeaux et al., 2007).

When I assessed the $Pax7^+$ population at 5 and 10 d post-injury, $SC_{A\text{-}CREB}$ mice showed over 90% fewer $Pax7^+$ cells compared to controls (Figure 12). No $Pax7^+$ cells were observed in damaged areas 35 d post-injury (Figure 11). Because of the lack of new myofibers, the absence of SCs at 35 d may be due to unavailable myofiber niches. These results indicate that inhibiting CREB in SCs leads to loss of $Pax7^+$ SCs after injury, directly or indirectly.

DISCUSSION

The success of regeneration depends on the proper response of SCs to injury stimulus. I found that CREB activity has a distinct role in the regenerative capacity of SCs and muscle regeneration. While CREB inhibition in the SC does not cause stem cell defects in terms of survival, cell fate, nor quiescence, once challenged by injury, $SCs_{A\text{-}CREB}$ do not respond correctly to injury stimulus. CREB inhibition leads to drastically reduced myofiber formation (Figure 9A, 10A,B). Newly formed fibers are smaller and fewer are formed, indicating either lack of myocytes fusion or lack of SC proliferation. Because I didn't see an abundance of nGFP positive cells in the interstitial space (Figure 10), , I predicted that the inability to form new fibers could be caused by lack of a sufficient progenitor pool rather than a lack of ability to fuse. Because a few fibers do form, a fusion defect likely does not explain the severe inability to regenerate new fibers.

SCs must also self-renew its population to provide a source of stem cells for future rounds of regeneration. The number of $Pax7^+$ cells at 5 and 10 days after injury were significantly reduced upon A-CREB expression in the SC lineage. Day 5 is a time point in which a portion of proliferating progenitors have fused to form terminally differentiated myofibers although a portion of myoblasts are proliferating in the interstitial space. At this time point, myoblasts represent both the transit amplifying population as well as the cellular population that will go on to form the reserve SC pool. I found that the number of $Pax7^+$ cells was significantly reduced, indicating a lack of expansion of progenitors and/or self-renewing SCs. A further reduction in $Pax7^+$ cells at day 10 after injury indicates that the smaller progenitor pool is not due to a delay in

expansion. Further, day 10 after regeneration, SCs will begin to reenter the niche and reestablish quiescence. In A-CREB expressing myoblasts, very few SCs are present compared to control (Figure 12A,B) suggesting A-CREB mice cannot self-renew the SC population after injury.

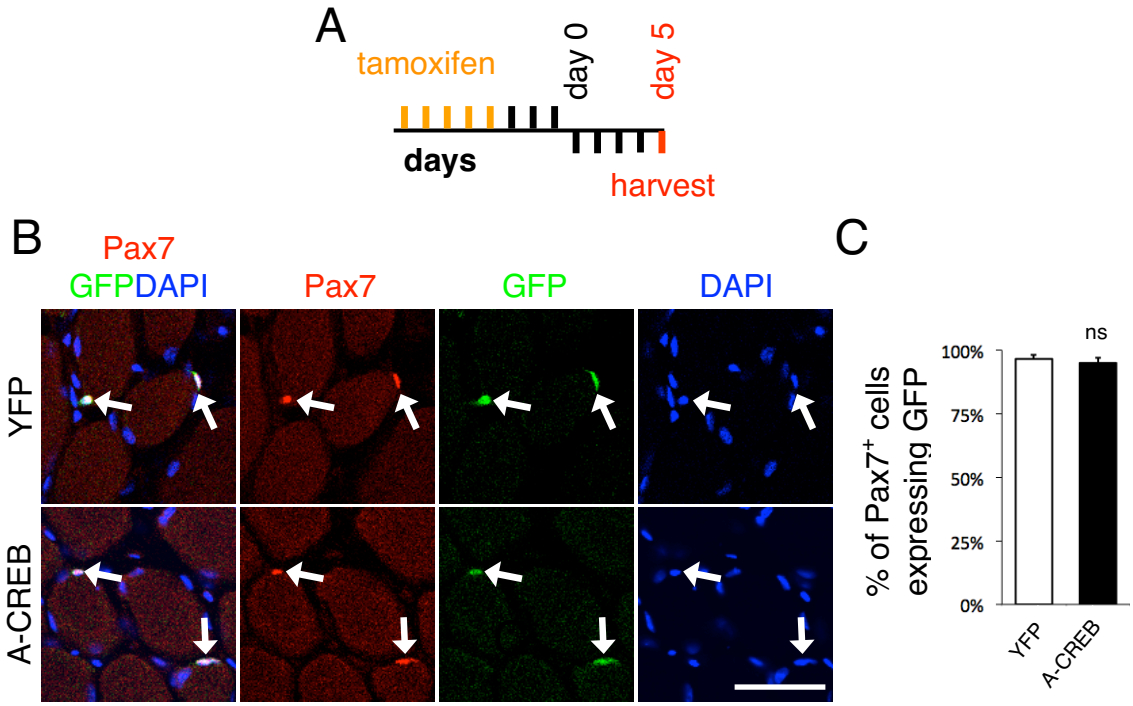

Figure 5. YFP and nGFP labeling efficiency in the Pax7-lineage (A) Timeline depicting tamoxifen injection regiment and TA muscle harvest 5 days after tamoxifen treatment. (B) Pax7 expression in lineage marked tamoxifen treated YFP and A-CREB mice at day 5 post-tamoxifen treatment as depicted in (A). (C) Quantification of labeling efficiency by determining YFP or nGFP expression in $Pax7^{+}$ cells in YFP or A-CREB mice, respectively, by immunofluorescence. Scale bars 50μm. N=3 mice, n≥50 cells per animal. Data represented as mean +/- 1 standard deviation.

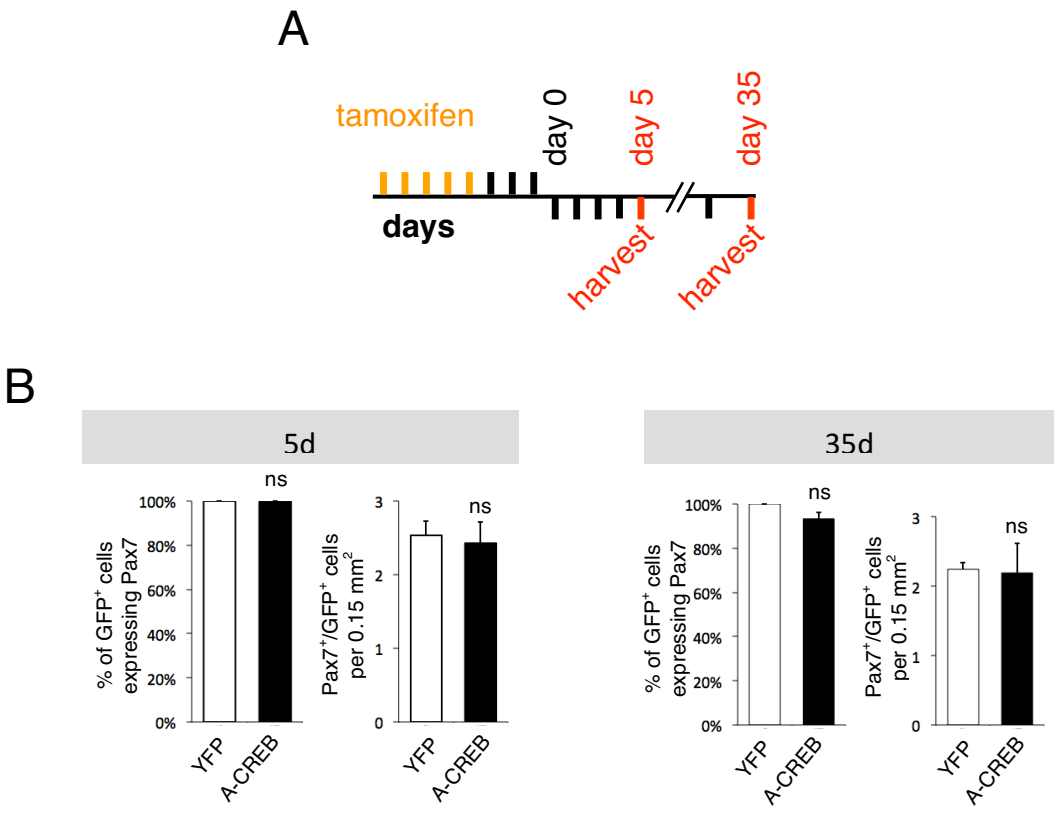

Figure 6. CREB inhibition does not affect Pax7^{+} cell number during quiescence (A) Timeline depicting tamoxifen injection regiment and TA muscle harvest at 5 and 35 days after tamoxifen treatment. (B) Maintenance of Pax7 expression was assessed by determining Pax7 expression in lineage marked cells at day 5 and day 35 and total number of Pax7 positive cells per area at day 5 and day 35 after tamoxifen treatment. N=3 mice, n≥50 cells per animal. Data represented as mean +/- 1 standard deviation.

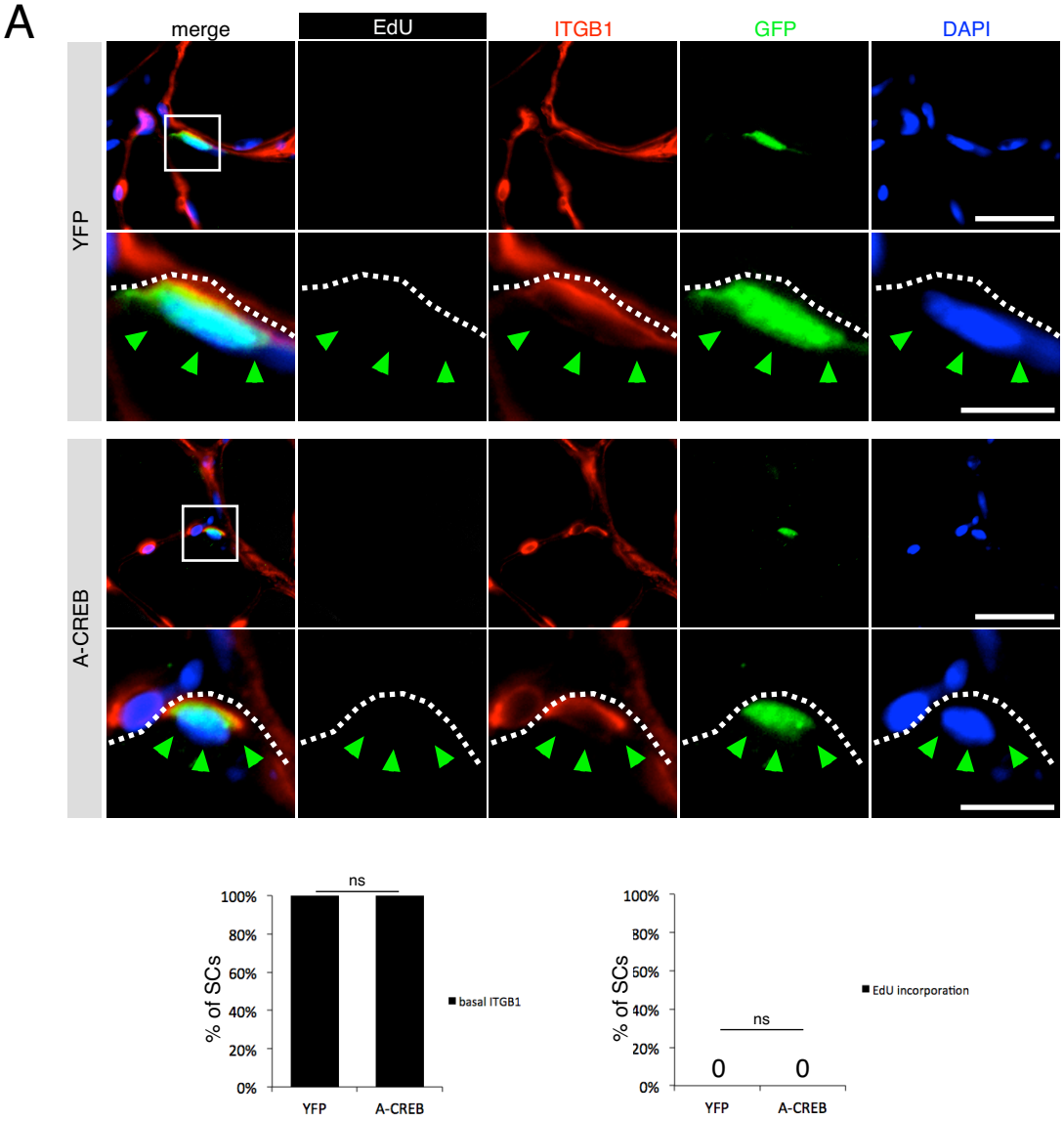

Figure 7. CREB inhibition does not disrupt basal domain nor quiescence of SCs

Representative images of ITGB1 expression and EdU detection analyzed by immunofluorescence in uninjured TAM treated TA muscle of YFP and A-CREB mice. Daily EdU injections performed during 5 days of TAM treatment and 2.5 weeks after last TAM injection. Boxed region is enlarged below. Dotted line marks basal lamina edge of myofiber. Arrowhead indicates apical side of SC. Scale bars 30 μm (top row), 10μm (bottom row, enlarged image)

A

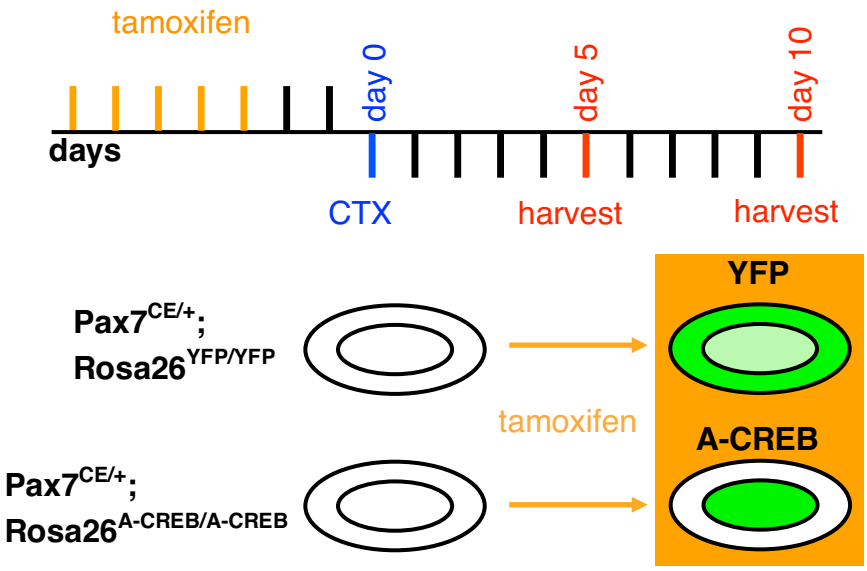

Figure 8. Schematic illustrating tamoxifen treatment for day 5 and day 10 muscle injury regiment

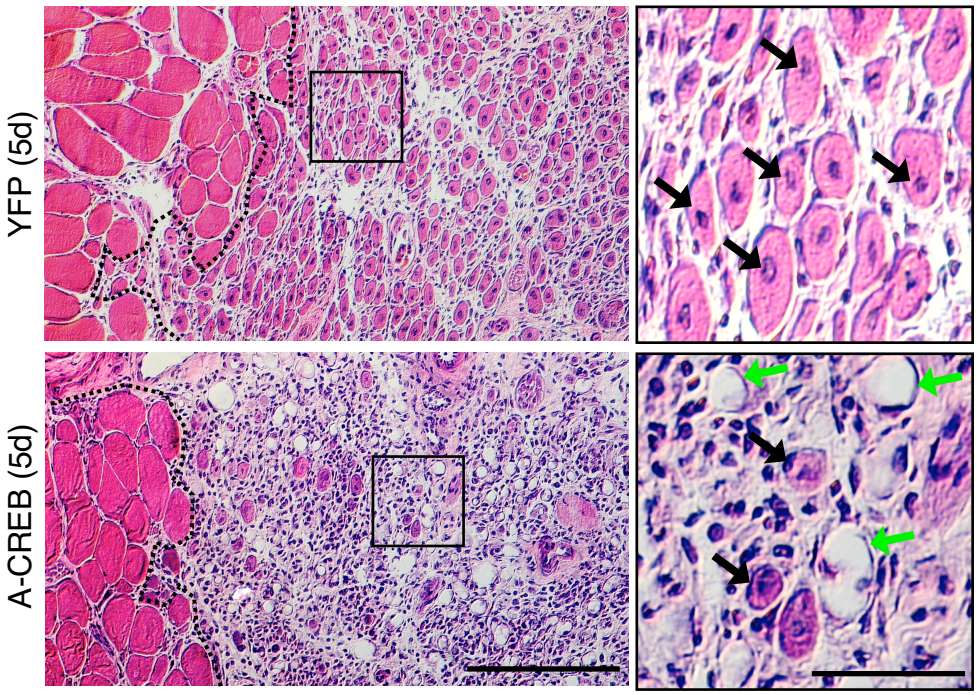

Figure 9. CREB inhibition leads to drastically reduced regeneration of myofibers after CTX injury (A) Hematoxylin and Eosin histological sections 5 days after cardiotoxin injury of YFP (control) and A-CREB TA muscles. Dotted line (left panels) demarcate uninjured area on the left and regenerated area on the right. Boxed region in left panel is enlarged in the right panel. Black arrows indicate newly formed centrally nucleated myofibers. Green arrows indicate vacuoles. Scale bars 200μm (left) and 50μm

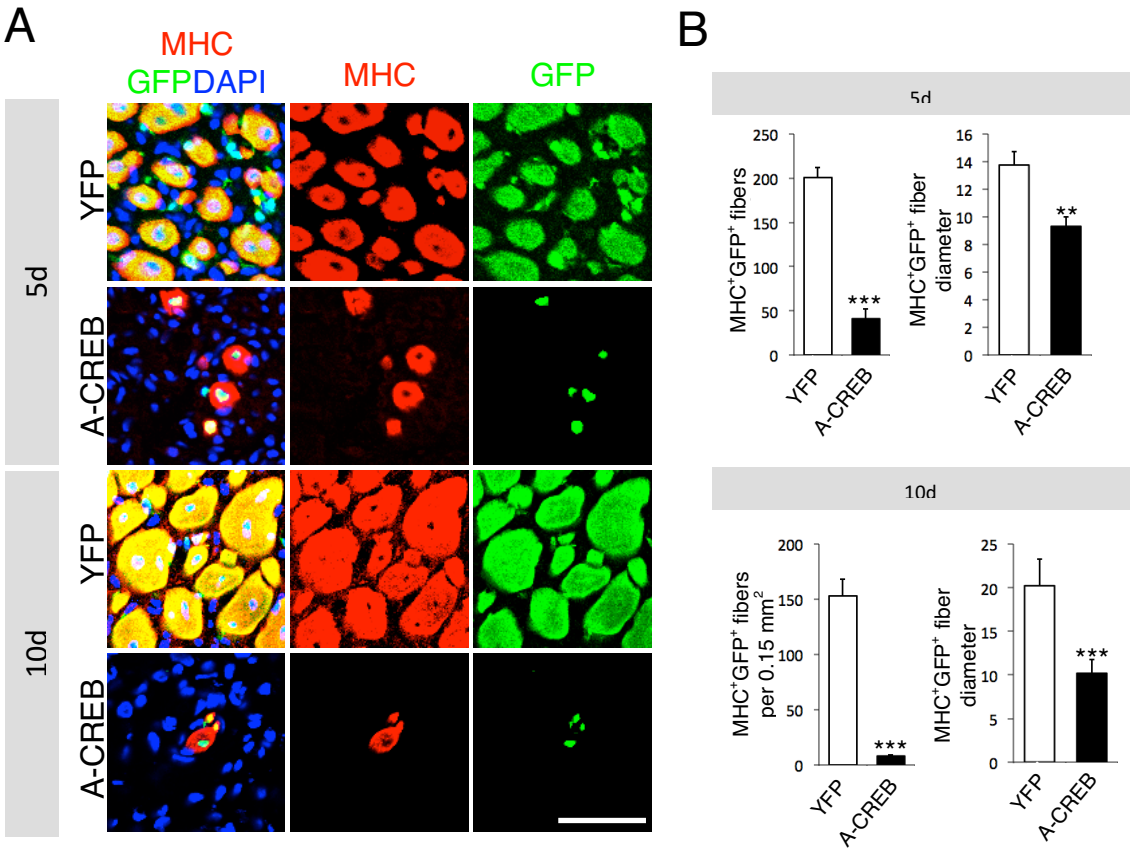

Figure 10. CREB inhibition leads to significantly reduced newly formed myofiber number and myofiber size after CTX injury (A) Representative images of embryonic myosin heavy chain (MHC) expression analyzed by immunofluorescence at day 5 and day 10 after injury. (B) Quantification of MHC^+ myofibers per indicated area (left) and average myofiber diameter (right) at day 5 and 10 after injury. Data represented as mean +/- 1 standard deviation. ***$p<0.001$, $p<0.01$, Student's t-test. Scale bar 50µm.

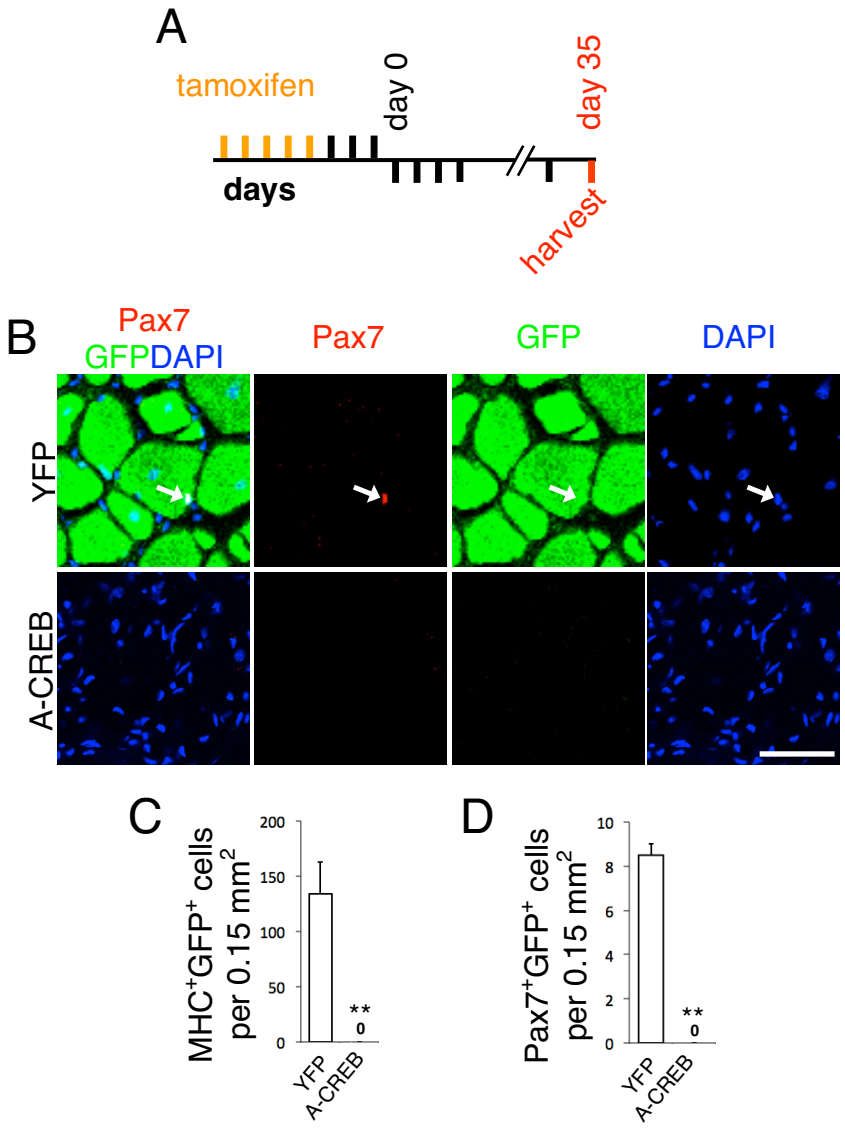

Figure 11. CREB activity is required for myofiber maintenance and Pax7$^+$ cell maintenance after injury (A) Schematic illustrating tamoxifen treatment and day 35 muscle injury regiment. (B) Representative images of Pax7 expression analyzed by immunofluorescence at day 35 after injury. Arrow indicates Pax7$^+$ cell. (C) Quantification of MHC$^+$ cells per indicated area at day 35 after injury. (D) Quantification of MHC$^+$ cells per indicated area at day 35 after injury. Data represented as mean +/- 1 standard deviation. **p<0.01, Student's t-test. Scale bar 50μm.

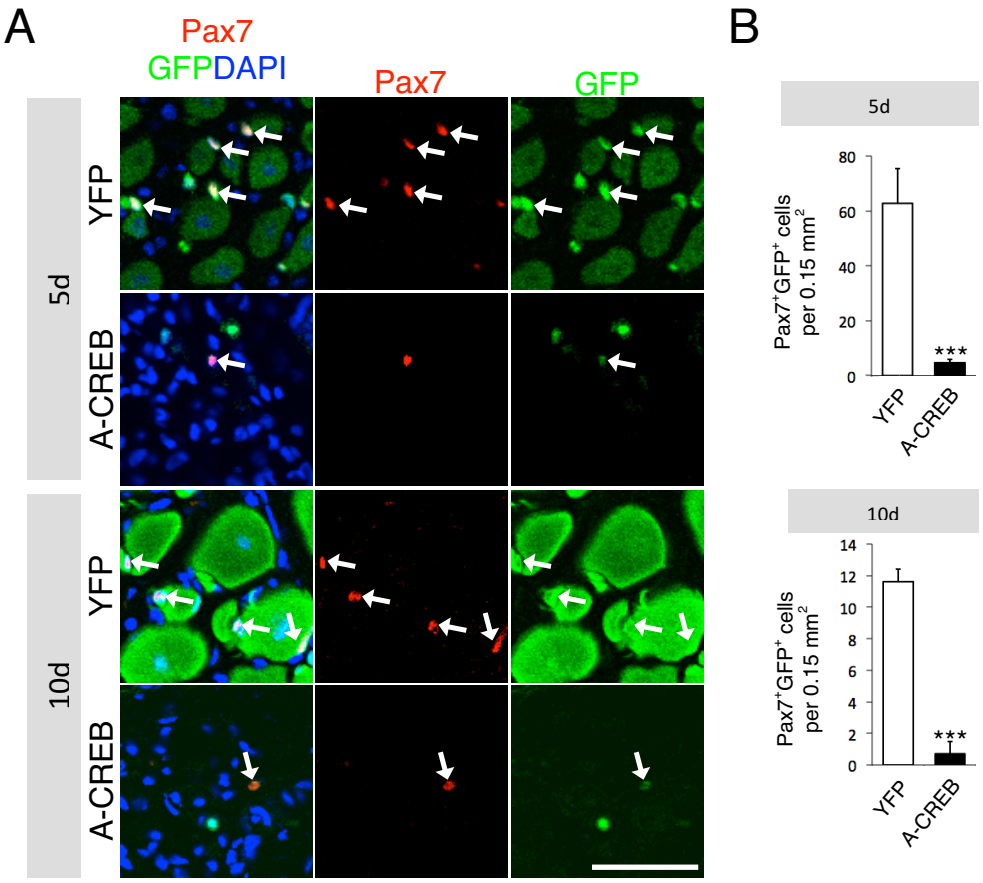

Figure 12. CREB inhibition leads to loss of Pax7^{+} cells during regeneration (A) Representative images of Pax7 expression analyzed by immunofluorescence at day 5 and day 10 after injury. Arrows indicated Pax7^{+} cells. (B) Quantification of Pax7^{+} cells per indicated area at day 5 and 10 after injury. Data represented as mean +/- 1 standard deviation. ***p<0.001, Student's t-test. Scale bar 50μm.

METHODS

Mice

Appropriate mating schemes were performed to obtain $Pax7^{CE/+}Rosa26^{YFP/YFP}$ and $Pax7^{CE/+}Rosa26^{A\text{-}CREB/A\text{-}CREB}$ mice. Animal treatment and care conform to the requirements of institution and NIH guidelines.

Tamoxifen solution

Tamoxifen, catalog #T5648, Sigma, was prepared for intraperitoneal injections by dissolving in corn oil, catalog #C8267, Sigma, at 20 mg/mL. The mixture was incubated in a 37^{o}C shaker at high RPM. Tamoxifen was dissolved within 30-90 minutes and aliquoted into 10mL volumes and flash frozen in dry ice chilled EtOH. Frozen aliquots were stored at -80^{o}C until use. Thawed aliquots were stored at 4^{o}C for up to two weeks.

Tamoxifen injections for inducible Cre activation

250 μL of 20 mg/mL tamoxifen in oil solution was injected daily for 5 consecutive days intraperitoneally into adult mice using a 26 gauge needle.

EdU treatment

200 μL of 0.5 mg/mL EdU solution was injected intraperitoneally into mice daily for 3 weeks.

Cardiotoxin treatment

Cardiotoxin (CTX), catalog #C9759, Sigma, was resuspended in 1XPBS 10 μM and aliquoted into 1.5 mL Eppendorf tubes and flash frozen in dry ice chilled EtOH. Frozen aliquots were stored at -80^{o}C until use. Prior to injection, animals were anesthetized using intraperitoneal injection of Avertin (2,2,2-Tribromoethanol), TCI America at 15

μl/gram body weight of 20 mg/ml solution). TA muscles were injected with 50 μL of CTX using an insulin needle (1/10 mL), catalog #14-829-26, Fisher.

Tibialis anterior (TA) cryosections

See Chapter 2 for methods used for obtaining TA muscle cryosections.

Single fiber isolation

See Chapter 2 for methods used for obtaining single fibers.

Antibodies

Primary antibody used were rabbit anti-GFP monoclonal (1:500), catalog # G10362, Invitrogen; rat anti-Integrinβ1 (1:1000), catalog #MAB1997, Millipore. Secondary antibody used were goat anti-rat AlexaFluor 488 (1:500), catalog #A11077. See Chapter 2 for additional antibodies used.

Immunostaining

See Chapter 2 for methods used for immunostaining muscle tissue sections.

EdU detection

Primary and secondary antibody protocol was performed prior to EdU detection. After secondary antibody application, Click-iT EdU Alexa-Fluor 647 Imaging Kit, catalog #C10085, Invitrogen, was used following manufacture's suggested protocol.

Hematoxylin and Eosin staining

Muscle sections were fixed in ice cold 4% paraformaldehyde for 10 minutes and rinse in distilled water for 1 minute. Sections were incubated in Hematoxylin, catalog #01560, Surgipath, for 3.5 minutes and then rinse in running lukewarm tap water for 5-10 minutes. Sections were then incubated in Scott's tap, catalog #3802901, Leica biosystems, for 10 seconds and then rinsed in running lukewarm tapwater for 2 minutes.

Sections were stained in Eosin, catalog #01600, Surgipath, for 1 minute and dehydrated in EtOH series: dip 5 times in 95% EtOH, dip 5 times in newly made solution of 95% EtOH, dip 30 times in 100% EtOH, dip 30 times in xylene. Sections were mounted under coverslips using Permount, catalog #SP15, Fisher Chemical.

CHAPTER 4: CREB ACTIVITY IS REQUIRED FOR SC PROLIFERATION DURING REGENERATION

INTRODUCTION

Myoblast proliferation during regeneration

Upon injury, SCs undergo proliferation and then differentiation to generate new myofibers (Moss and Leblond, 1970; Snow, 1978). The proper timing of both of these events is crucial for generating sufficient, but not excessive myoblasts. The first SC division after injury can begin as early as 24 hours after injury induction (Zammit et al., 2002). Subsequent cell cycles can be more rapid with a cycling time of about 12 hours being average (Zammit et al., 2002). From day 0 to day 3 of regeneration, SC derived myoblasts are primarily proliferative with only a small portion of cells showing differentiation (Zammit et al., 2004). This allows for expansion of the progenitor pool for supplying the future myonuclei of the regenerated myofibers. After 3 days, the terminal differentiation markers Mgn and MHC begin to appear (Zammit et al., 2004). The beginning of myofiber formation coincides with further myoblast proliferation, however as proliferation ceases, myocyte fusion dominates and myocytes are largely incorporated into myofibers (Robertson et al., 1993).

RESULTS

CREB activity is necessary for SC proliferation

To determine whether the reduction of $Pax7^+$ $SC_{A\text{-}CREB}$ cells at 5 d post-injury (Figure 12B) is due to defective proliferation, I examined the rate of *in vivo* EdU incorporation during muscle repair from day 0 through 5 after CTX injury (Figure 13A). I observed a marked reduction in $SC_{A\text{-}CREB}$ proliferation, compared to robust expansion of control YFP^+ SCs during the 2-5 d period, when assaying for total lineage marked cells and for percent of cells incorporating EdU at each time point (Figure 13B,C). I next tested whether precocious differentiation might contribute to failed expansion. Indeed, the fraction of lineage marked SCs positive for the myocyte marker Mgn at 2-4 days post-injury were significantly higher in $SC_{A\text{-}CREB}$ mice compared to controls (Figure 14). To further test $SC_{A\text{-}CREB}$ proliferative performance and differentiation kinetics, I used myofiber culture assays, in which injury is absent. The majority of $SCs_{A\text{-}CREB}$ remained as single cells after 3 d in culture, while most control SCs expanded to form multi-cell clusters (Figure 15). At 1 d, when most cells had not undergone cell cycle, single $SCs_{A\text{-}CREB}$ expressed Mgn, while control SCs did not (Figure 16), indicating that at least a portion of $SCs_{A\text{-}CREB}$ undergo differentiation without cell division. Consistent with our *in vivo* studies, these findings demonstrated that $SCs_{A\text{-}CREB}$ proliferate poorly and differentiate early during the expansion phase.

Reduced SC expansion explains fewer newly regenerated myofibers in $SC_{A\text{-}CREB}$ mice. However, smaller fiber diameter might also be compounded by reduced fusion

efficiency. To test this possibility, I purified $SCs_{A\text{-}CREB}$ and control SCs by fluorescence activated cell sorting (FACS) based on GFP/YFP signal, and plated them at the same density in differentiation media. I found $SCs_{A\text{-}CREB}$ showed similar fusion efficiency as controls (Figure 17). Together, the findings provide evidence that $SCs_{A\text{-}CREB}$ are defective in proliferation but capable of transitioning through the differentiation program to form new muscle fibers.

DISCUSSION

Expression of A-CREB in the SC causes significantly reduced ability to mount a proliferative program. The lack of proliferation explains the observed regeneration phenotype in which newly regenerated myofibers were reduced as well as their size (Figure 9,10). This indicates that CREB activity promotes a proliferation factor and since few $SCs_{A\text{-}CREB}$ expanded or incorporated EdU throughout the expansion period, it is likely that the proliferation defects occurs early. Additionally, myoblast begin to terminally differentiate as early as 1 day after activation (Figure 16), which is usually when the first cell division occurs. These suggest that the first division of $SCs_{A\text{-}CREB}$ is defective which leads to loss of an amplifying progenitor pool.

I ruled out the possibility that $SCs_{A\text{-}CREB}$ were lost to apoptosis based on their survival after short and long term tamoxifen treatment (Figure 6) as well as their ability to form myofibers in culture without noticeable loss of total cell number (Figure 17). I assayed the differentiation marker Mgn in the A-CREB expressing myoblast population and found a greater percentage of myoblasts had entered terminal differentiation compared to control. This indicated that the loss of proliferation coincides with accelerated differentiation. Loss of RBP-J kappa in SCs also results in accelerated differentiate however these mutant cells also break quiescence and fuse into existing myofibers without injury (Bjornson et al., 2012; Mourikis et al., 2012). This indicates that $SCs_{A\text{-}CREB}$ defects likely do not involve Notch signaling completely. The events that regulate the correct balance of proliferation and differentiation are biased towards

differentiation in $SCs_{A\text{-}CREB}$, which leads to severe inability to activate upon injury stimulus.

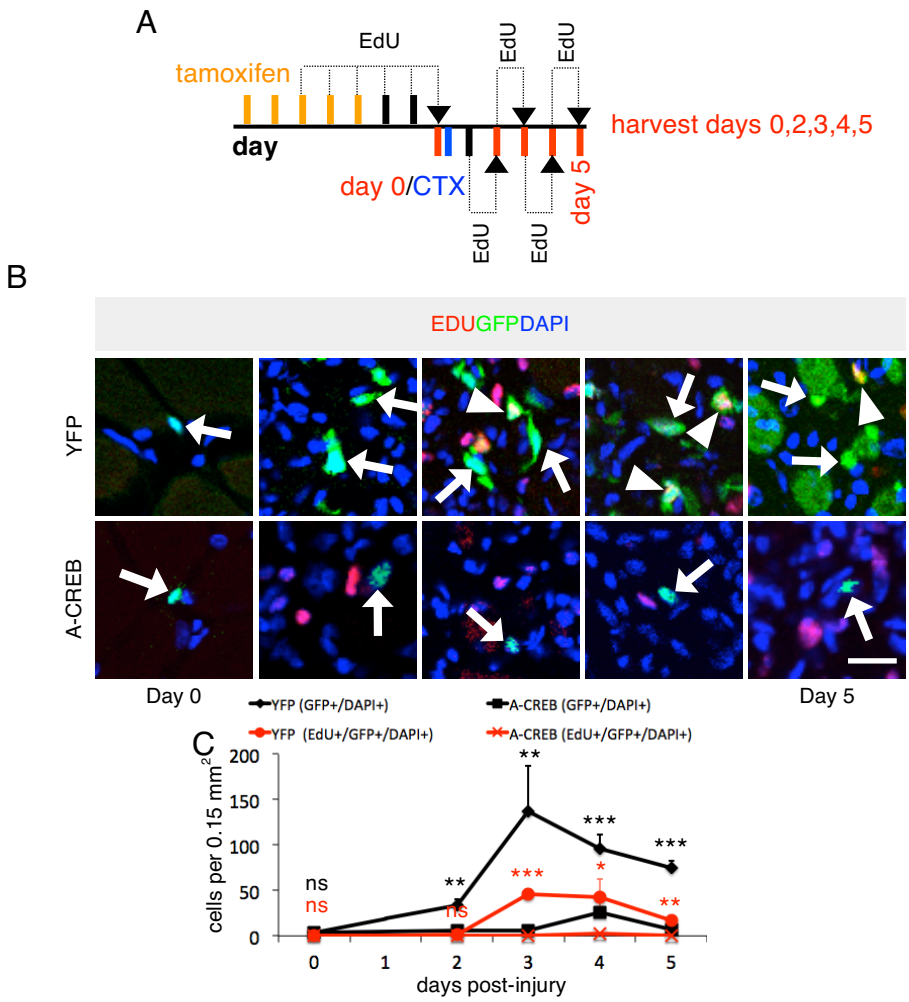

Figure 13. CREB is required for proper SC proliferation (A) Schematic illustrating tamoxifen treatment and EdU injections used for day 0,2,3,4 and 5 muscle injury regiments. (B) Representative images of EdU incorporation detection in YFP and A-CREB TA muscle at indicated time points after CTX injury. Arrows indicate lineage marked EdU^- myoblasts and arrowheads indicated lineage marked EdU^+ myoblasts. (C) Quantification of YFP and A-CREB lineage-marked myoblast number and EdU^+ myoblast number on day 0,2,3,4, and 5 after CTX injury. Data represented as mean +/- 1 standard deviation. **p<0.01, ***p<0.001, Student's t-test. Scale bars 20μm.

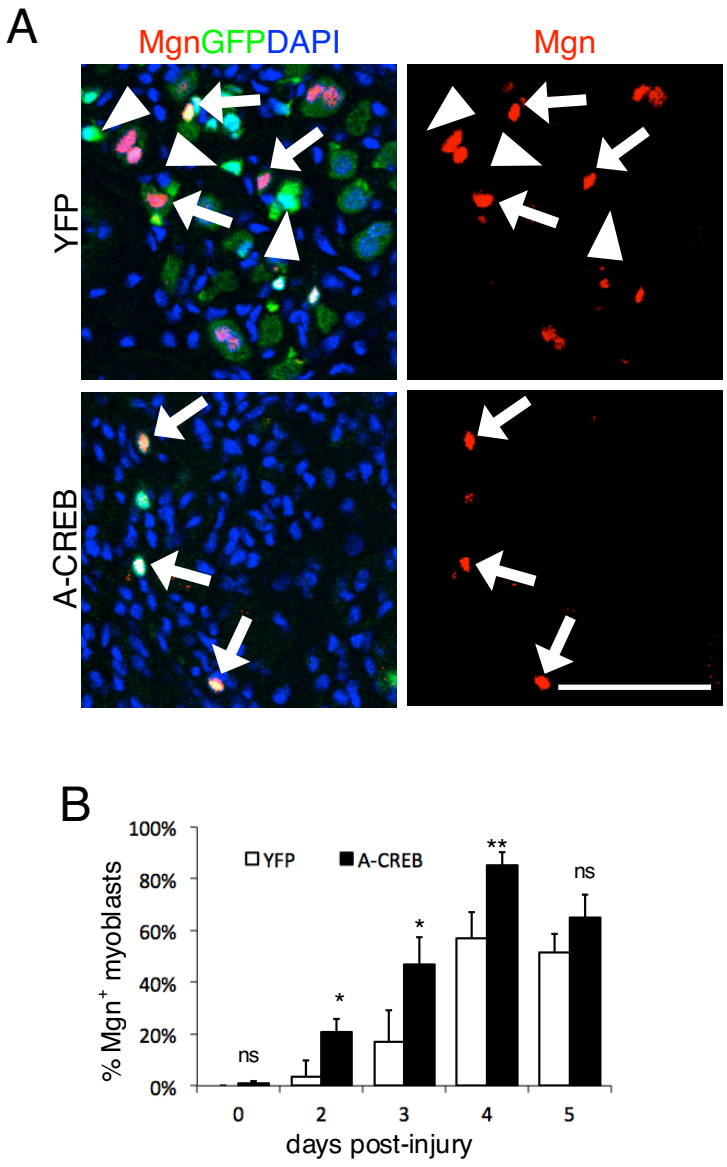

Figure 14. CREB inhibition leads to premature differentiation (A) Representative images of Mgn expresion in YFP and A-CREB myoblasts from TA muscle at 4 days after CTX injury. Arrows indicate lineage marked Mgn^+ myoblasts. Arrowheads indicate lineage marked Mgn^- myoblasts. (B) Quantification of Mgn^+ cells as a percentage of total GFP^+ lineage marked myoblasts. Data represented as mean +/- 1 standard deviation.*$p<0.05$, **$p<0.01$, Student's t-test. Scale bar 50µm.

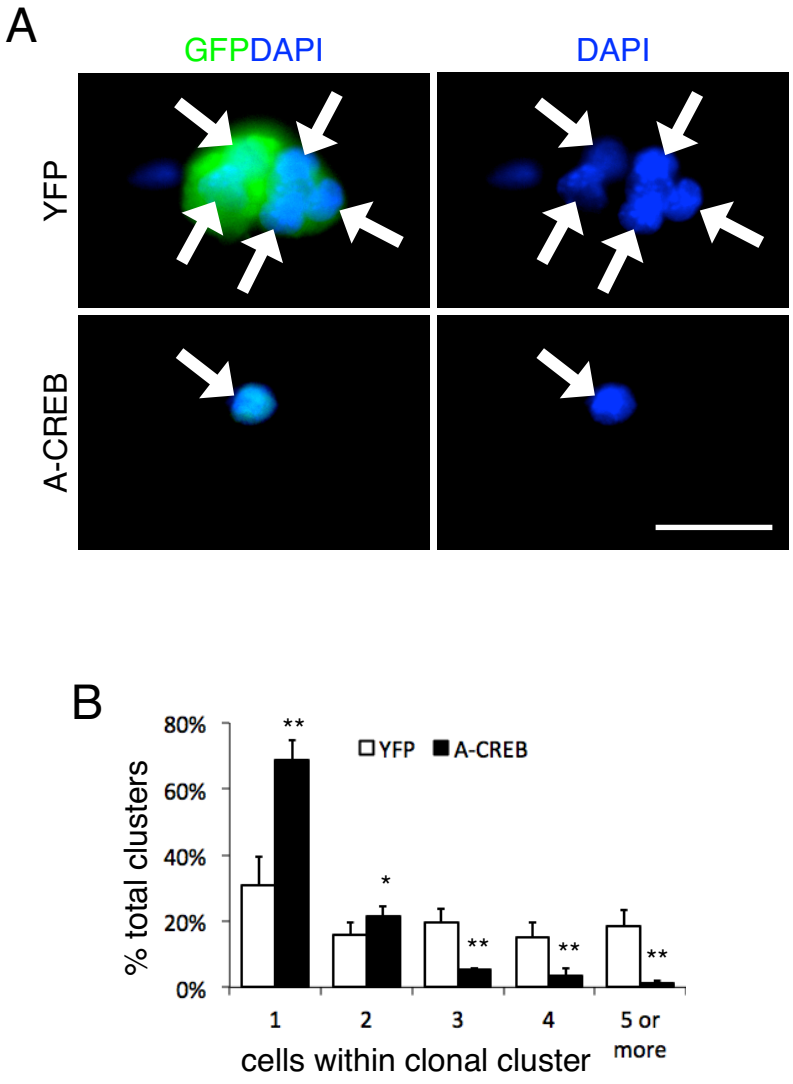

Figure 15. CREB inhibition in the SC leads to reduced proliferation *in vitro* (A) Representative images of YFP and A-CREB myofiber-associated myoblast clusters after 3 days of culture in plating medium. Arrows indicated lineage marked DAPI+ myoblasts from within a cluster. (B) Quantification of cluster size after 3 days of culture in plating medium. Data represented as mean +/- 1 standard deviation. *p<0.05, **p<0.01, Student's t-test. Scale bar 20 μm.

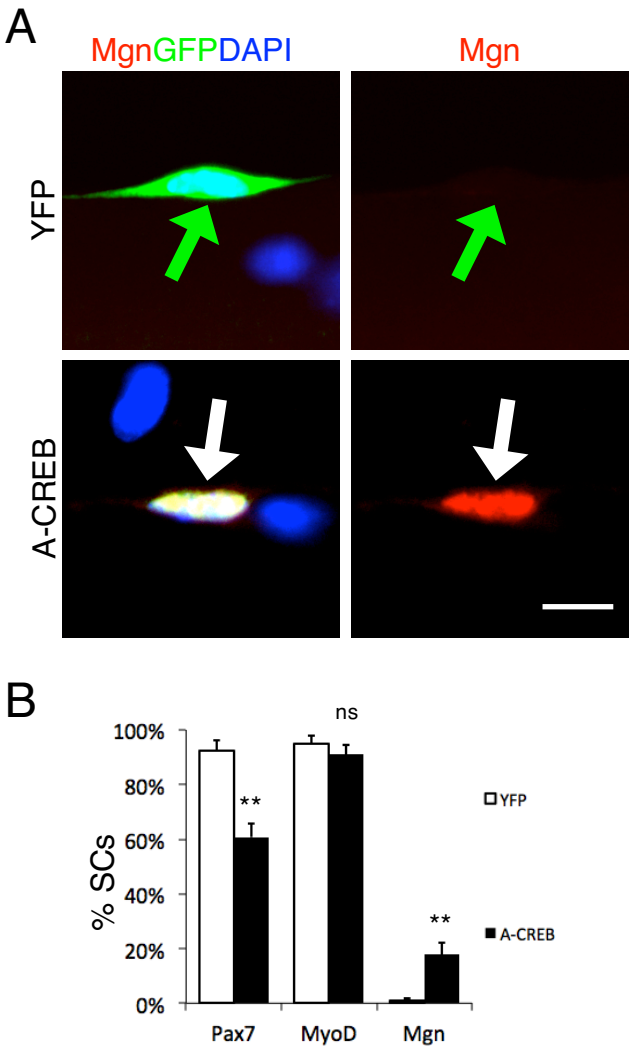

Figure 16. CREB inhibition leads to premature differentiation at the expense of Pax7$^+$ cell maintenance *in vitro* (A) Immunofluorescence of single myofiber-associated SCs cultured in plating medium for 1 day shows A-CREB SCs undergo premature differentiation. Green arrows mark Mgn$^-$ SCs. White arrows mark Mgn$^+$ SCs. (B) Quantification of Pax7, MyoD or Mgn expression shows A-CREB SCs have reduced Pax7 and enhanced Mgn. N=3 mice/genotype, n≥100 cells/animal. Data represented as mean +/- 1 standard deviation. **p<<0.01, Student's t-test. Scale bar 10 μm.

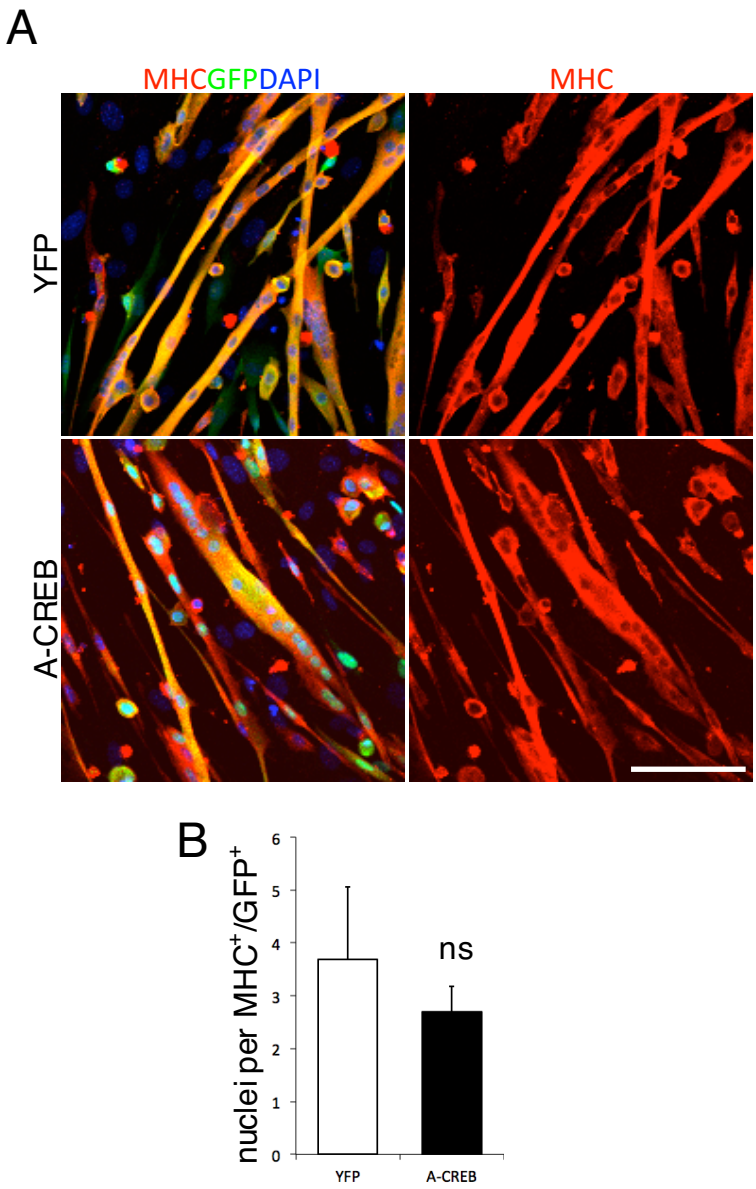

Figure 17. CREB is not necessary for terminal differentiation (A) YFP and A-CREB satellite cells were purified by FACS and plated at equal densities for 5 days in DM. Immunofluorescence analysis of MHC expression shows proper myofiber formation by A-CREB satellite cells. (B) Quantification of fusion index shows A-CREB myoblast differentiation is comparable to control. N=3 technical replicates, n≥200 cells/replicate. Data is expressed as the mean±standard deviation. Scale bar 100 μm.

METHODS

Mice

See Chapters 2 and 3 for mice used.

Tamoxifen injections for inducible Cre activation

See Chapter 3 for methods used for tamoxifen injections.

Tibialis anterior (TA) cryosections

See Chapter 2 for methods used for obtaining TA muscle sections.

Single fiber isolation

See Chapter 2 for methods used for obtaining single myofibers.

EdU treatment

200 μL of 0.5 mg/mL EdU solution was injected intraperitoneally into mice 24 hours prior to harvesting muscle tissue for analysis.

Cardiotoxin treatment

See Chapter 3 for methods used for cardiotoxin injury.

EdU detection

See Chapter 3 for methods used for detecting EdU incorporation.

Antibodies

See Chapter 2,3 for methods used for antibodies used.

Fluorescence activated cell sorting (FACS)

SCs of hindlimb muscle from TAM treated YFP and A-CREB mice were isolated in the manner described in "Myoblast isolation" section of methods of Chapter 2. SCs were

resuspended in 1XPBS prior to enrichment by positively selecting for YFP or nGFP signal in lineage marked SCs by FACS.

Tissue culture

FACS sorted myoblasts were cultured on matrigel (1mg/10mL dilution in DMEM), catalog #356234, BD Biosciences, coated Permanox tissue culture slides, catalog #62407-335, VWR Scientific, in differentiation media (10% horse serum, PENSTREP, 1% Glutamax, in 1XDMEM).

CHAPTER 5: CREB ACTIVITY PROMOTES SELF-RENEWAL OF THE SC POPULATION

INTRODUCTION

The capacity of SCs to self-renew is evident in their ability to regenerate muscle after multiple rounds of injury. Two studies suggest a role for CREB in cell fate decisions. First, embryonic CREB mutants showed decreased expression of Pax3 (a paralog of Pax7) and MyoD in myogenic progenitors (Chen et al., 2005). Second, germline expression of an activation sensitive form of CREB, CREB-YF, resulted in greater levels of Pax7 protein in myoblasts between 6-12 hours of culturing in differentiation media (Stewart et al., 2011). The inability to regain $Pax7^{+}$ cells during regeneration (Figure 12) and the lack of proliferation of SCs after injury (Figure 13) promoted me to investigate the self-renewal capability of SCs. The role of CREB in cell fate regulation suggests the possible role for CREB in self-renewing the $Pax7^{+}$ population during regeneration.

RESULTS

$SCs_{A\text{-}CREB}$ have a defect in self-renewal

Reduced $Pax7^+$ cells after injury in $SC_{A\text{-}CREB}$ mice suggests a SC self-renewal defect caused either directly by A-CREB expression in the SCs and/or secondarily by deficient newly formed myofiber niches and inadequate environmental conditions of poorly regenerated areas. The myofiber culture assay permits SC self-renewal examination within wild-type niches and adequate milieu (Day et al., 2007; Zammit et al., 2004). By assessing the fractions of lineage marked $Pax7^+MyoD^-$ (self-renewed), $Pax7^+MyoD^+$ (expanding progenitors), and $Pax7^-MyoD^+$ (committed progenitors) cells 4 d after activation, I found that the $SC_{A\text{-}CREB}$ lineage had reduced fractions of expanding progenitors and renewed SCs (Figure 18A,B). Furthermore, I found that FACS purified $SCs_{A\text{-}CREB}$ generated fewer $Pax7^+$ reserve cells compared to controls in 5 d differentiated cultures (Figure 19A,B). As reserve cells are suggested to be similar to quiescent SCs, $SCs_{A\text{-}CREB}$ may be defective in re-acquiring quiescence.

I next examined SC symmetric versus asymmetric divisions by probing for Pax7, MyoD or Mgn expression after the first cell cycle in myofiber cultures. In 2 d cultures, 80% of control SCs divided once to form doublets, whereas only 23% of A-CREB clusters were doublets (Figure 20). Over 80% of control doublets contained at least one $Pax7^+$ daughter, conversely over 80% of A-CREB daughters were both $Pax7^-$ (Figure 21B). Both YFP and A-CREB doublets were mostly $MyoD^+$ (Figure 21B). Notably, many A-CREB doublets contained daughters that were both Mgn^+, whereas this combination was rarely seen in controls (Figure 21A,B). Based on the observation that SC self-

renewal occurs in the first cell division (Troy et al., 2012), these data show that the small fraction of $SCs_{A\text{-}CREB}$ that divide have a high propensity towards differentiation and limited self-renewal. All together, I conclude that CREB activity maintains the $Pax7^{+}$ SC population after they are activated.

DISCUSSION

Self-renewal is a hallmark characteristic of SCs, which enables multiple rounds of muscle repair throughout the lifetime of the organism. CREB inhibition in the SC abolishes the capacity to maintain the $Pax7^{+}/MyoD^{-}$ self-renewing population as well as the $Pax7^{+}/MyoD^{+}$ progenitor population after activation (Figure 18). This occurs on single fiber cultures in which the myofiber niche is not disrupted by damage and has not incorporated defective myoblasts. This shows that the $SC_{A\text{-}CREB}$ defect *in vivo* (Figure 9, 10,11,12,13,14) is not merely a secondary effect of disrupted myofibers and altered niche. Consistently, FACS purified A-CREB expressing cultured myoblasts could not reform the reserve cell phenotype (Figure 19). Therefore, the requirement for CREB in the ability to re-establish the $Pax7^{+}$ lineage is likely cell autonomous.

Upon activation, SCs are thought to be a heterogeneous mixture of myoblasts that have differential propensities towards self-renewal or differentiation (Kuang et al., 2008). In a recent study to determine when the SC might be commited for self-renewal, the authors found that SCs that regained quiescence at 4 days after activation (the reserve cell phenotype) were set aside during the first cell division (Troy et al., 2012). The inhibition of CREB in the SC prior to activation led to mostly an inability to expand (Figure 20), and those SCs that did undergo one cell division had high propensity to differentiation rather than self-renew (Figure 21). The direct terminal differentiation without proliferation explains some of the reason why few cells divide (Figure 16). Both the inability to proliferate as well as the accelerated differentiation rate of $SCs_{A\text{-}CREB}$ contribute to their lack of self-renewal.

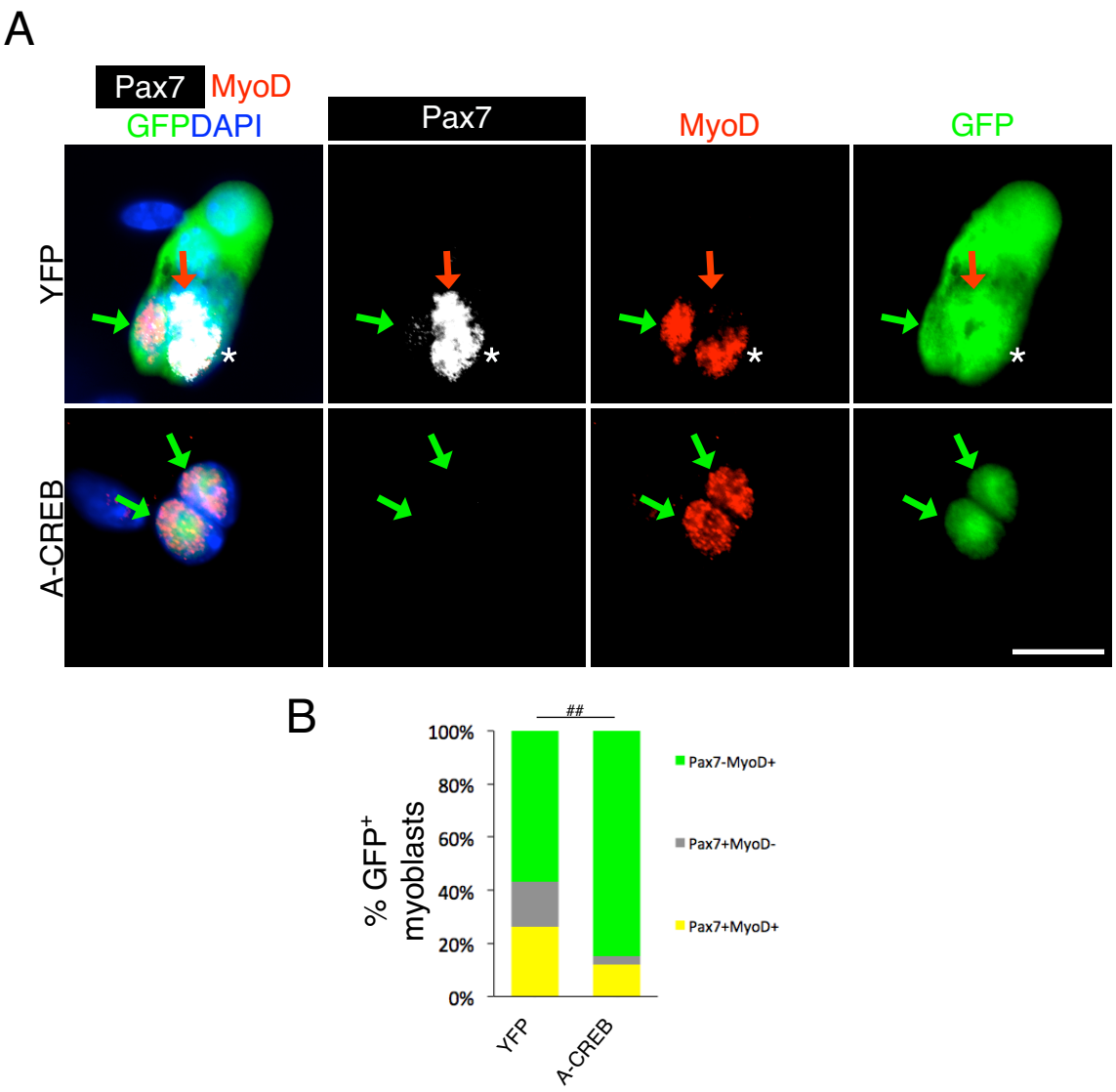

Figure 18. CREB inhibition leads to loss of Pax7 self-renewal after activation (A) Single myofiber-associated SCs were cultured for 4 days. Immunofluorescence analysis of myoblasts within clonal clusters. Red and green arrows mark $Pax7^{+}MyoD^{-}$ and $Pax7^{-}/MyoD^{+}$ myoblasts, respectively. Asterisks mark $Pax7^{+}MyoD^{+}$ myoblasts. (B) Quantification of Pax7 and MyoD expression pattern shows few $SCs_{A\text{-}CREB}$ renew the $Pax7^{+}/MyoD^{-}$ population after activation. N=3 mice/genotype, n≥150 cells/animal. ##p<0.01 Chi-squared test. Scale bar 20 μm.

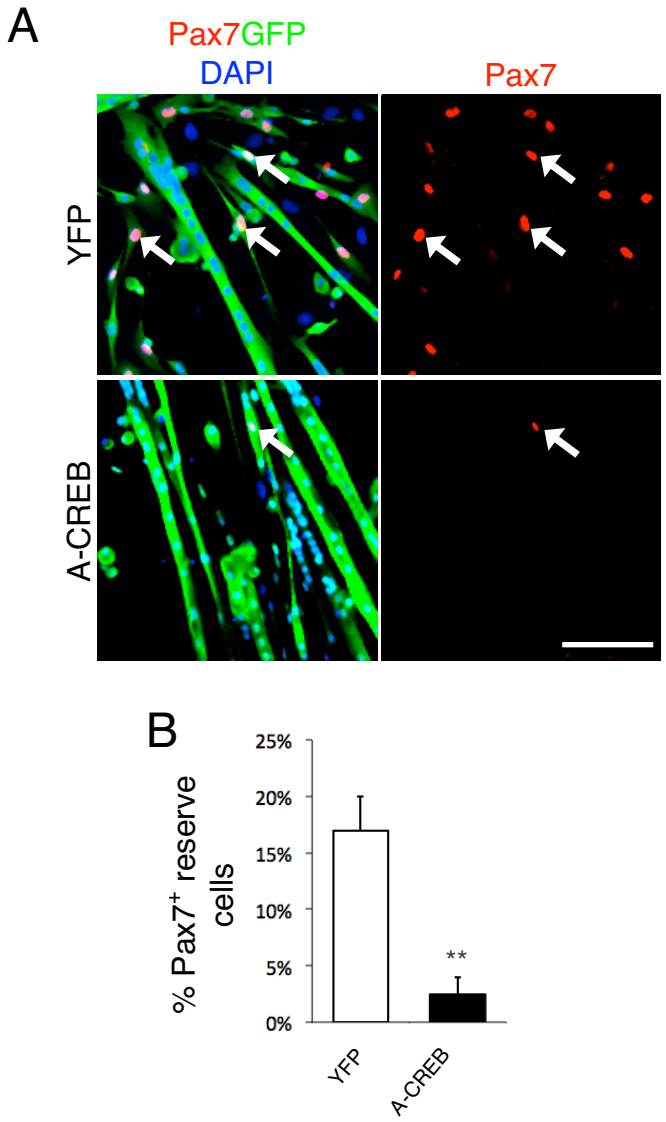

Figure 19. CREB inhibition leads to loss of Pax7$^+$ reserve cell population (A) YFP and A-CREB expressing SCs were purified by FACS and plated at identical densities for 5 days in DM. Immunofluorescence analysis of Pax7 shows reduced Pax7$^+$ population in $SCs_{A\text{-}CREB}$. Arrows mark Pax7$^+$ myoblasts. (B) Quantification of Pax7$^+$ cell number after differentiation shows $SCs_{A\text{-}CREB}$ reestablish fewer Pax7$^+$ reserve cells. N=3 technical replicates, n≥200 cells/replicate. Data represented as mean +/- 1 standard deviation. **p<0.01 Student's t-test. Scale bar = 50 μm.

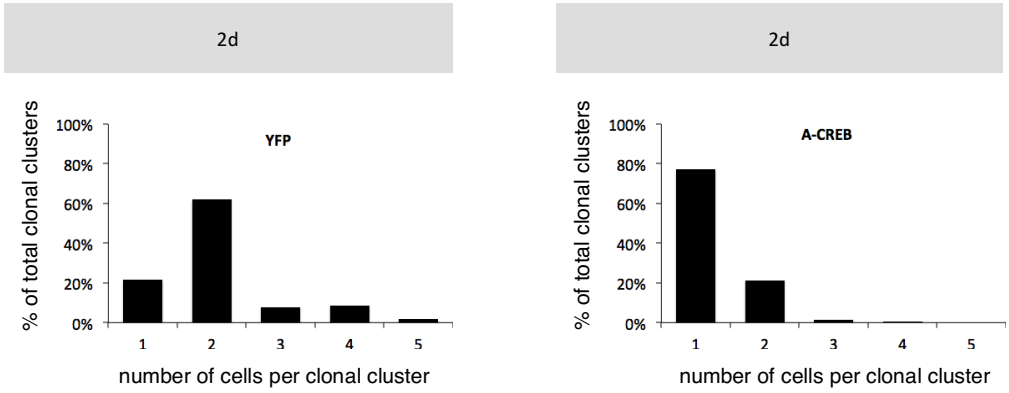

Figure 20. Proliferative cluster profile of SCs after 2 days in culture Quantification of cell number within myofiber-associated YFP and A-CREB myoblast clusters 2 days after activation. n≥100 cells/genotype.

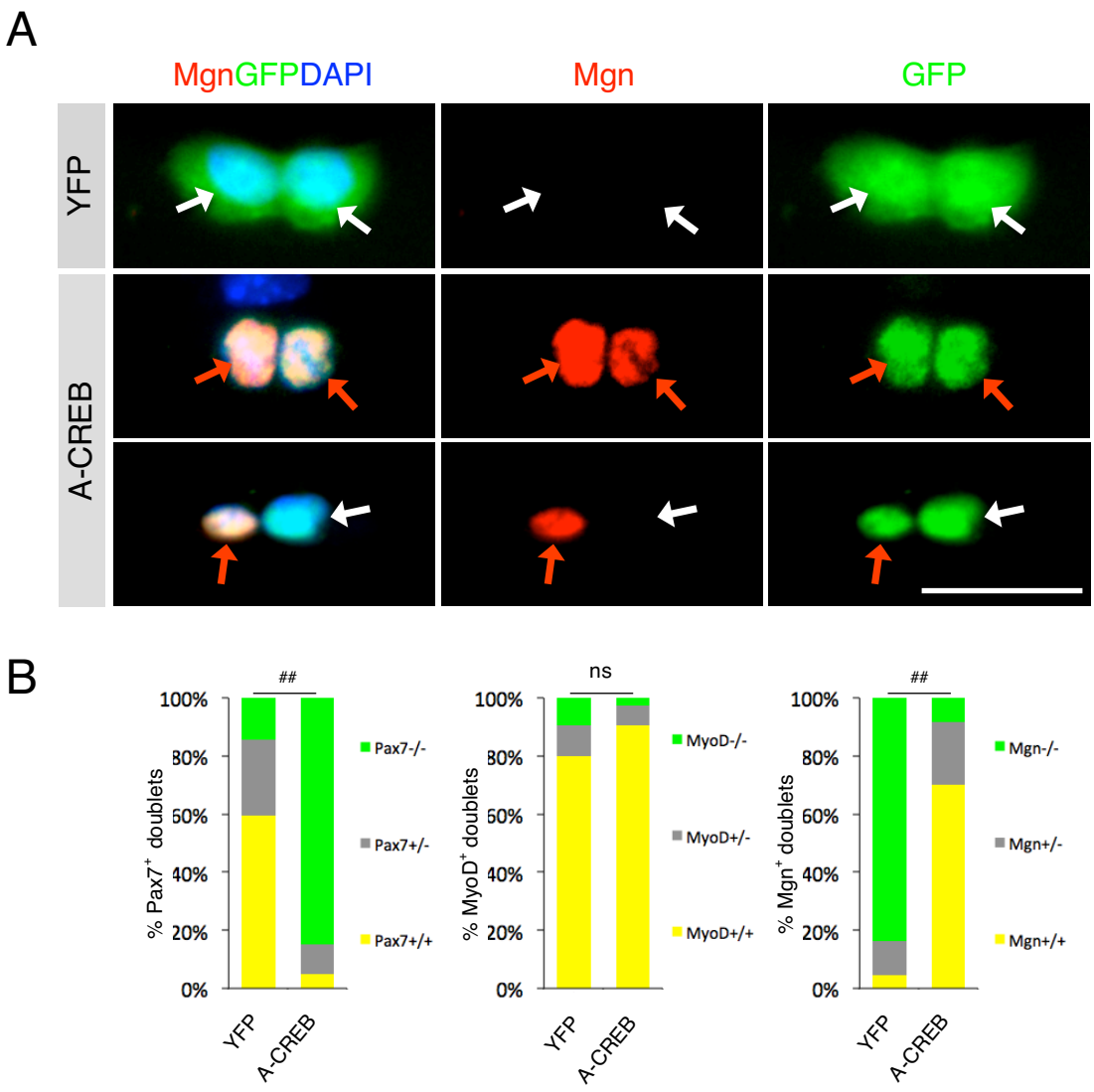

Figure 21. CREB inhibition leads to loss of Pax7$^+$ expression after the first cell division (A) EDL myofibers and associated SCs were cultured for 2 days in plating media. Immunofluorescence analysis of myoblast doublets. Mgn expression within myoblast doublets shows increased frequency of Mgn expression by $SCs_{A\text{-}CREB}$. White and red arrows mark Mgn$^-$ myoblasts and Mgn$^+$ myoblasts, respectively. (B) Quantification Pax7, MyoD, or Mgn expression within doublets. N=3 mice/genotype/marker, n≥50 doublets/marker/animal. ##p<0.01 Chi-squared test. Scale bar 20μm.

METHODS

Mice

See Chapters 2 and 3 for mice used.

Single fiber isolation

See Chapter 2 for methods used for obtaining single fibers.

Antibodies

See Chapter 2 antibodies used.

Tissue culture

See Chapter 4 for methods used for culturing FACS sorted SCs. See Chapter 2 for methods used for culturing myofibers.

CHAPTER 6: IDENTIFICATION OF CREB-DEPENDENT POLARITY PROTEIN MPP7 BY RNA-SEQ

INTRODUCTION

CREB regulation of transcription has been a long-term focus of studies. Since its original discovery as a transcriptional regulator of *somatostatin* in the nervous system (Montminy et al., 1986), hundreds of direct targets have been predicted for CREB and a subset have been validated based on gene expression levels, binding assays and sequencing analysis. The advent of high throughput sequencing has allowed for the discovery of non-canonical CREB family binding sites, in additional CREB responsive elements (CREs). ChIP-seq assays have determined these are actively transcribed CREB binding sites and are able to activate downstream targets (Martianov et al., 2010; Mayr and Montminy, 2001). Using a comparative RNA-seq approach to determine genes that are directly or indirectly regulated by CREB along with ChIP-PCR to determine direct binding of CREB to conventional and novel CRE sites, I have discovered the transcriptional changes that are important for CREB-mediate SC function, as described below.

RESULTS

Identification of CREB downstream genes in quiescent SCs

To ascertain the mechanism by which CREB controls SC proliferation and self-renewal, I identified CREB transcriptional targets in SCs. $SCs_{A\text{-}CREB}$ display precocious Mgn expression after injury/isolation, signifying early onset of defects. Therefore, to improve our prospects of finding primary CREB targets responsible for this effect, I harvested freshly isolated control and $SCs_{A\text{-}CREB}$ from hind limb muscles by FACS for immediately RNA preparation and RNA-seq. Although CREB family members are transcriptional activators, there was a much larger set of up-regulated (1517) than down-regulated (17) genes in $SCs_{A\text{-}CREB}$ compared to controls (Figure 22, Table 1, Table 2). A KEGG pathway database search (Huang et al., 2009a, 2009b) using the up-regulated gene set as input did not reveal pathway changes that could suggest abnormal signal transduction of $SCs_{A\text{-}CREB}$ (Table 3). Rather, 81 up-regulated genes could be categorized into 38 KEGG pathways, with many of them being metabolic pathways (Table 4), which has already been linked to CREB function (Altarejos and Montminy, 2011).

For identifying primary CREB targets, I focused on the 17 downregulated genes (Table 2). Using bioinformatics to query their promoter regions (-5kb - +1kb of the transcription start site), I found 16 of these genes contained at least one half-CRE and/or novel half-CRE site (Martianov et al., 2010); half-CRE sites have been shown to be highly functional in enhancing transcription of gene targets (Lesiak et al., 2013; Mayr and Montminy, 2001). Using the CREB database search tool (Zhang et al., 2005), 3 genes were found to contain CRE sites near a TATA box and 1 gene contained a CRE site

without a proximal TATA box (Table 2). *Nr4a2* and *Nr4a3* are canonical CREB target genes that are essential for dopaminergic differentiation and oncogenic functions, respectively (Ke et al., 2004; Le et al., 2003). The remaining genes have no documented function in SC proliferation or self-renewal. I chose to focus on Mpp7, because it is a polarity protein with tangential links to both aspects of SC function in the literature.

$SCs_{A\text{-}CREB}$ display altered apical protein distribution

Mpp7, the membrane-associated guanylate kinase (MAGUK) p55 subfamily member 7, is a homolog to *Drosophila* polarity protein Stardust. It shows the highest transcriptional change (≥10 fold) of the down-regulated genes within $SCs_{A\text{-}CREB}$ (Table 2) and greatest transcriptional abundance among the 7 *Mpp* family members (Figure 23). Chromatin immunoprecipitation (ChIP) analysis of SC-derived myoblasts confirmed pCREB binding to two predicted half-CRE sites in the *Mpp7* promoter (Figure 24) suggesting its regulation by CREB. Mpp7 has been studied in epithelial cell lines and shown to localize to adherens junctions and tight junctions for their maintenance (Bohl et al., 2007; Stucke et al., 2007). To determine Mpp7 distribution in SCs, I analyzed 3-D reconstructed immunofluorescence images of freshly isolated SCs on myofibers and found Mpp7 was preferentially localized to the apical side, opposite to β1-integrin basal localization, in the majority of SCs (Figure 25A-E). Consistent with *Mpp7* being a target of CREB, the majority of $SCs_{A\text{-}CREB}$ displayed low to undetectable Mpp7 (Figure 25D,E).

This prompted me to ask whether additional SC polarity proteins were affected in $SCs_{A\text{-}CREB}$, irrespective of direct CREB regulation. M-cadherin and its intracellular effector β-catenin are both localized to the apical surface of SCs (Figure 26A,C,G,I). M-cadherin is restricted apically in quiescent SCs, but invaded the basal domain of $SCs_{A\text{-}}$

$_{CREB}$ (Figure 26B,C). Similarly, the altered pattern of β-catenin localization followed that of M-cadherin (Figure 26H,I). Because $SCs_{A\text{-}CREB}$ are defective in proliferation, I examined the localization of a SC activation determinant, polarity protein Par-3. Unexpectedly, it was drastically reduced in $SCs_{A\text{-}CREB}$, compared to its apically concentrated pattern in control SCs (Figure 26D-F). Conversely, distribution of the basally enriched β1-integrin was unperturbed in $SCs_{A\text{-}CREB}$ (Figure 26J-L), consistent with *in vivo* localization pattern during quiescence (Figure 7A). All together, these data suggest that $SCs_{A\text{-}CREB}$ have a partial defect in maintaining apical polarity, while retaining the basal domain.

DISCUSSION

CREB activity has been implicated in myoblast proliferation (Stewart et al., 2011) however its role in the SC has not been determined. Here, I found that it has a direct role in promoting the expression of transcript and protein of Mpp family member Mpp7, the membrane-associated guanylate kinase (MAGUK) p55 subfamily member 7 (Figure 23, 24, 25). Mpp family has PDZ domains that allows for protein-protein interactions and categorized as a scaffolding protein (Bohl et al., 2007; Stucke et al., 2007). Mpp7 has been found to be required for proper tight junction function and localized to tight and adherens junction (Bohl et al., 2007; Stucke et al., 2007). Here, I found that Mpp7 colocalizes to the apical domain as does β-catenin, an adherens junction associated protein (Figure 25A-E,26G-I). Mpp7, is a homolog to *Drosophila* polarity protein Stardust of Drosophila. Stardust is apically localized in Drosophila epithelial cells usually through interactions with its binding partner Crumbs (Bachmann et al., 2001). Interestingly, mammalian Crumbs paralogs are not expressed in SCs as assessed by RNA-seq of a very low FPKM (data not shown). This provides evidence that Mpp7 does not coordinate with the conventional Crumbs containing Stardust complex in SCs.

CREB inhibition in SCs did not cause a loss in SCs (Figure 5A-C,7) however I found a redistribution of polarized localization of proteins (Figure 25,26). By immunofluorescence, Mpp7 was enriched on the apical side of quiescent SCs. Consistent with the role of CREB in regulating Mpp7 expression, $SCs_{A\text{-}CREB}$ had reduced Mpp7 expression. Furthermore, M-cadherin, Par-3 and β-catenin were mislocalized of reduced (Figure 26). This shows that has a distinct defect in the apical domain during quiescence.

Interestingly, Par-3 has a role in SC progenitor expansion (Troy et al., 2012) which is consistent with the lack of proliferation of $SCs_{A\text{-}CREB}$.

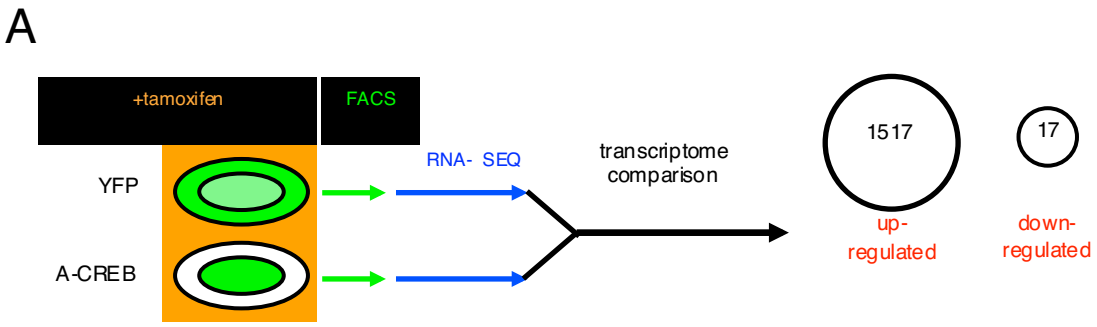

Figure 22. Flowchart followed to identify candidate CREB targets in quiescent satellite cells by RNA-seq (A) YFP and A-CREB satellite cells were purified by FACS and subjected to RNA-seq analysis. Transcriptome comparison performed using Cufflinks.

gene	FPKM		log2(fold_change)	p_value
	YFP	A-CREB		
Krt8	0.0610069	5.80513	6.57221	0.000705358
Krt18	0.117395	6.7619	5.84799	0.00208073
Prrg4	0.420092	21.8121	5.69828	6.78448E-06
Chrnd	0.30967	12.5592	5.34187	7.20199E-05
Spp1	3.86619	147.259	5.2513	0.020749
Ccnb1	0.610967	23.221	5.24819	1.41816E-05
Chrng	0.212469	7.85277	5.20788	0.000939425
Cdca3	0.248599	9.18565	5.20749	0.000883882
Myh3	0.811127	24.8661	4.93811	6.19024E-07
Pbk	0.652271	18.8544	4.85329	0.000121794
Gm12603	0.203343	5.68829	4.80601	0.0214647
Hist1h3c	6.15005	169.949	4.78836	7.37343E-05
Mgst2	0.202607	5.47671	4.75656	0.0101087
Murc	0.835802	22.4516	4.74752	6.35749E-05
Msln	0.22054	5.85	4.72932	0.0022977
Gmnn	0.341123	8.94634	4.71293	0.00481958
Fgfbp1	0.419735	10.7456	4.67812	0.00201107
Cdk1	0.67579	17.2808	4.67645	8.16873E-05
Hist1h2ak	1.91841	48.9948	4.67465	0.0042933
Hist1h1b	1.95106	49.7697	4.67294	0.000451499
Hist1h2bl	3.44375	83.184	4.59425	0.00144934
Nusap1	0.287121	6.88272	4.58325	0.0211736
Hist1h3g	2.09432	49.6631	4.56762	0.00264656
Top2a	2.09103	49.4078	4.56245	6.35102E-07
Gm7325	0.538143	12.6001	4.5493	0.0120778
Hist1h4f	14.73	340.199	4.52955	0.000188324
Prune2	0.601729	13.8294	4.52248	1.15375E-06

gene	FPKM		log2(fold_change)	p_value
Ect2	0.382772	8.59593	4.4891	0.00996682
Myog	8.63139	192.452	4.47876	5.0278E-06
Hist1h2bb	12.9431	288.445	4.47803	0.000024766
Hist1h2bj	7.79772	172.004	4.46324	0.000316663
Itgb6	0.260547	5.73362	4.45983	0.0177773
Shcbp1	0.352113	7.67954	4.44691	0.00195261
Anln	0.716098	15.609	4.44607	9.98315E-06
Prc1	0.988491	21.4337	4.43851	2.95164E-05
Hist1h2bk	10.5465	225.338	4.41726	0.000148156
Trip13	0.274261	5.72116	4.38269	0.00161692
Psrc1	0.257311	5.3346	4.37379	0.00981444
Spc25	0.418631	8.62798	4.36527	0.0542072
Dusp27	0.279961	5.70974	4.35013	0.00174998
Actc1	1.93521	39.1846	4.33972	0.000140228
Hist1h2ab	4.05998	82.0682	4.33728	0.00103979
Kcnn4	0.376084	7.5661	4.33042	0.0797248
Hist1h2af	3.34683	67.2394	4.32844	0.00325721
Hist1h2ba	0.521692	10.3284	4.30728	0.0169398
Hist1h3b	7.54715	148.766	4.30097	0.000541508
Kif11	0.694711	13.655	4.29687	0.000021231
Bub1	0.298498	5.83293	4.28843	0.0024357
Hist1h1d	0.728856	14.0345	4.2672	0.000198936
Hist1h2bn	5.89505	113.326	4.26483	0.00101912
Tnni1	2.0232	38.8533	4.26332	0.00104059
Aspm	0.269771	5.04854	4.22606	2.89529E-05
Cenpa	0.766645	14.2212	4.21334	0.0025437
Cep55	0.323382	5.90628	4.19094	0.0328782
Hist1h4m	16.5358	301.832	4.19008	0.00029195

gene	FPKM		log2(fold_change)	p_value
Hist1h1a	8.13973	147.842	4.18294	2.66167E-05
Spag5	0.351058	6.33346	4.17321	0.000382954
Hmmr	0.560736	10.0554	4.16451	7.12076E-05
Hist1h3d	3.89222	68.8217	4.1442	0.00356633
Mki67	0.631921	11.123	4.13766	5.8531E-06
Hist1h2ag	3.94952	69.4359	4.13593	0.00247943
Tpx2	0.390426	6.77729	4.11759	0.056262
Uhrf1	0.898948	15.6012	4.11727	0.0310635
Tnnc1	1.06363	18.4239	4.11451	0.00329239
Hist1h2bg	4.49213	76.8128	4.09587	0.000822821
Ube2c	0.303493	5.09588	4.0696	0.0341713
Hist1h2bp	1.37799	23.1291	4.06907	0.00774465
Igfbp2	0.660231	10.9144	4.04712	0.00432712
Hist1h2bf	2.96651	48.878	4.04234	0.00639965
Hist1h3i	4.18951	68.8941	4.03953	0.00196157
Sgol2	0.356316	5.8446	4.03588	0.0271036
Hist1h2bm	5.29126	86.5	4.03102	0.00206985
Aif1l	2.98511	48.6471	4.0265	3.63753E-05
Racgap1	0.636699	10.3626	4.02464	0.00172723
2810417H13Rik	1.09323	17.7882	4.02425	0.0383771
D2Ertd750e	0.330869	5.35009	4.01523	0.00144521
Kbtbd5	1.29306	20.8702	4.01258	0.000261065
Smyd1	0.312835	5.04495	4.01137	0.0170771
Cav3	1.49574	23.9157	3.99902	0.00152257
Hist1h2an	4.23212	67.427	3.99387	0.00538499
Nek2	0.358574	5.69622	3.98966	0.00117659
Ccna2	1.42767	22.5486	3.9813	0.0155669
Cdh2	0.357134	5.58229	3.96632	0.000905901

gene	FPKM		log2(fold_change)	p_value
Arpp21	0.938508	14.5758	3.95706	0.0822589
Ttn	2.0755	32.11	3.95149	0.000765459
Hist1h2ai	6.40865	98.9015	3.9479	0.00257753
Hist1h2ah	4.77552	73.5864	3.94571	0.00497041
2700094K13Rik	3.7065	56.818	3.93822	0.0246614
Hist1h3h	5.28735	79.6643	3.91332	0.00197924
Stac3	0.468083	7.03342	3.90939	0.00427357
Eno3	9.11585	136.216	3.90137	0.00166074
Hist1h4k	24.3361	361.54	3.89298	0.000411899
Nudt14	0.882054	13.0772	3.89005	0.0173537
H19	5.22312	76.8187	3.87847	0.000163085
Cdc20	1.13976	16.6726	3.87068	0.0528587
Cacng1	0.902149	13.1727	3.86804	0.00455258
Lgals3	5.12196	74.7202	3.86673	0.0104449
Tnnt2	0.801315	11.6273	3.85901	0.0270604
Dut	1.14455	16.5298	3.85221	0.0178526
Nuf2	0.714633	10.3166	3.85162	0.00137291
Hist1h4n	20.6985	296.742	3.84161	0.000891219
Tmem182	1.081	15.2003	3.81367	0.00634408
Mylpf	10.7118	149.086	3.79887	0.000177689
Trim55	0.719291	9.88994	3.78131	0.00350241
Hist1h2ac	0.471242	6.44222	3.77302	0.00465428
Srl	1.61045	21.9847	3.77096	0.00014586
Itgb1bp2	0.437323	5.95466	3.76725	0.0112376
Haus1	0.468338	6.37375	3.76652	0.0213344
Myl4	3.66878	49.7998	3.76277	0.000563846
Lgals1	89.7829	1216.53	3.76019	1.84622E-05
Adamts14	0.487962	6.52965	3.74216	0.000297199

gene	FPKM		log2(fold_change)	p_value
Smc2	0.969872	12.9755	3.74185	0.000125888
Hist1h2ad	5.65152	75.313	3.73619	0.00559619
Myof	1.57599	20.9667	3.73376	5.63823E-05
Mcm6	2.31092	30.5999	3.72699	0.000121451
Mcm2	0.654841	8.57903	3.7116	0.000949709
Tsfm	1.00946	13.1915	3.70795	0.00397252
Zwilch	0.456233	5.93805	3.70215	0.0147231
Bex1	0.888376	11.5585	3.70164	0.0105173
Hist1h2ae	1.56247	20.2859	3.69857	0.0104257
Mycl1	0.402195	5.2206	3.69825	0.00245776
Ncaph	0.611187	7.88302	3.68906	0.00107509
Stmn1	4.19734	53.8542	3.68151	0.000341137
Bub1b	0.84162	10.7281	3.67208	0.000391795
1190002F15Rik	0.59415	7.54399	3.66643	0.0286886
Plk4	0.646099	8.17909	3.66211	0.00157634
Hist1h4b	17.9269	226.003	3.65615	0.00159054
Hells	0.646259	7.96357	3.62323	0.00149399
Nme4	0.56471	6.94987	3.6214	0.0178287
Dctpp1	3.07821	37.7633	3.61682	0.00319067
Dctn3	3.08958	37.8868	3.61621	0.0102343
Myom2	0.576925	7.01103	3.60317	0.000479567
Hist1h4j	17.6014	212.147	3.5913	0.00211257
Nrcam	0.442375	5.31083	3.5856	0.00925236
Rbm24	1.26533	15.0901	3.57601	0.000603908
Mrpl34	0.8674	10.3379	3.57511	0.0189404
Psmd10	1.01646	12.0981	3.57315	0.0572882
Ccnb2	0.865692	10.3021	3.57294	0.00317641
Phgdh	6.15414	73.0785	3.56982	7.04845E-05

gene	FPKM		log2(fold_change)	p_value
Nudcd2	2.13504	25.2905	3.56626	0.000597026
Gsta4	1.99721	23.6551	3.56609	0.00308834
Casq2	0.925278	10.9524	3.56521	0.00211228
Apool	1.14265	13.5229	3.56495	0.00698334
Chchd10	0.530107	6.26443	3.56283	0.0287829
Ap1s1	0.899273	10.6186	3.56169	0.00812268
Ccng1	6.13296	72.3863	3.56106	4.45431E-05
Ak1	1.94922	22.913	3.5552	0.0145878
Mad2l1	0.522768	6.10649	3.5461	0.0117978
Cdk6	0.631918	7.29922	3.52993	0.00315714
Me2	1.21926	14	3.52134	0.000758006
Dnajc15	4.07296	46.4516	3.51158	0.00274103
Cdc45	0.935008	10.6463	3.50922	0.0461434
Hist1h4i	1.75232	19.9513	3.50915	0.0185431
Actn3	3.56459	40.2252	3.49629	0.000288917
Rrm2	2.8386	31.8434	3.48774	0.000215263
Ncapd2	0.869063	9.63894	3.47134	0.000663799
Prim1	0.968265	10.7031	3.46649	0.00452179
Nudt2	0.902328	9.90573	3.45654	0.0118296
Pafah1b3	0.484241	5.30542	3.45367	0.0394393
Acta1	10.6041	115.49	3.44508	0.000320268
Dapk2	1.27262	13.8532	3.44434	0.00207483
Dnajc9	2.82799	30.5503	3.43334	0.000457785
Hist1h3a	7.37846	79.383	3.42744	0.00269139
C1qtnf3	7.56952	80.7693	3.41553	0.0026738
Hist1h2bh	3.22186	33.8774	3.39436	0.0305482
Hist1h3e	9.52358	99.6752	3.38766	0.00483157
Ckap2	1.5352	15.9509	3.37714	0.000744866

gene	FPKM		log2(fold_change)	p_value
Prkar2b	1.18133	12.2454	3.37375	0.00110333
Chrna1	3.0464	31.4756	3.36906	0.000278343
Mrpl42	2.09957	21.5927	3.36238	0.00893058
Hist1h1c	3.09472	31.6168	3.35281	0.000890371
Tpm2	5.76486	58.6368	3.34645	0.000659327
Hes6	2.73434	27.7661	3.34406	0.00103892
Tmem55a	2.61027	26.4869	3.34301	0.000503576
Areg	0.87217	8.83603	3.34072	0.00786068
Tk1	1.32765	13.4486	3.3405	0.0174134
Akr1b8	3.50389	35.3599	3.33508	0.00150882
1110058L19Rik	0.759261	7.65609	3.33394	0.0365074
C330027C09Rik	1.14529	11.5197	3.33032	0.000711035
Galk1	1.7998	18.0023	3.32227	0.0216532
Arl4c	1.60746	16.0589	3.32052	0.00047194
0910001L09Rik	1.21697	12.1479	3.31934	0.0106243
Tacc3	1.53976	15.3506	3.31751	0.000901576
Lage3	1.36654	13.578	3.31268	0.0171489
2410022L05Rik	0.933729	9.25029	3.30842	0.0242232
Neb	0.95373	9.27666	3.28195	0.000959378
Igj	0.594314	5.77177	3.27971	0.00989248
Ccdc141	1.13137	10.9543	3.27536	0.000812113
Fam96a	2.13378	20.5979	3.27101	0.00296089
Kbtbd10	2.21618	21.2996	3.26468	0.00134234
Trim72	0.829943	7.95265	3.26035	0.00417146
D4Bwg0951e	1.02873	9.84456	3.25847	0.0077031
Atp5k	61.0285	581.55	3.25235	0.000599814
Mrps12	2.11835	19.908	3.23233	0.00998593
Acn9	0.588897	5.48989	3.22069	0.0472928

gene	FPKM		log2(fold_change)	p_value
Ppil1	1.64228	15.299	3.21967	0.00628551
Mrps16	4.64134	43.1723	3.21749	0.00538989
1110008P14Rik	1.19606	11.0144	3.20303	0.0282628
Hist2h3b	11.1235	102.375	3.20219	0.00462107
Rpa3	2.25051	20.6703	3.19924	0.0172431
Snrnp25	0.667184	6.11154	3.19538	0.0316589
Adam19	0.633718	5.79645	3.19326	0.00152469
Dclk1	1.94523	17.7841	3.19257	0.0598647
Cdkn2b	0.84144	7.66335	3.18704	0.0135695
Lrrc17	2.37897	21.6449	3.18562	0.00131897
Nup37	1.02032	9.11376	3.15902	0.0663399
Pdlim3	2.7805	24.8233	3.15828	0.00196301
Hddc2	1.02945	9.15467	3.15264	0.0377383
Eno1	10.2201	90.8806	3.15256	0.00280531
Tead2	0.939973	8.33697	3.14883	0.0083773
Nes	3.71339	32.8716	3.14603	0.000488737
Smcr7	0.86569	7.60858	3.1357	0.0145176
Bok	1.76929	15.4504	3.1264	0.00567382
Ccdc23	2.44296	21.2824	3.12296	0.082238
Fkbp11	0.781832	6.79886	3.12036	0.0491901
Egln3	0.731147	6.35254	3.1191	0.00496473
Tubg1	0.592469	5.14592	3.11862	0.0163906
Ptgr1	1.21295	10.5294	3.11783	0.00420353
Rnaseh2b	0.658501	5.7022	3.11426	0.0208662
Rfc3	1.49518	12.8894	3.10778	0.00795064
Amacr	0.607792	5.23167	3.10562	0.0117405
Nudt8	0.608095	5.22067	3.10187	0.0488496
Emid2	0.863847	7.40034	3.09874	0.00431267

gene	FPKM		log2(fold_change)	p_value
Pkig	3.85294	32.9161	3.09476	0.077653
Fdps	6.51671	55.313	3.0854	0.00517903
Mrpl22	1.98279	16.7649	3.07984	0.0129141
Ccnd1	4.41861	37.1723	3.07256	0.000321199
Hist1h4h	34.1516	285.958	3.06578	0.00175102
Hmgb3	1.90477	15.8825	3.05975	0.00342075
Hist1h2bc	11.1145	91.9067	3.04773	0.00206594
Mgmt	1.0489	8.63358	3.04108	0.0305682
Tnnc2	5.53723	45.3397	3.03354	0.00321645
Tmem98	0.648072	5.30024	3.03183	0.0262774
Dpp3	1.07833	8.80964	3.03028	0.00343722
Mybl1	0.81628	6.63999	3.02404	0.00438392
Serf1	0.916599	7.45046	3.02297	0.0770973
Mrpl18	2.91918	23.6859	3.0204	0.00501231
Nudt5	2.49416	20.2355	3.02027	0.00260948
Ccne1	0.687196	5.54932	3.01352	0.0146047
Cd69	0.666292	5.37687	3.01254	0.0192949
Pnmal2	0.685093	5.51415	3.00877	0.00365086
3110040N11Rik	0.622419	5.00896	3.00855	0.0728047
Hist1h2be	1.34318	10.7955	3.0067	0.0834289
Has2	1.09892	8.82473	3.00547	0.00242377
Cib1	1.21517	9.75438	3.00489	0.0292729
Tmem35	0.731855	5.85565	3.0002	0.0182247
Idh2	13.7866	110.157	2.99821	0.000547276
Jph2	0.960969	7.63258	2.98961	0.0046784
Tmeff1	0.819822	6.4848	2.98368	0.0181103
Hist2h2bb	42.5627	336.308	2.98212	0.00161678
Fbxo5	0.720966	5.67165	2.97577	0.0162204

gene	FPKM		log2(fold_change)	p_value
Armcx6	0.719307	5.63565	2.9699	0.0137855
Rfc5	1.00574	7.86925	2.96797	0.0102404
Mcm5	2.94399	23.0175	2.96689	0.00138911
Psmd5	3.73823	29.1274	2.96195	0.00211551
Hist1h4d	51.4587	399.938	2.95829	0.00300882
1810009A15Rik	3.82965	29.7489	2.95756	0.0113167
Terc	4.48482	34.774	2.95489	0.0335068
Mrpl14	1.27841	9.86159	2.94747	0.0534651
Mrpl40	1.23219	9.49816	2.94642	0.0180325
Adam8	1.08866	8.36119	2.94116	0.00702354
Mfap3l	0.818986	6.27498	2.9377	0.0259372
Anxa1	40.0269	306.028	2.93462	0.000628472
Esrra	1.30604	9.96623	2.93185	0.0693923
Tmsb10	85.7844	652.922	2.92812	0.00928161
Uqcr11	35.4022	268.243	2.92163	0.00133273
2900010M23Rik	11.2034	84.5361	2.91562	0.00434666
Pmf1	1.29396	9.73385	2.91122	0.0223828
Rpa1	2.60534	19.5964	2.91104	0.00244433
Cdk4	9.20746	69.1363	2.90857	0.00150971
Mcm3	2.49495	18.5756	2.89632	0.00227066
Ndufb8	13.8007	102.703	2.89567	0.00213436
Ahcy	11.4787	84.8351	2.88571	0.000510468
Slc25a24	2.52642	18.5808	2.87864	0.00213941
Mtap	2.16507	15.8766	2.87442	0.00338023
Parp1	2.34011	17.1327	2.8721	0.0023247
Cul7	1.37554	9.97924	2.85893	0.00245801
Cks1b	4.68139	33.8724	2.8551	0.00807111
Zfp238	1.99988	14.4523	2.85331	0.0161145

gene	FPKM		log2(fold_change)	p_value
Myl1	10.8991	78.5637	2.84965	0.00922713
Atpif1	12.0029	86.2479	2.8451	0.00500859
Nradd	1.38188	9.92925	2.84505	0.0200585
Med30	2.36834	17.0089	2.84434	0.0155696
9130401M01Rik	1.6213	11.6095	2.84009	0.0145027
S100a4	85.4526	611.347	2.8388	0.00110323
Mcat	0.719019	5.13592	2.83652	0.0247853
Mrpl11	1.05113	7.45409	2.82609	0.00676978
Nfu1	1.97298	13.9879	2.82573	0.0446009
Gamt	1.16742	8.2672	2.82407	0.0421083
Fam83g	0.860256	6.07953	2.82112	0.00441826
Coq9	1.62253	11.4147	2.81458	0.00852916
Spg21	3.73883	26.2219	2.81011	0.00253978
Rnaseh2a	0.866974	6.07412	2.80861	0.015719
Trp53i11	0.902372	6.29013	2.8013	0.0153552
Ass1	3.59798	25.0375	2.79883	0.00238793
Rfc2	1.44193	10.0224	2.79717	0.0158493
Tmem147	3.51928	24.3866	2.79274	0.0124894
Acads	1.23546	8.53553	2.78843	0.0145392
Slpi	1.1319	7.81891	2.78822	0.0360467
Asns	2.0593	14.1673	2.78234	0.0096898
Arl2	0.849033	5.84041	2.78218	0.0587651
Pdzd11	1.1852	8.1297	2.77807	0.0276273
Prdx2	24.5054	167.433	2.77242	0.00183671
Sdhb	10.5298	71.9439	2.7724	0.00282304
Sccpdh	2.49552	16.9869	2.76701	0.00559405
Ppp1r14b	37.7857	256.9	2.7653	0.00132898
Cox17	4.66461	31.6424	2.76203	0.0331241

gene	FPKM		log2(fold_change)	p_value
Acp1	2.91083	19.737	2.76139	0.00845341
Suclg1	3.05889	20.7316	2.76075	0.00541395
Hist1h4a	65.0302	439.608	2.75704	0.00473778
Sdhd	16.146	109.058	2.75584	0.00218289
Hist1h3f	5.03229	33.9458	2.75395	0.00966586
N6amt2	1.62048	10.9091	2.75104	0.0424629
Ufsp2	1.38107	9.29164	2.75015	0.0201867
Commd3	4.73416	31.6891	2.74281	0.00696143
Ndufv2	5.81403	38.9081	2.74246	0.00403883
Atp5c1	23.6024	157.432	2.73772	0.00434578
1810013D10Rik	1.71511	11.3731	2.72926	0.0295101
2310009B15Rik	0.87617	5.80299	2.72751	0.0770067
Mrps21	8.21687	54.3108	2.72458	0.0191469
Coq7	1.37779	9.08033	2.72039	0.0417983
Dtymk	5.55725	36.5696	2.7182	0.0646543
Tpi1	21.7296	142.981	2.71809	0.00256302
Mycbp	1.30135	8.53477	2.71334	0.0247857
D10Jhu81e	1.89548	12.4311	2.71332	0.0149865
Ormdl3	3.15125	20.6484	2.71203	0.00381428
Eci1	3.02814	19.7613	2.70617	0.0081674
Sdhc	10.801	70.4747	2.70594	0.00298625
Tubb5	25.9198	169.088	2.70565	0.00144319
Mrps5	3.29922	21.4742	2.70241	0.00600658
Pmaip1	2.42773	15.801	2.70234	0.00315509
Arhgap22	2.69561	17.5444	2.70233	0.00337646
Jub	0.793496	5.13975	2.6954	0.0127095
Ict1	2.26326	14.6568	2.69509	0.0276588
Gtf2h4	0.917052	5.93771	2.69483	0.0300046

gene	FPKM		log2(fold_change)	p_value
Ndufb3	7.79186	50.2538	2.68919	0.0125634
Tes	1.96741	12.6826	2.68848	0.0109146
Lmnb2	5.122	32.9799	2.68681	0.00197756
Tufm	4.51903	29.0483	2.68437	0.021234
Cpped1	0.802359	5.15573	2.68386	0.0203064
Mrps33	4.23073	27.0893	2.67874	0.0601441
4930455C21Rik	1.20241	7.69124	2.67729	0.0135986
Ola1	5.43569	34.7162	2.67507	0.0513103
Mrpl13	8.82534	56.2028	2.67092	0.00712413
Pgk1	46.8011	297.959	2.6705	0.0013466
Cops6	3.51246	22.2758	2.66492	0.0109017
Isyna1	1.98578	12.5678	2.66195	0.0114982
Fbxo32	1.51254	9.57161	2.66179	0.0034141
Mrpl28	4.69631	29.5796	2.655	0.00832266
Prdx3	5.98417	37.6859	2.6548	0.00632785
Gart	3.12018	19.6478	2.65467	0.0034992
Hn1l	2.89814	18.2461	2.65439	0.00563005
Fam162a	8.87064	55.8407	2.65421	0.00734923
Pgm2	1.55066	9.72614	2.64899	0.00742076
Ldhb	1.36665	8.54838	2.64501	0.031357
Ndufa9	8.12606	50.8158	2.64465	0.00470858
Hmgn2	13.7461	85.9056	2.64373	0.00285312
Xpo1	7.11437	44.3288	2.63944	0.0102184
Exosc5	1.56758	9.76151	2.63857	0.0298454
1500001M20Rik	1.16729	7.26787	2.63837	0.0349259
Cisd1	2.81148	17.5046	2.63833	0.020841
Ppic	9.62764	59.8745	2.63669	0.00452051
Ndufa4	25.7888	160.273	2.63572	0.00581385

gene	FPKM		log2(fold_change)	p_value
Clpp	2.12168	13.1799	2.63505	0.018566
Ndufs8	4.64097	28.8277	2.63496	0.0116405
Uqcr10	39.9593	248.111	2.63438	0.00404865
Fen1	1.91137	11.8155	2.628	0.00847324
Prkcsh	3.62889	22.2962	2.6192	0.00455956
Atp5o	25.4937	156.545	2.61836	0.00360761
Bin1	10.6369	65.2456	2.61681	0.0106622
Zfand1	1.10683	6.7864	2.61622	0.0290421
Kcnq4	1.17018	7.16997	2.61523	0.0133918
Ndufb4	12.9872	79.5673	2.61508	0.00835863
Popdc3	3.44945	21.133	2.61506	0.0061527
Acta2	18.0666	110.625	2.61429	0.00613518
Ap2s1	4.27457	26.148	2.61285	0.0156817
Plk2	54.6685	334.188	2.61188	0.00215768
Ano8	1.25848	7.68352	2.61009	0.0788439
Aldh3b1	0.932016	5.68321	2.60828	0.0317848
Commd9	0.976503	5.94763	2.60662	0.0476976
Nans	2.66745	16.1972	2.60221	0.00880916
Lsm7	11.8436	71.7512	2.5989	0.0116042
Plxna1	1.91468	11.5942	2.59822	0.00354462
Med11	1.4766	8.93579	2.59732	0.0356564
Samm50	5.39604	32.644	2.59684	0.00644374
Ndufc2	10.1669	61.4578	2.59571	0.0102093
Polr2g	4.08377	24.6697	2.59477	0.0132015
Lsm5	4.31636	26.0553	2.59369	0.0325903
Ifngr2	1.47917	8.90735	2.59021	0.0165405
Tmem70	3.13447	18.8733	2.59005	0.00927694
Fam125a	2.43664	14.6546	2.58839	0.0182286

gene	FPKM		log2(fold_change)	p_value
Mrpl39	1.52007	9.13865	2.58785	0.016912
Htra2	2.2472	13.4737	2.58395	0.0653898
Ndufc1	9.0917	54.4323	2.58184	0.0313794
Mrps35	1.90495	11.3434	2.57403	0.0374113
Tnni2	7.04029	41.9069	2.57348	0.0108808
Dmpk	5.6556	33.6558	2.5731	0.0408264
Igfbp3	3.45477	20.5294	2.57103	0.00807963
Urod	3.79241	22.5087	2.5693	0.00924171
Uqcrc1	10.6345	63.0488	2.56772	0.00377492
Cmtm7	1.86456	11.0417	2.56606	0.0537777
Adh5	6.5042	38.4865	2.56491	0.00508006
Mrpl27	2.97184	17.5521	2.56222	0.0285934
Mpi	1.04057	6.1446	2.56195	0.0240756
Frmd8	1.74735	10.3113	2.56099	0.0107853
Zfp637	1.10529	6.51629	2.55962	0.04284
Rcc1	3.11814	18.3605	2.55784	0.0194489
Pgam2	1.13854	6.69808	2.55656	0.0556714
Gpx7	1.26741	7.44859	2.55508	0.0392576
Fbxw9	1.03618	6.08539	2.55408	0.030329
Ndufab1	2.77407	16.2646	2.55166	0.0288424
Ociad2	1.2849	7.53238	2.55145	0.0214852
B3gnt5	1.21868	7.13655	2.5499	0.0546907
Phb	10.9286	63.9538	2.54892	0.00379803
Park7	11.2452	65.7978	2.54872	0.0050108
Myg1	1.1671	6.823	2.54748	0.0320455
Rars2	1.01505	5.9331	2.54724	0.0329538
Etfb	5.56315	32.5117	2.54698	0.0122427
Nln	1.95638	11.4304	2.54662	0.0054764

gene	FPKM		log2(fold_change)	p_value
Phlda3	6.82296	39.843	2.54586	0.00677625
Dap	1.45607	8.48605	2.54301	0.020197
Stoml2	4.77482	27.8251	2.54287	0.00680528
Apeh	0.874591	5.09218	2.5416	0.0197262
Psmb3	23.3022	135.392	2.53861	0.00459157
Mrpl33	21.9194	127.228	2.53714	0.00659561
Asnsd1	2.39622	13.9015	2.53641	0.00936196
Nnt	1.23541	7.16702	2.53639	0.02521
Usp5	4.65152	26.9712	2.53564	0.00413074
Rab31	4.10151	23.776	2.53528	0.00602771
Rsad2	4.06253	23.5438	2.5349	0.00832752
Aarsd1	1.74288	10.0982	2.53455	0.0234025
AI462493	1.1022	6.38239	2.53371	0.0607689
Vdac1	15.26	88.1224	2.52975	0.00382331
Psat1	15.7297	90.8263	2.52962	0.0160897
Ndufa8	2.83485	16.3644	2.52921	0.0301162
Ifi27l2a	4.76147	27.4727	2.52852	0.0468776
Vim	214.735	1238.47	2.52793	0.00482379
Ndufs5	7.74215	44.6323	2.52728	0.031299
Dbf4	1.19286	6.86588	2.52502	0.0167149
Lsm4	5.26897	30.268	2.5222	0.0121831
Rnf187	4.83263	27.719	2.52	0.00642599
Tusc3	3.18331	18.244	2.51882	0.00928254
Cetn2	2.10595	12.0604	2.51773	0.0253279
Smc4	5.77547	33.0678	2.51742	0.00442726
Clybl	1.16628	6.66897	2.51555	0.0649606
Atpaf2	1.02567	5.86092	2.51456	0.0355284
Casp3	5.64539	32.1899	2.51146	0.0073858

gene	FPKM		log2(fold_change)	p_value
Mrpl53	4.7579	27.1256	2.51126	0.0548335
Hist2h3c2	2.17322	12.3897	2.51123	0.0479978
Xrcc5	2.40122	13.6885	2.51112	0.00676195
Pkia	2.80474	15.9496	2.50759	0.00588565
Rps27l	70.7523	401.524	2.50464	0.00420758
Cpsf3	1.64319	9.32378	2.50442	0.0106542
Ptcd2	1.76635	10.0088	2.50242	0.0169824
Lars2	34.6654	196.367	2.50199	0.00242359
Gpt2	0.94176	5.32566	2.49953	0.0147476
Topbp1	2.70598	15.2902	2.49839	0.00551949
Bid	0.967529	5.46626	2.49818	0.037816
Prdx5	11.4459	64.5909	2.4965	0.00609618
Atp5g3	43.4211	244.676	2.4944	0.00439085
Lrwd1	1.85605	10.4551	2.4939	0.0123509
Dcakd	1.23269	6.94015	2.49316	0.0308714
Gipc1	1.22327	6.87353	2.4903	0.0312052
Ndufb7	9.46544	53.1779	2.49008	0.0181536
Fh1	6.03729	33.8915	2.48895	0.00741187
Trappc1	1.57991	8.86531	2.48833	0.0769083
Chchd1	10.5583	59.231	2.48798	0.0138833
Cinp	1.70708	9.57572	2.48785	0.0378266
Ruvbl2	6.50131	36.4537	2.48726	0.00543583
Ptk7	1.73569	9.7317	2.48718	0.00670031
Hibch	1.42985	8.0157	2.48697	0.0252131
Cox6b1	58.9343	329.789	2.48436	0.00507975
Xrcc1	1.03528	5.79244	2.48416	0.0248435
Atp5j2	32.7863	183.44	2.48414	0.00673682
Prmt7	3.08654	17.2689	2.48412	0.00755246

gene	FPKM		log2(fold_change)	p_value
Calm3	9.65793	53.9576	2.48204	0.0056173
Metrn	0.974552	5.44444	2.48197	0.0514142
Mrpl47	2.89992	16.197	2.48164	0.0287604
2010107E04Rik	84.8631	473.734	2.48087	0.00454226
Lmo7	0.906044	5.05675	2.48056	0.0132938
Pfn1	43.2448	241.292	2.48018	0.00511232
Dscr3	1.89391	10.567	2.48013	0.0105518
Ccdc56	3.60278	20.0903	2.47932	0.0303262
Myh1	1.35071	7.52884	2.47871	0.00995452
Cap2	2.21994	12.3152	2.47185	0.00959334
Ndufa5	4.51242	24.9152	2.46505	0.0359941
Psmd13	8.44441	46.5715	2.46338	0.0054453
Adprh	1.79603	9.89389	2.46173	0.023434
Bnip1	1.44381	7.94201	2.45963	0.0508476
Mfn2	2.26258	12.4448	2.4595	0.00621337
3110003A17Rik	8.65905	47.5702	2.45778	0.0126051
Layn	1.25905	6.9082	2.45597	0.0292791
Pdgfa	2.84508	15.6008	2.45508	0.0275262
Ncapg2	1.57605	8.63396	2.45371	0.00642435
Fhl2	1.371	7.50734	2.45307	0.0348748
Ttc13	1.09649	6.00131	2.45239	0.0182033
Psmb5	13.8487	75.7482	2.45146	0.00991047
Prelid1	5.10478	27.9009	2.45039	0.0154503
Vars	3.21125	17.5508	2.45033	0.00604327
Mrps18c	6.18212	33.7874	2.45031	0.0389498
Ndufa12	17.664	96.4865	2.44951	0.00964631
Cox7b	22.6147	123.23	2.44602	0.00518664
Inppl1	3.72944	20.2518	2.44102	0.0491127

gene	FPKM		log2(fold_change)	p_value
Decr1	1.82469	9.9017	2.44003	0.0107773
Tomm22	16.1873	87.7427	2.43842	0.00749307
Rpa2	1.69499	9.15626	2.43348	0.0239906
2310030N02Rik	1.44605	7.80174	2.43168	0.0510104
Dynlt1a	1.8617	10.0418	2.43132	0.0610042
Slc25a11	2.88966	15.551	2.42804	0.013295
Tnc	8.78433	47.1899	2.42547	0.00360709
Psmc3	24.0191	129.026	2.4254	0.00408112
Glipr2	3.4226	18.3838	2.42527	0.0120392
Gpc1	16.7136	89.7537	2.42495	0.0136753
Snrpd2	44.1727	237.152	2.42458	0.00685154
Sdf2l1	2.26065	12.126	2.42329	0.0331843
Iffo1	2.79991	15.017	2.42314	0.0604756
1110004E09Rik	1.01859	5.45848	2.42193	0.0582695
Slc25a4	57.1236	305.558	2.41929	0.00399249
2610034B18Rik	1.20291	6.4337	2.41912	0.0265936
Ankrd32	1.06614	5.69871	2.41823	0.0149122
Cacybp	8.86487	47.3422	2.41695	0.00701859
Psma4	22.9432	122.413	2.41562	0.00803688
S100a6	76.7199	409.264	2.41536	0.0057917
Ndufa10	7.79307	41.5577	2.41485	0.00771548
Pepd	6.22672	33.1018	2.41037	0.00721299
Lzic	3.6957	19.6322	2.40931	0.0122289
Rpap3	1.1059	5.86803	2.40766	0.0280649
Mdh1	7.97933	42.2833	2.40575	0.00832929
Tmem209	0.938024	4.96751	2.40483	0.025287
Polr3g	0.980942	5.19417	2.40465	0.022674
Mrpl38	2.31325	12.2258	2.40194	0.032151

gene	FPKM		log2(fold_change)	p_value
Slc38a4	1.48684	7.85663	2.40166	0.0110967
Psmg3	1.3827	7.29959	2.40032	0.0691977
Ifit3	2.60013	13.7185	2.39947	0.0211123
Bnip3	2.69086	14.1961	2.39936	0.0180447
Ndufs7	6.96019	36.7134	2.39911	0.0191511
Ndufs6	6.48909	34.2111	2.39837	0.072992
Mex3b	1.2083	6.36926	2.39815	0.0164426
Cbx3	10.9803	57.7246	2.39427	0.00596273
Usp18	1.04344	5.48315	2.39366	0.0512774
Shmt2	4.38021	23.0143	2.39346	0.0471418
Chchd3	11.0933	58.2854	2.39344	0.0072387
Uqcrc2	14.7059	77.2634	2.39339	0.00873767
Phb2	13.3841	70.2724	2.39244	0.00645355
Deb1	3.57556	18.7318	2.38924	0.0544558
Cox5b	47.0313	245.874	2.38623	0.00716804
Lyrm2	1.08814	5.68003	2.38404	0.0590361
Ppip5k2	1.23111	6.42107	2.38285	0.0103695
Mrpl45	1.42332	7.41527	2.38124	0.0220947
Ndufb6	26.5877	137.746	2.37318	0.00976671
3200002M19Rik	1.62846	8.42781	2.37165	0.0564414
Sec11c	5.28766	27.3388	2.37025	0.0193494
Idh3a	4.47044	23.1102	2.37004	0.00891096
Dbi	18.5729	95.9471	2.36904	0.0406035
Ndufb9	22.1362	114.353	2.36902	0.010026
Prkaca	2.87219	14.8317	2.36846	0.0123733
Nudt22	1.3216	6.81436	2.3663	0.0773917
Ppap2c	1.70267	8.77035	2.36483	0.0256111
Timm50	3.87994	19.9793	2.3644	0.0214249

gene	FPKM		log2(fold_change)	p_value
Tipin	3.73416	19.212	2.36315	0.019792
Gfm1	3.35117	17.2339	2.36251	0.0133497
Psma7	22.155	113.9	2.36206	0.00839072
Asna1	3.15528	16.2185	2.3618	0.0219144
Ndufs1	11.0345	56.6695	2.36054	0.0363311
Fam136a	2.95759	15.1889	2.36052	0.0148829
Tmem160	2.40755	12.3625	2.36033	0.0535449
Cox5a	21.0428	107.991	2.35952	0.00969392
Mrpl10	1.51828	7.78406	2.35808	0.0317777
Hspa14	4.95317	25.383	2.35744	0.00923488
Creld1	1.52251	7.79475	2.35605	0.0242009
Mlf2	8.12076	41.5416	2.35487	0.0418443
Ndufb5	11.5703	59.1657	2.35433	0.0127352
Zfyve21	1.49066	7.61812	2.35348	0.0390453
Naa10	6.09365	31.0964	2.35137	0.0428228
Stbd1	1.89398	9.66408	2.35121	0.0173089
Sae1	4.65478	23.7046	2.34838	0.0130719
Mat2b	2.54203	12.9337	2.34708	0.0579036
Sap30	5.26046	26.7584	2.34673	0.0141395
Ndufs4	4.00749	20.3824	2.34655	0.0165617
Gnpat	1.93713	9.84429	2.34537	0.0131567
Psmb10	2.40022	12.1958	2.34515	0.0276827
Avpi1	1.59604	8.10058	2.34353	0.0621137
Abcb8	0.985436	4.98793	2.33961	0.0308902
Mapk6	12.1365	61.3578	2.33789	0.0218146
Vasp	5.19369	26.2521	2.3376	0.0144818
Fam49b	1.92548	9.73099	2.33737	0.0121034
Dlat	3.31738	16.7646	2.33731	0.00850844

gene	FPKM		log2(fold_change)	p_value
2400001E08Rik	1.54479	7.78535	2.33335	0.0627144
Pts	1.50736	7.59442	2.33291	0.0688842
Atad2	2.1769	10.9628	2.33227	0.00714785
Gcsh	6.39815	32.1927	2.33101	0.0104961
Mrpl21	4.25105	21.3833	2.33059	0.0211724
Ptpla	8.69054	43.6784	2.3294	0.056747
Tmx2	2.86803	14.3971	2.32765	0.0156388
Mrpl3	6.34436	31.8025	2.3256	0.015209
Gnb4	2.10462	10.5313	2.32305	0.0178784
S1pr2	1.27509	6.37586	2.32202	0.0285087
Tspan6	3.21904	16.0799	2.32056	0.0245915
Cnpy2	3.14567	15.6793	2.31743	0.0363416
Hmbs	1.00349	4.99901	2.31662	0.0787719
Atp6v0a2	2.22276	11.0597	2.31489	0.0186609
Wdr1	17.5484	87.3131	2.31486	0.00652637
Ndufs3	7.67493	38.1716	2.31427	0.0172211
Anxa2	89.6448	445.171	2.31207	0.0116863
Cmas	2.187	10.8541	2.31122	0.0265422
Tbca	36.5723	181.487	2.31105	0.00852655
Hist2h2aa1	27.8692	138.188	2.30989	0.0370329
1110059E24Rik	2.29453	11.3631	2.30808	0.0314597
Ash2l	2.85661	14.1091	2.30425	0.0169789
Ubac1	1.20141	5.9246	2.30199	0.0183963
Vdac3	16.7211	82.4536	2.30191	0.029373
Bckdk	1.07178	5.27108	2.29809	0.0367065
Snrpe	55.9957	275.085	2.29649	0.00939246
Mlec	4.31456	21.1747	2.29505	0.0083823
Itpa	8.03137	39.4143	2.295	0.013255

gene	FPKM		log2(fold_change)	p_value
Cox7c	77.1195	377.893	2.29281	0.0080167
Nme1	24.0069	117.214	2.28763	0.0069689
Mrpl51	4.06831	19.854	2.28693	0.0181562
Atox1	12.5475	61.0254	2.28201	0.0370334
Mpdu1	2.0542	9.98836	2.28167	0.0432648
Cops7a	3.18702	15.4949	2.28151	0.0676157
Chmp6	1.8752	9.11194	2.28072	0.0302103
Atp5g1	17.0904	82.9926	2.27979	0.0569471
Nup133	2.01637	9.78014	2.2781	0.009832
Hist1h4c	112.814	546.943	2.27744	0.0155155
Ssna1	2.88393	13.9517	2.27433	0.0494939
Atp5f1	26.7869	129.264	2.27072	0.0589843
Mcm7	6.9556	33.5474	2.26995	0.0136152
Rala	2.00372	9.64286	2.26678	0.0222295
Hspb8	15.8291	76.0927	2.26518	0.00836654
Pvrl2	2.6887	12.917	2.2643	0.046508
Ccdc104	1.91718	9.19713	2.2622	0.0285092
Plin3	3.77832	18.0948	2.25976	0.0132183
Dll1	3.13445	15.0066	2.25932	0.0165271
Cyc1	11.1789	53.5191	2.25928	0.0149345
Tmem63b	1.33953	6.41267	2.2592	0.0201461
Tbcd	2.81659	13.4825	2.25907	0.0255387
Dnmt1	3.09621	14.8007	2.25709	0.0421779
Mtx2	3.28758	15.7094	2.25653	0.0335635
Dnpep	2.73045	13.0434	2.25611	0.0376731
Efha1	3.00305	14.345	2.25605	0.0190442
Cmpk2	1.34184	6.4058	2.25516	0.0278174
Clic1	25.6297	122.294	2.25446	0.00970006

gene	FPKM		log2(fold_change)	p_value
Lias	1.31211	6.25694	2.25357	0.0455409
Tomm5	18.8372	89.8064	2.25323	0.0506988
Prpf31	2.43624	11.6138	2.25311	0.0547039
Ankrd1	13.0208	62.0266	2.25207	0.00859573
Crip2	8.48826	40.4339	2.25202	0.0149443
Anapc4	3.84936	18.3338	2.25182	0.0133058
Setd8	3.31395	15.7784	2.25133	0.0194114
Tmem38a	2.01789	9.60106	2.25035	0.0253052
Psmc1	13.4496	63.925	2.24882	0.0110734
Polr2e	6.18854	29.4046	2.24837	0.0211194
Fbxl19	1.04614	4.96962	2.24806	0.0283601
Snrnp27	3.57504	16.9692	2.24689	0.0409478
H1f0	1.70315	8.07711	2.24563	0.0326096
Ndufaf2	2.38593	11.3068	2.24456	0.0682632
Atp5g2	29.8823	141.422	2.24265	0.0145032
March8	3.32018	15.705	2.24189	0.0120623
Cdc123	3.41193	16.1282	2.24093	0.0216967
Vamp8	3.97986	18.8009	2.24001	0.0403227
Sox11	1.47082	6.94279	2.23889	0.0128834
Mrpl36	2.66441	12.5663	2.23766	0.0582679
Nedd8	12.733	59.9996	2.23639	0.0177565
Mrpl9	8.08195	38.0769	2.23614	0.0137008
Taldo1	16.0276	75.5085	2.23608	0.0108119
Bod1	6.59	31.0418	2.23586	0.0162726
5730437N04Rik	6.42561	30.203	2.23279	0.020246
Uqcrfs1	13.9384	65.5065	2.23257	0.0128744
Pebp1	34.5223	162.089	2.23118	0.00843761
Itga7	35.4656	166.511	2.23112	0.0121212

gene	FPKM		log2(fold_change)	p_value
Dnajc2	3.19625	14.9862	2.22918	0.0132916
Mrps27	1.86295	8.72895	2.22822	0.0481874
Zfp367	3.46121	16.2144	2.22793	0.0102234
Arl6ip1	7.0157	32.856	2.2275	0.0133861
Aifm1	1.16239	5.44065	2.22668	0.037949
Nit2	1.79867	8.40911	2.22503	0.0476405
Atic	5.54284	25.9092	2.22477	0.0130955
2810004N23Rik	2.72521	12.7348	2.22434	0.0278652
Taf12	1.9887	9.28758	2.22348	0.0543414
Pfdn1	5.81574	27.1499	2.22291	0.0210851
Trappc2l	3.0921	14.4233	2.22174	0.0718674
Prmt5	1.98112	9.22427	2.21912	0.0205911
Fam111a	2.13271	9.92061	2.21774	0.0195029
Ccdc134	3.44177	16.0066	2.21745	0.0159728
Vdac2	20.7207	96.305	2.21654	0.011736
Nono	19.7148	91.6077	2.21619	0.0243929
Fzr1	1.18955	5.52409	2.21532	0.039204
Mre11a	1.34885	6.26101	2.21466	0.0265973
Dhrs1	2.2443	10.4164	2.21452	0.0390195
Cox7a2	38.8248	179.941	2.21247	0.0107292
Myzap	1.32905	6.15819	2.21211	0.0398943
Smarcc1	1.98565	9.18938	2.21035	0.0123241
Psmb2	15.6259	72.3024	2.2101	0.0196889
Exosc9	5.32826	24.6431	2.20945	0.0432177
Nipsnap3b	1.82728	8.44627	2.20862	0.048784
Il33	7.83594	36.2069	2.20808	0.0592863
Atp2a1	4.39552	20.3068	2.20786	0.0299324
Bst2	8.41589	38.8341	2.20614	0.0202668

gene	FPKM		log2(fold_change)	p_value
Hmgb1	39.5937	182.536	2.20484	0.00732762
Cpsf3l	1.94288	8.95564	2.2046	0.0625531
Fkbp4	13.1049	60.4	2.20445	0.00967832
Polr2f	8.51876	39.2244	2.20303	0.0424886
Cops5	6.28979	28.9554	2.20275	0.0179292
Pycr2	4.51294	20.775	2.20271	0.0171067
Lap3	5.81449	26.7631	2.20252	0.0159745
2810405K02Rik	2.69824	12.4013	2.2004	0.0693638
Gins4	1.67622	7.69072	2.19791	0.0536535
Tmem14c	6.01911	27.6091	2.19752	0.0223595
Polr2i	3.08796	14.1421	2.19527	0.0683858
Timm13	4.57269	20.9196	2.19374	0.030617
Ppa2	1.7624	8.06126	2.19346	0.0619436
Bax	10.1894	46.5523	2.19178	0.0213076
Tceal8	3.80299	17.373	2.19165	0.0500367
Acadl	4.94377	22.5589	2.19001	0.018281
Alg5	1.66498	7.59591	2.18972	0.0465145
Tsta3	1.75515	8.00661	2.1896	0.0465645
Snap47	1.831	8.35208	2.1895	0.0331034
Col18a1	4.80413	21.9136	2.18948	0.0842557
Mrpl37	1.49583	6.81942	2.1887	0.0611183
Ppp1ca	26.47	120.55	2.1872	0.0167651
Got1	2.99766	13.6313	2.18501	0.0294386
Slc35a1	2.02406	9.20266	2.1848	0.0316693
Mdh2	21.6036	98.1796	2.18415	0.0122389
Ttc33	2.12881	9.67155	2.1837	0.0310839
Cdk5rap3	1.42067	6.45397	2.18362	0.0376709
Parl	3.61916	16.4369	2.18321	0.0248935

gene	FPKM		log2(fold_change)	p_value
Ints4	1.91807	8.70732	2.18257	0.0228018
Gfod1	2.81368	12.7649	2.18165	0.0134448
Ccdc8	1.10238	5.00067	2.18149	0.0406064
Hist2h2ac	22.0473	99.9454	2.18054	0.0342955
Elof1	3.87324	17.5551	2.18028	0.0334311
Myeov2	19.5656	88.5714	2.17852	0.0582137
Ndufb10	13.1347	59.4119	2.17736	0.020052
Immt	6.23689	28.205	2.17705	0.0668266
Atp5e	79.7158	360.495	2.17704	0.0116875
Psmg1	3.36238	15.1966	2.1762	0.0365003
Cks2	8.77196	39.6416	2.17605	0.025857
Psmd6	16.3531	73.8261	2.17457	0.0138394
Naa38	4.60002	20.7658	2.1745	0.0452354
Uba3	11.0446	49.8469	2.17416	0.0460641
Cyld	2.07861	9.37942	2.17388	0.0760655
Ostc	8.14916	36.767	2.17369	0.0220255
Ppa1	14.7997	66.7414	2.17301	0.012684
Ndufa7	19.2436	86.7283	2.17212	0.0225473
Qdpr	1.3733	6.18608	2.17138	0.0558031
Apoa1bp	4.96312	22.3347	2.16997	0.0364552
Pgls	4.57636	20.5925	2.16984	0.0454154
Foxred1	2.46354	11.0741	2.16839	0.0187405
Spc24	3.06852	13.7933	2.16835	0.0246364
Eif2b5	6.7319	30.1788	2.16445	0.0137287
2310016M24Rik	4.60266	20.6125	2.16298	0.0520383
Ppia	421.189	1883.54	2.16091	0.0102246
Ssu72	4.01914	17.9689	2.16054	0.0235571
Hist2h4	15.7852	70.5393	2.15986	0.0626319

gene	FPKM		log2(fold_change)	p_value
6330578E17Rik	1.77391	7.9131	2.15731	0.024179
Gtf2h2	1.46666	6.52897	2.15432	0.0453213
Cdc26	3.32639	14.7937	2.15295	0.0540202
Tmem132a	2.38406	10.6007	2.15267	0.0249269
Afg3l1	1.16944	5.19928	2.15249	0.0805996
Cars2	1.13545	5.03028	2.14737	0.0597979
Mrpl44	1.74906	7.74261	2.14624	0.0551484
Mustn1	2.04932	9.06932	2.14585	0.0648217
Commd1	10.3967	45.9776	2.1448	0.0639147
Prim2	1.94639	8.60752	2.14479	0.0364799
Dgkz	2.22822	9.85173	2.14448	0.0643848
Slc44a2	3.45645	15.2748	2.14379	0.0398007
Nup93	3.22256	14.2405	2.14372	0.0170013
Prep	4.27117	18.8658	2.14307	0.019856
Polr2k	11.4815	50.6964	2.14257	0.0607946
Psmb1	32.9609	145.538	2.14257	0.010874
Iqsec3	1.97756	8.71759	2.14021	0.0165314
Cog4	2.8174	12.403	2.13825	0.0196465
AI314976	1.52097	6.69245	2.13754	0.0667552
Exoc7	1.46071	6.42545	2.13713	0.0534254
Ublcp1	2.63554	11.5855	2.13615	0.026975
Ric8	3.0436	13.3524	2.13325	0.030623
Aimp1	7.30475	32.0204	2.13208	0.0228961
Cstf2	2.70492	11.8402	2.13004	0.0253991
Abhd8	1.38153	6.0304	2.12598	0.0496794
Suds3	4.40149	19.2037	2.12532	0.050484
Rpp30	2.8432	12.3919	2.12381	0.0474875
Trim59	2.16232	9.41435	2.12228	0.021891

gene	FPKM		log2(fold_change)	p_value
Rcn1	6.93806	30.2057	2.12222	0.0152107
Pomp	21.2409	92.4582	2.12196	0.0194203
Cnn2	2.87584	12.5143	2.12153	0.0374232
0610037P05Rik	3.26532	14.1986	2.12045	0.0389912
Psmd14	14.6692	63.7305	2.11919	0.0138016
H2afj	2.17157	9.42359	2.11754	0.0391565
Psma5	23.307	101.02	2.1158	0.0129325
Got2	6.66198	28.8485	2.11447	0.0212769
Tsc22d1	12.061	52.2155	2.11413	0.0519005
Rab1b	6.23002	26.9686	2.11397	0.0249934
Acat1	4.5574	19.727	2.11389	0.0157703
Thop1	4.46625	19.3228	2.11317	0.02056
Ubr7	1.96641	8.50704	2.1131	0.026139
Coro1c	5.62478	24.3316	2.11296	0.0183737
Prkag1	4.88335	21.1238	2.11293	0.0271953
Stambpl1	1.50917	6.52806	2.1129	0.0438251
Sfxn1	1.49534	6.45698	2.11039	0.0338328
Pkm2	131.407	567.266	2.10998	0.0110944
Ino80c	2.08279	8.97899	2.10804	0.0364011
Nae1	4.24419	18.2901	2.1075	0.0280328
4930503L19Rik	1.31233	5.65441	2.10725	0.0523444
Atp6v1c1	3.85755	16.6187	2.10705	0.0298769
Mrps11	2.18407	9.40871	2.10698	0.0711246
Fitm1	2.39912	10.3274	2.1059	0.0782815
Ywhah	7.79244	33.4405	2.10145	0.0237238
Atp5a1	81.6715	350.418	2.10117	0.0113529
Idh1	3.28772	14.1018	2.10071	0.0819549
Ndufs2	20.4728	87.8104	2.10069	0.0155833

gene	FPKM		log2(fold_change)	p_value
Cs	11.2988	48.4048	2.09898	0.0145637
Olfml2b	12.0383	51.5336	2.09788	0.0129886
Polr2j	9.05317	38.7244	2.09675	0.0384325
Clns1a	2.21882	9.48067	2.09519	0.0250517
Psma6	22.8882	97.7881	2.09506	0.0178766
Edf1	11.5364	49.2648	2.09436	0.0321384
Sesn3	2.04728	8.74201	2.09426	0.0334709
Xrcc6	1.91585	8.17079	2.09249	0.0357749
Mrps24	3.7853	16.1098	2.08946	0.0441471
Plekho1	1.60027	6.80648	2.08859	0.0803215
Exosc4	1.78208	7.57855	2.08836	0.0446844
Tssc1	1.55403	6.60366	2.08726	0.0555556
Poldip2	4.94137	20.9797	2.08601	0.0256769
Pgam1	21.8802	92.8809	2.08575	0.0132425
Pdia4	15.4557	65.5361	2.08415	0.0176883
Elp2	3.72826	15.7739	2.08097	0.0227772
Mif	32.1395	135.928	2.08042	0.0251438
Traf3ip3	1.27456	5.38919	2.08007	0.0752786
Ammecr1	1.20692	5.1008	2.07939	0.0454845
1110002B05Rik	5.60369	23.6458	2.07714	0.0302021
Tmem199	2.29663	9.69077	2.07709	0.0477981
Prpf19	4.54875	19.1898	2.0768	0.0776143
Ccdc72	16.9511	71.5087	2.07674	0.0235969
Med21	7.04011	29.6334	2.07356	0.0364509
Hadh	2.63042	11.0703	2.07332	0.031292
Ap1b1	2.19633	9.24111	2.07297	0.0706386
C1d	2.0338	8.54813	2.07143	0.0306263
Txndc15	2.48281	10.4311	2.07085	0.0454953

gene	FPKM		log2(fold_change)	p_value
Mtch2	7.13812	29.977	2.07024	0.0244968
Scd2	5.67748	23.8027	2.0678	0.0206144
Ahsa1	21.0018	88.0411	2.06766	0.0167624
Nup43	1.78336	7.47354	2.0672	0.0727777
1810006K21Rik	14.8539	62.2001	2.06607	0.0759236
Sf3b5	5.75508	24.0815	2.06502	0.05339
Il13ra1	1.70626	7.13523	2.06412	0.0355183
Ppib	43.5194	181.909	2.06349	0.0426019
Tsen15	2.26794	9.47678	2.06301	0.064412
Ckb	8.38623	35.0178	2.06199	0.0275515
Sft2d2	1.67182	6.98057	2.06193	0.0232308
2810474O19Rik	5.12524	21.3854	2.06093	0.013389
Larp7	7.01877	29.145	2.05395	0.0244938
Paics	19.7448	81.9839	2.05387	0.0426938
Cad	2.34016	9.70114	2.05155	0.0197299
Npm3	15.1954	62.9649	2.05092	0.0236262
Serpinh1	79.3591	328.203	2.04812	0.0305215
Pmpcb	14.9461	61.7897	2.04759	0.0172757
Commd8	1.57394	6.50599	2.04739	0.032543
Spg7	2.8785	11.895	2.04697	0.0265695
Ddx1	13.2988	54.927	2.04622	0.0153345
Psmb6	33.4566	138.031	2.04463	0.0176963
Lrpprc	5.50567	22.6956	2.04343	0.0178768
Ei24	2.66202	10.961	2.04179	0.0795095
Traf4	1.73238	7.12695	2.04053	0.0356303
Mrps22	3.67222	15.0995	2.03977	0.0449608
Pdcd5	8.9898	36.8625	2.03579	0.0455262
Pole3	4.25896	17.4377	2.03364	0.0783235

gene	FPKM		log2(fold_change)	p_value
Atp6v1e1	8.13399	33.2207	2.03005	0.0327898
Pop4	6.21974	25.3778	2.02864	0.030523
Rtn2	9.06006	36.9602	2.02838	0.0855513
Eif4ebp1	10.2523	41.8039	2.02768	0.0313278
Vps36	5.13257	20.9213	2.02722	0.03168
Ncoa7	3.80846	15.5227	2.0271	0.0594533
Rapsn	5.51555	22.4743	2.0267	0.0309586
Mrpl54	8.92394	36.3557	2.02643	0.0490171
Pycrl	2.50286	10.189	2.02536	0.0530109
Mfsd11	1.61768	6.5823	2.02467	0.0419593
Kifap3	1.3067	5.31659	2.02458	0.0327427
Fech	1.68998	6.86836	2.02296	0.0397171
Leprot	4.10523	16.6825	2.0228	0.0358369
Cog6	1.4389	5.846	2.02248	0.0501074
Cdk2ap1	13.5323	54.9145	2.02078	0.0233438
Aco2	18.3301	74.3606	2.02032	0.0238699
Isca2	2.28878	9.27875	2.01935	0.0824718
Khdrbs3	3.47796	14.0958	2.01895	0.0359199
Nudt21	14.4232	58.3905	2.01734	0.0264913
Stard7	7.12129	28.8226	2.01699	0.019754
Pld3	1.94477	7.86624	2.01608	0.0462395
Mipep	1.51209	6.1148	2.01576	0.0798602
Ccdc12	4.35944	17.629	2.01574	0.0466375
Adsl	5.35176	21.6058	2.01333	0.0253845
Rbfa	1.5647	6.30859	2.01143	0.0770641
Psma2	33.4715	134.861	2.01047	0.0189148
Swi5	24.1017	97.0983	2.01031	0.0211282
Maz	2.89144	11.6399	2.00922	0.0364552

gene	FPKM		log2(fold_change)	p_value
Cd83	2.27188	9.13687	2.00781	0.0348761
Stard3nl	2.26265	9.09728	2.00742	0.0827412
Mrps28	7.88982	31.7136	2.00704	0.0415904
BC003965	2.06635	8.30477	2.00686	0.040174
Krcc1	2.64446	10.6182	2.0055	0.0384308
Mrpl20	13.3267	53.506	2.00538	0.0330346
Ttc9c	2.02004	8.1074	2.00485	0.0318204
Gga2	1.27356	5.11034	2.00455	0.0343175
Fbxl6	1.51054	6.05874	2.00395	0.0780474
Isoc1	2.19961	8.81487	2.00269	0.0422024
5430437P03Rik	2.32643	9.32204	2.00253	0.0477616
Hint2	5.51041	22.0662	2.00161	0.0790645
Dnaja3	3.26623	13.0726	2.00085	0.0804597
Actn1	4.3106	17.246	2.0003	0.024846
Ankrd10	17.9497	71.7932	1.99989	0.0614615
Cox8a	42.7339	170.887	1.99959	0.0282898
Rp9	3.53385	14.1287	1.99931	0.0445406
Mrps31	2.01487	8.05352	1.99893	0.0580432
Ppie	5.27312	21.0743	1.99875	0.0370228
Bloc1s2	3.0401	12.1261	1.99592	0.0619456
Alkbh3	2.26594	9.03709	1.99575	0.0719086
Snrpg	65.9579	262.966	1.99526	0.0292972
Arpc5l	3.40297	13.5671	1.99525	0.047297
Glrx5	5.68695	22.6688	1.99498	0.0469276
Tuba1b	57.9886	231.041	1.99431	0.01603
Kdelc1	1.43959	5.73392	1.99386	0.0550283
Me1	1.98414	7.90226	1.99375	0.0787404
Tspo	22.6744	90.2642	1.99309	0.0262139

gene	FPKM		log2(fold_change)	p_value
Cd320	1.29165	5.13869	1.99219	0.0726578
Pop5	3.00561	11.9542	1.99179	0.0811028
Naa20	8.50461	33.8201	1.99156	0.084593
Psma1	19.0929	75.8942	1.99095	0.021742
Fam60a	3.45185	13.7194	1.99077	0.0288984
Ssrp1	11.6735	46.3782	1.99021	0.049988
Sc4mol	6.60402	26.2214	1.98933	0.0340125
Tomm7	14.4321	57.2482	1.98795	0.0282363
Atp5b	161.547	639.993	1.9861	0.0326041
Ptges2	2.01538	7.97966	1.98528	0.0551061
Sgcb	2.25039	8.88597	1.98135	0.0294194
St13	16.2301	64.0769	1.98114	0.0241345
Mrpl12	6.13649	24.2198	1.9807	0.0399968
Gm13253	5.15202	20.3317	1.98052	0.0595096
Acaa2	5.19071	20.4701	1.97951	0.0343733
Cnot8	3.56861	14.062	1.97836	0.0397652
Nxn	3.32536	13.1014	1.97814	0.0334449
Dhrsx	2.47822	9.75337	1.9766	0.0548158
Cnih4	1.90787	7.50709	1.97629	0.0459443
Cox6c	58.2749	229.279	1.97615	0.0234871
Coro1a	1.82934	7.19647	1.97596	0.0575286
Mrpl2	2.88851	11.3561	1.97507	0.0668606
Tbcb	5.42958	21.3386	1.97455	0.0403471
Esd	43.6044	171.341	1.97432	0.0200908
Sepw1	14.983	58.8131	1.97281	0.039074
Actl6a	6.04327	23.6995	1.97146	0.0305098
Maged2	4.72377	18.5214	1.97118	0.0851931
Pef1	2.11856	8.30595	1.97106	0.0622489

gene	FPKM		log2(fold_change)	p_value
Hspd1	74.8671	293.323	1.97009	0.0176661
2700060E02Rik	12.7152	49.748	1.96809	0.0778517
Il1b	3.91798	15.3129	1.96656	0.0405945
Dyrk2	2.84398	11.1139	1.96639	0.0401744
Fabp5	7.0951	27.7236	1.96622	0.0485113
Acadm	5.48991	21.4275	1.96461	0.0331042
Snx1	15.0187	58.5855	1.96379	0.0206294
Abcb7	1.87494	7.31184	1.96339	0.0280373
Wbp5	28.5041	111.141	1.96314	0.0220936
Atp5l	99.2072	386.491	1.96192	0.0219131
Rchy1	2.60983	10.1596	1.96081	0.0602996
Atp6v1d	2.94029	11.439	1.95993	0.0604716
Psph	2.58901	10.0665	1.95909	0.0561099
Cfdp1	11.6565	45.2532	1.95688	0.031039
Txndc17	5.54738	21.53	1.95647	0.0440206
Cops4	11.326	43.9039	1.95471	0.0273674
Uxs1	6.17027	23.9103	1.95422	0.0339157
Vps37b	2.79149	10.807	1.95285	0.0488482
Cbx1	2.97166	11.4923	1.95132	0.0702127
Sec61b	17.6264	68.0608	1.94908	0.0462842
Ppm1f	2.12752	8.20825	1.9479	0.0376923
Mff	4.37802	16.8789	1.94687	0.0349855
Rassf8	2.21305	8.52027	1.94487	0.0444261
Angptl2	4.60446	17.7159	1.94395	0.0429214
Trap1	6.2835	24.1667	1.94338	0.0373125
Asl	1.61848	6.21823	1.94186	0.0706307
Maea	8.00655	30.7451	1.94111	0.0305452
Prps2	1.3446	5.16296	1.94102	0.0445556

gene	FPKM		log2(fold_change)	p_value
Cyb5r1	3.48358	13.3701	1.94037	0.0467742
Pdcl3	3.46907	13.2852	1.9372	0.0505475
Bcas2	6.96026	26.6167	1.93512	0.0313753
Lsm3	11.6869	44.6714	1.93446	0.0467887
Ktn1	6.73862	25.7464	1.93384	0.0226934
Impa1	2.15237	8.2192	1.93307	0.0474848
Spr	4.52732	17.2765	1.93208	0.0516467
Gtf3c3	1.52656	5.82182	1.93119	0.0534947
Tmem126a	6.43392	24.5134	1.9298	0.0606313
Akr1a1	19.4276	74.0082	1.92958	0.0278299
Fam18b	2.75446	10.4835	1.92829	0.0507673
Smarcd3	2.65373	10.0979	1.92796	0.0517689
Lta4h	4.67594	17.7422	1.92386	0.0356365
Wdr18	2.79888	10.6186	1.92368	0.0391079
Mrpl16	3.51909	13.3398	1.92247	0.0606759
Etfdh	4.48806	17.0095	1.92218	0.0378123
Armc1	2.91686	11.0534	1.922	0.0363485
Lgmn	5.25042	19.8745	1.92042	0.0413793

Table 1. 1000 genes significantly differentially up-regulated in $SCs_{A\text{-}CREB}$ compared to YFP

gene	FPKM		log2(fold-change)	p-value	half-CRE sites			CREB database
	YFP	A-CREB			tgacg	cgtca	tggcg	
Mpp7	54.35	4.99	-3.44	0.0041	+		+++	unknown
Alpl	7.85	1.04	-2.91	0.0018		+	++	no
Slc10a6	31.33	5.05	-2.63	0.0017	++		++	no
Slc15a2	8.12	1.37	-2.57	0.0070	++	+++	++	no
Sele	4.88	1.04	-2.23	0.0302	+	+	+	no
Nr4a3	9.01	1.99	-2.18	0.0174	+	+	++	no
Timp4	8.80	2.09	-2.07	0.0678				no
Mpz	10.59	2.64	-2.01	0.0555	+++		+	no
Eltd1	4.96	1.36	-1.87	0.0622		++	+	CRE_NoTATA
Chrdl2	5.19	1.48	-1.81	0.0651	+	+	++++	no
Nr4a2	5.68	1.68	-1.76	0.0854	++++	++++	+++++	CRE_TATA
Esm1	9.88	2.98	-1.73	0.0778	+++++	+	+	CRE_TATA
Akap12	8.68	2.71	-1.68	0.0656		+++		no
Apold1	9.52	3.09	-1.62	0.0852	+++		++	CRE_TATA
Alpk1	5.45	1.82	-1.58	0.0578			+	no
Map3k6	23.20	8.13	-1.51	0.0650	+	+	++++++	no
Tnfaip6	126.07	47.13	-1.42	0.0696	+			no

+ indicates one respective site

Table 2. Genes significantly differentially down-regulated in $SCs_{A\text{-}CREB}$ compared to control and corresponding predicted CRE sites within gene promoters

Wnt pathway*

	YFP	A-CREB
Axin1	8.25	16.21
Axin2	0.55	1.94
Ctnnb1	74.86	149.21
Dvl1	16.75	43.13
Dvl2	2.17	4.05
Dvl3	1.21	2.38
Fzd1	3.94	4.92
Fzd10	0.16	0.50
Fzd2	0.74	1.61
Fzd3	0.66	1.71
Fzd4	6.56	6.66
Fzd5	3.32	4.69
Fzd6	0.28	0.45
Fzd7	4.21	10.55
Fzd8	3.37	4.78
Fzd9	0.79	1.52
Gsk3a	3.27	11.74
Gsk3b	3.27	8.75
Lrp5	3.61	5.06
Lrp6	14.40	14.29
Wnt1	0.10	0.04
Wnt10a	0.18	1.30
Wnt10b	0.13	0.14
Wnt11	1.37	1.51
Wnt16	0.06	0.07
Wnt2	0.05	0.02
Wnt2b	0.25	0.24
Wnt3	0.06	0.04
Wnt3a	0.05	0.01
Wnt4	1.46	1.76
Wnt5a	0.15	0.30
Wnt5b	0.22	0.39
Wnt6	0.33	0.39
Wnt7a	0.04	0.00
Wnt7b	0.11	0.91
Wnt8a	0.06	0.05
Wnt8b	0.06	0.03
Wnt9a	0.36	0.95
	FPKM	

Notch pathway*

	YFP	A-CREB
Dll1	3.10	14.95
Dll3	0.08	0.09
Dll4	1.28	0.91
Jag1	6.51	14.35
Jag2	1.14	4.29
Notch1	8.58	13.48
Notch2	17.11	24.95
Notch3	30.96	36.71
Notch4	0.38	0.25
Rbpj	20.70	34.22
	FPKM	

Hippo pathway*

	YFP	A-CREB
AMOT	1.73	1.73
AMOTl1	4.61	8.68
AMOTl2	11.73	21.50
Fat1	6.51	17.61
Fat2	0.03	0.06
Fat3	0.08	0.06
Fat4	1.91	1.89
Frmd6	32.34	43.73
Lats1	9.76	14.36
Lats2	6.14	9.34
Mob1a	23.56	46.18
Mob1b	6.04	10.82
Mob2	7.45	12.48
Nf1	15.01	18.97
Nf2	3.85	7.83
Sav1	7.31	12.42
Stk3	5.29	9.47
Stk4	3.13	6.85
Taz	3.38	6.33
Tead1	7.29	14.97
Tead2	0.93	8.33
Tead3	3.67	4.48
Tead4	0.47	2.55
Wwc1	0.02	0.07
Wwc2	2.96	4.30
Yap1	12.06	12.26
	FPKM	

Fgf pathway*

	YFP	A-CREB
Fgf1	0.54	0.21
Fgf10	0.06	0.04
Fgf11	1.13	3.74
Fgf12	0.06	0.16
Fgf13	0.68	1.61
Fgf14	0.02	0.00
Fgf15	0.10	0.03
Fgf16	0.77	1.40
Fgf17	0.16	0.01
Fgf18	0.18	0.20
Fgf2	4.91	3.21
Fgf20	0.09	0.00
Fgf21	0.81	2.69
Fgf22	0.19	0.05
Fgf23	0.33	0.01
Fgf3	0.00	0.06
Fgf4	0.04	0.03
Fgf5	0.13	0.07
Fgf6	0.06	0.06
Fgf7	0.25	0.44
Fgf8	0.10	0.17
Fgf9	3.27	3.15
Fgfr1	72.06	84.80
Fgfr2	0.23	0.31
Fgfr3	1.50	2.32
Fgfr4	15.08	26.95
Frs2	3.18	5.10
Grb2	7.56	15.56
Sos1	3.14	4.91
Sos2	5.17	8.43
	FPKM	

Polarity complexes*

	YFP	A-CREB
Ccdc42	0.07	0.00
Cldn5	15.90	9.47
Crb3	0.02	0.08
Dlg1	9.38	13.20
Dlg2	0.18	0.37
Dlg3	1.01	2.11
Dlg4	1.06	1.72
Dlg5	1.54	3.75
Inadl	0.52	3.04
Llgl1	1.23	4.05
Llgl2	0.07	0.20
Ocln	0.08	0.10
Pard3	4.05	7.76
Pard3b	1.67	1.83
Pard6a	0.82	3.14
Pard6b	0.13	0.13
Pard6g	0.46	1.47
Prkci	6.63	15.77
Scrib	2.38	6.67
Tjp1	8.57	13.82
Tjp2	5.35	9.15
Tjp3	0.03	0.03
	FPKM	

low		high

***no differences in FPKM between YFP and A-CREB expressing cells were significant by cuffdiff analysis**

Table 3. Signaling pathways unperturbed in $SCs_{A\text{-}CREB}$ during quiescence

Term	Genes	p_value	FDR
mmu05016:Huntington's disease	UQCRC2, ATP5E, UQCRC1, AP2S1, ATP5B, CYC1, NDUFAB1, UQCRFS1, COX5A, COX5B, NDUFS7, GPX1, NDUFS6, NDUFS5, CASP3, UQCR10, UQCR11, NDUFS4, NDUFS8, ATP5O, NDUFS3, NDUFS2, ATP5H, NDUFS1, NDUFB10, SLC25A4, CYCS, NDUFC2, COX4I1, NDUFC1, NDUFA10, COX6C, DCTN2, UQCRH, ATP5C1, UQCRB, NDUFB3, POLR2H, NDUFB4, POLR2G, POLR2F, NDUFB5, NDUFB6, POLR2E, NDUFB7, NDUFB8, POLR2K, NDUFB9, POLR2J, POLR2I, COX7B, COX7C, ATP5G2, ATP5G1, ATP5G3, POLR2C, NDUFB2, COX6B1, NDUFA4, NDUFA5, NDUFA2, COX7A2, NDUFA8, NDUFA9, NDUFA6, COX8A, NDUFA7, ATP5F1, VDAC2, VDAC3, NDUFA1, VDAC1, SDHA, SDHB, HDAC2, NDUFV1, BAX, SDHC, NDUFV2, SDHD, ATP5A1	1.04E-33	1.27E-30

Term	Genes	p_value	FDR
mmu00190:Oxidative phosphorylation	UQCRC2, ATP5E, UQCRC1, ATP5B, CYC1, NDUFAB1, UQCRFS1, COX5A, COX5B, NDUFS7, NDUFS6, NDUFS5, UQCR10, UQCR11, NDUFS4, NDUFS8, ATP5L, ATP5O, NDUFS3, NDUFS2, ATP5H, COX17, NDUFS1, ATP5K, NDUFB10, NDUFC2, COX4I1, NDUFC1, NDUFA10, ATP6V1D, COX6C, ATP6V1C1, ATP6V1A, UQCRH, ATP5C1, UQCRB, NDUFB3, NDUFB4, NDUFB5, NDUFB6, NDUFB7, NDUFB8, NDUFB9, COX7B, COX7C, ATP5G2, ATP6V1B2, ATP5G1, ATP6V1G1, ATP5G3, NDUFB2, COX6B1, NDUFA4, NDUFA5, NDUFA2, ATP5J2, COX7A2, NDUFA8, NDUFA9, NDUFA6, NDUFA7, COX8A, ATP5F1, NDUFA1, PPA2, PPA1, SDHA, SDHB, NDUFV1, ATP6V1E1, SDHC, NDUFV2, SDHD, ATP5A1, ATP6V0A2	2.66E-41	3.23E-38

Term	Genes	p_value	FDR
mmu05010:Alzheimer's disease	UQCRC2, ATP5E, UQCRC1, ATP5B, IDE, CYC1, NDUFAB1, UQCRFS1, COX5A, COX5B, NDUFS7, NDUFS6, NDUFS5, CASP3, UQCR10, UQCR11, NDUFS4, NDUFS8, IL1B, ATP5O, NDUFS3, NDUFS2, ATP5H, NDUFS1, NDUFB10, CYCS, NDUFC2, COX4I1, NDUFC1, NDUFA10, COX6C, UQCRH, ATP5C1, GM12070, UQCRB, NDUFB3, BID, NDUFB4, NDUFB5, NDUFB6, NDUFB7, NDUFB8, NDUFB9, COX7B, COX7C, ATP5G2, ATP5G1, ATP5G3, NDUFB2, COX6B1, GAPDH, NDUFA4, NDUFA5, NDUFA2, COX7A2, NDUFA8, NDUFA9, NDUFA6, NDUFA7, COX8A, ATP5F1, CAPN2, NDUFA1, NAE1, SDHA, SDHB, NDUFV1, SDHC, NDUFV2, ATP2A1, SDHD, CALM3, ATP5A1	3.15E-26	3.83E-23

Term	Genes	p_value	FDR
mmu05012:Parkinson's disease	UQCRC2, ATP5E, UQCRC1, ATP5B, CYC1, NDUFAB1, UQCRFS1, COX5A, COX5B, NDUFS7, NDUFS6, NDUFS5, UQCR10, CASP3, UQCR11, NDUFS4, HTRA2, NDUFS8, ATP5O, NDUFS3, ATP5H, NDUFS2, NDUFS1, NDUFB10, SLC25A4, CYCS, NDUFC2, COX4I1, NDUFC1, NDUFA10, COX6C, UQCRH, ATP5C1, UQCRB, NDUFB3, NDUFB4, NDUFB5, NDUFB6, NDUFB7, NDUFB8, NDUFB9, COX7B, COX7C, ATP5G2, ATP5G1, ATP5G3, NDUFB2, COX6B1, NDUFA4, NDUFA5, NDUFA2, COX7A2, NDUFA8, NDUFA9, NDUFA6, NDUFA7, COX8A, ATP5F1, VDAC2, VDAC3, NDUFA1, PARK7, VDAC1, SDHA, SDHB, NDUFV1, SDHC, NDUFV2, SDHD, ATP5A1	5.20E-35	6.31E-32
mmu04110:Cell cycle	FZR1, DBF4, CDC16, SKP1A, RBX1, CCNE1, CDC45, MCM7, CDKN2B, BUB1, CCNA2, BUB3, TFDP1, ANAPC1, CDK1, ANAPC4, CDK6, CDC20, MCM2, CDC26, CDK4, MCM3, MCM4, MCM5, MCM6, CCNB1, CCND1, YWHAH, CCNB2, HDAC2, MAD2L1, MDM2, BUB1B	6.94E-07	8.43E-04

Term	Genes	p_value	FDR
mmu03040:Spliceosome	NCBP1, CCDC12, 0610009D07RIK, PPIL1, CWC15, LSM7, SNRPD1, SNRPD2, SF3B5, NAA38, SF3B2, CTNNBL1, PRPF19, LSM5, LSM4, LSM3, BCAS2, SNRPA1, PRPF31, EFTUD2, PRPF6, SF3A3, PPIE, SNRNP200, SNRNP40, SNRPC, SNRNP27, SNRPE, THOC3, SNRPG	9.65E-06	0.011728551
mmu00230:Purine metabolism	POLR2H, POLR2G, POLR2F, POLR2E, POLR2K, POLR2J, POLR2I, PNPT1, POLA1, POLR2C, PRIM1, ATIC, POLE3, PRIM2, PAPSS1, POLR3G, NUDT2, AK1, NUDT5, GART, NME4, ITPA, NME1, PKM2, RRM2, RRM1, ADSL, PAICS, PRPS2	0.001733591	2.086207315
mmu03050:Proteasome	PSMB10, SHFM1, PSMA7, PSMB5, PSMB4, PSMB7, PSMB6, PSMB1, PSMB3, PSMB2, PSMD3, PSMD4, PSMD6, PSMD7, PSMD8, PSMA2, PSMA1, PSMD14, PSMC5, PSMD13, PSMA6, PSMC4, PSMA5, PSMC3, PSMC2, PSMA4, PSMC1, POMP	9.66E-16	1.21E-12
mmu00240:Pyrimidine metabolism	POLR2H, POLR3G, POLR2G, POLR2F, NUDT2, POLR2E, POLR2K, POLR2J, DTYMK, PNPT1, POLR2I, POLA1, CAD, POLR2C, CMPK1, TK1, NME4, PRIM1, ITPA, NME1, POLE3, RRM2, PRIM2, RRM1, DUT	1.74E-05	0.02109712

Term	Genes	p_value	FDR
mmu05322:Systemic lupus erythematosus	SNRPD1, CBX3, HIST2H2AA1, HIST1H2BP, HIST1H2BM, HIST1H2BN, H2AFV, HIST1H2BK, HIST1H2BL, HIST2H2AC, HIST1H2BJ, H2AFZ, HIST3H2A, H2AFX, ACTN1, ACTN3, H2AFJ, HIST2H4, HIST2H2BB, HIST1H2AB, HIST1H2AC, HIST1H4M, HIST1H4K, HIST1H2AF, HIST1H2AG, HIST1H2AD, HIST1H2AE, HIST2H3C2, TROVE2, HIST1H4A, HIST1H4B, HIST1H4F, HIST1H4C, HIST1H4D, HIST1H4I, HIST1H4J, HIST1H4H, HIST1H2BA, HIST1H2BB, HIST2H3B, HIST1H2BC, HIST1H2BE, HIST1H2BF, HIST1H2BG, HIST1H2BH, HIST1H3A, HIST1H3B, HIST1H2AI, HIST1H3C, HIST1H2AH, HIST1H3D, HIST1H2AK, HIST1H3E, HIST1H3F, HIST1H3G, HIST1H3H, HIST1H2AN, HIST1H3I	6.02E-05	0.073090203
mmu04120:Ubiquitin mediated proteolysis	ANAPC1, FZR1, DDB1, ANAPC4, SAE1, CDC20, CDC34, CDC16, SKP1A, UBE3C, CDC26, UBE2C, RBX1, TRIM37, PRPF19, UBE2E3, FBXW8, RNF7, CUL7, CUL4A, UBA2, UBA3, MDM2, RCHY1	0.008394426	9.735806348

Term	Genes	p_value	FDR
mmu04260:Cardiac muscle contraction	UQCRC2, ACTC1, UQCRC1, COX7A2, TNNC1, COX8A, CYC1, COX7B, COX7C, COX4I1, UQCRFS1, TPM2, COX5A, CACNG1, COX5B, COX6C, TNNT2, UQCR10, UQCR11, UQCRH, COX6B1, UQCRB	1.73E-05	0.021058447
mmu00020:Citrate cycle (TCA cycle)	DLST, ACO2, ACO1, SUCLG2, SUCLG1, CS, DLAT, PDHB, IDH3A, SDHA, SDHB, IDH3G, SDHC, DLD, SDHD, IDH2, IDH1, FH1, SUCLA2, MDH2, MDH1	2.40E-13	2.92E-10
mmu03030:DNA replication	POLA1, MCM2, RNASEH2A, MCM3, RNASEH2B, MCM4, MCM5, RNASEH2C, RPA3, MCM6, RPA1, PRIM1, RFC5, RPA2, RFC3, MCM7, RFC2, POLE3, PRIM2, FEN1	7.28E-11	8.84E-08
mmu04115:p53 signaling pathway	BID, CDK1, CYCS, CDK6, PMAIP1, CDK4, CCNG1, SESN3, CCNB1, CCNE1, CCND1, EI24, CASP3, CCNB2, RRM2, BAX, MDM2, RCHY1, IGFBP3	1.08E-04	0.130998812
mmu04114:Oocyte meiosis	ANAPC1, CDK1, ANAPC4, CDC20, SKP1A, CDC16, CDC26, RBX1, CCNB1, CCNE1, PPP1CA, YWHAH, MAD2L1, CCNB2, BUB1, FBXO5, CALM3, PRKACA	0.06656057	56.69646477
mmu00010:Glycolysis / Gluconeogenesis	LDHB, LDHA, ADH5, PGAM1, PGAM2, DLAT, GPI1, PDHB, ALDH3B1, PGM2, TPI1, PKM2, DLD, ENO3, PGK1, GM12070, GAPDH, ENO1	8.97E-04	1.084769492
mmu03018:RNA degradation	EXOSC8, CNOT8, EXOSC9, EXOSC4, LSM7, PNPT1, EXOSC5, NAA38, LSM5, LSM4, ENO3, LSM3, HSPD1, HSPA9, ENO1, C1D	6.55E-04	0.793172778

Term	Genes	p_value	FDR
mmu03420:Nucleotide excision repair	DDB1, GTF2H4, CETN2, GTF2H2, RBX1, RPA3, RFC5, RPA1, MNAT1, RPA2, RFC3, CUL4A, POLE3, RFC2	1.99E-04	0.241856194
mmu00620:Pyruvate metabolism	AKR1B8, ME1, LDHB, LDHA, ME2, PKM2, DLD, DLAT, ACAT1, PDHB, MDH2, MDH1	0.001833984	2.205788211
mmu00280:Valine, leucine and isoleucine degradation	BCKDHA, ACAA2, ACADM, ACADS, DLD, ECHS1, ACAD8, HIBCH, HADH, ACAT1, HADHA, HADHB	0.004871633	5.761254943
mmu00480:Glutathione metabolism	LAP3, GSS, GSR, GPX1, GSTA4, RRM2, PGD, RRM1, IDH2, IDH1, GPX7, MGST2	0.012687893	14.37168314
mmu00071:Fatty acid metabolism	ACAA2, ACADM, ACADS, ADH5, ECHS1, ACADL, HADH, ACAT1, HADHA, ACSL5, HADHB	0.012155444	13.80888701
mmu00640:Propanoate metabolism	LDHB, LDHA, ACADM, SUCLG2, SUCLG1, ECHS1, HIBCH, SUCLA2, ACAT1, HADHA	0.002035733	2.445691187
mmu00970:Aminoacyl-tRNA biosynthesis	RARS2, RARS, HARS2, FARSB, LARS, GARS, CARS2, LARS2, VARS, KARS	0.021359921	23.07595235
mmu00520:Amino sugar and nucleotide sugar metabolism	CYB5R3, PGM2, GALK1, CYB5R1, NANS, MPI, CMAS, TSTA3, UXS1, GPI1	0.028378737	29.51788213
mmu00330:Arginine and proline metabolism	GOT2, LAP3, PYCRL, PYCR2, GOT1, ASS1, GATM, GAMT, ASL, CKB	0.07967585	63.53695884
mmu03020:RNA polymerase	POLR2H, POLR3G, POLR2G, POLR2F, POLR2E, POLR2K, POLR2J, POLR2I, POLR2C	0.003913295	4.652575124
mmu00250:Alanine, aspartate and glutamate metabolism	GOT2, GOT1, ASS1, ADSL, ASNS, CAD, ASL, GPT2	0.02619196	27.56602692
mmu00260:Glycine, serine and threonine metabolism	SHMT1, SHMT2, GATM, DLD, PHGDH, GAMT, PSPH, PSAT1	0.036367699	36.24556914
mmu00270:Cysteine and methionine metabolism	GOT2, LDHB, LDHA, AHCY, GOT1, DNMT1, MTAP, MAT2B	0.042313527	40.86438339

Term	Genes	p_value	FDR
mmu00360:Phenylalanine metabolism	GOT2, GOT1, NAA20, PRDX6, NAA10, ALDH3B1, MIF	0.018470326	20.27024605
mmu00630:Glyoxylate and dicarboxylate metabolism	MTHFD1, ACO2, ACO1, CS, MDH2, MDH1	0.017238108	19.04548742
mmu03430:Mismatch repair	RFC5, RPA1, RPA2, RFC3, RFC2, RPA3	0.062999258	54.64572602
mmu00680:Methane metabolism	SHMT1, SHMT2, PRDX6, ADH5, CAT	0.002763738	3.30689194
mmu00062:Fatty acid elongation in mitochondria	ACAA2, ECHS1, HADH, HADHA, HADHB	0.005090288	6.012548831
mmu00670:One carbon pool by folate	MTHFD1, SHMT1, SHMT2, ATIC, GART	0.069287987	58.20908645
mmu00290:Valine, leucine and isoleucine biosynthesis	LARS, LARS2, VARS, PDHB	0.090567793	68.44796082

Table 4. KEGG Pathway Analysis of up-regulated genes in $SCs_{A\text{-}CREB}$

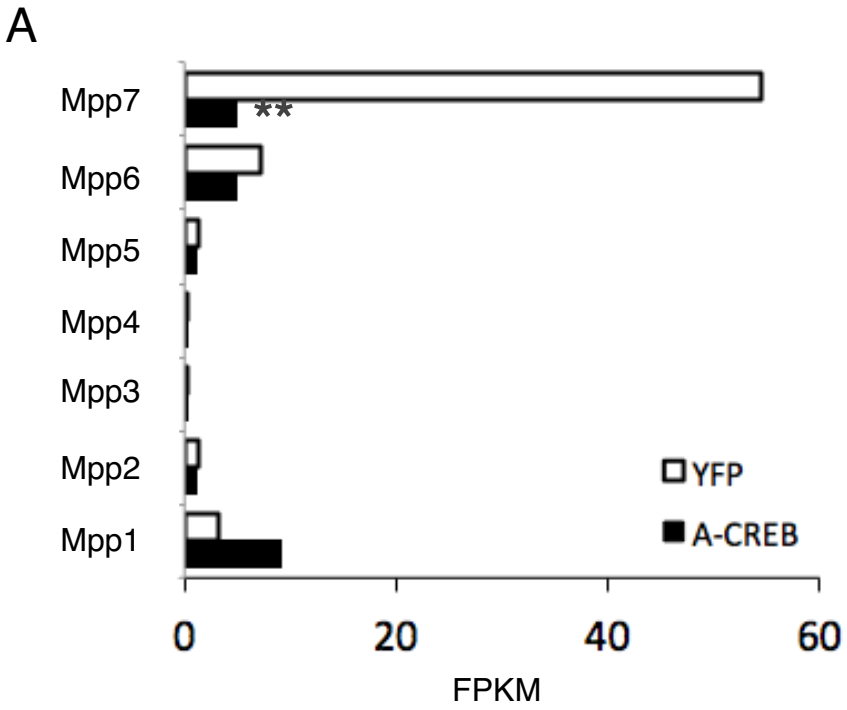

Figure 23. *Mpp7* is highly expressed in control satellite cells and drastically reduced in $SCs_{A\text{-}CREB}$ (A) FPKMs of Mpp family proteins in SCs shows significant reduction of *Mpp7* transcript in $SCs_{A\text{-}CREB}$. N=2 mice/genotype. **p<0.01.

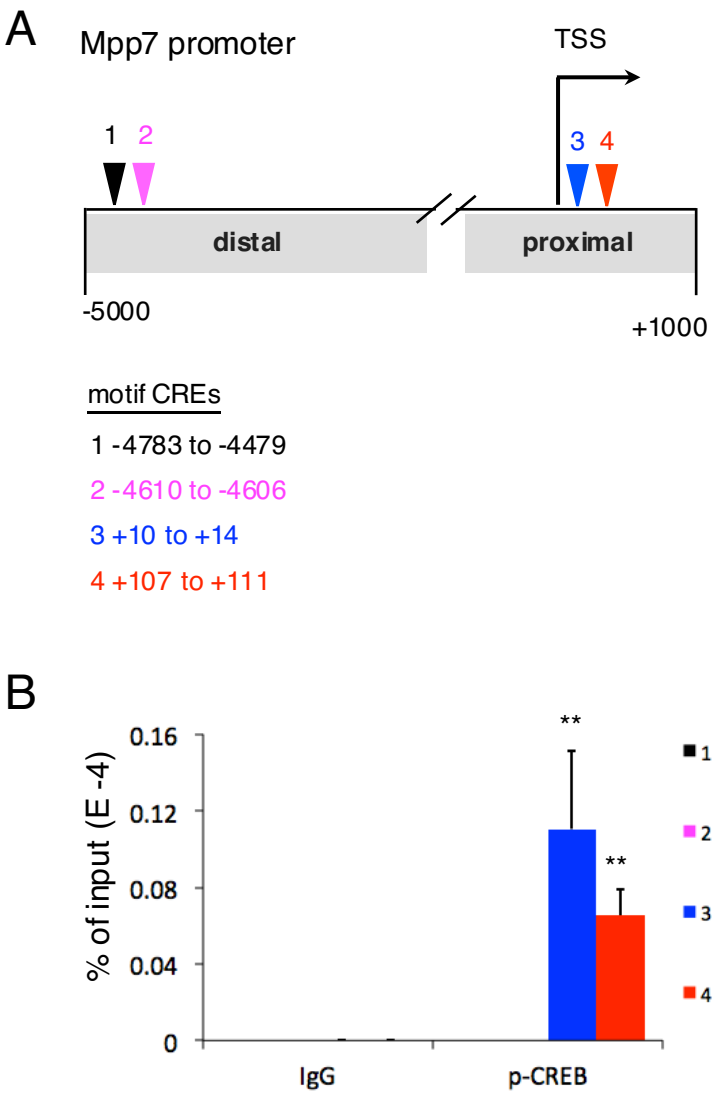

Figure 24. pCREB binds to the Mpp7 promoter (A) Schematic of Mpp7 promoter including the loci of candidate CREB binding sites relative to the TSS. (B) pCREB occupancy at the Mpp7 promoter in primary myoblasts was analyzed by ChIP-qPCR. Percent of precipitated DNA compared to input DNA (not immunoprecipitated) shown. N=3 biological replicates. Data is expressed as the mean±standard deviation.**$p<0.01$ Student's t-test.

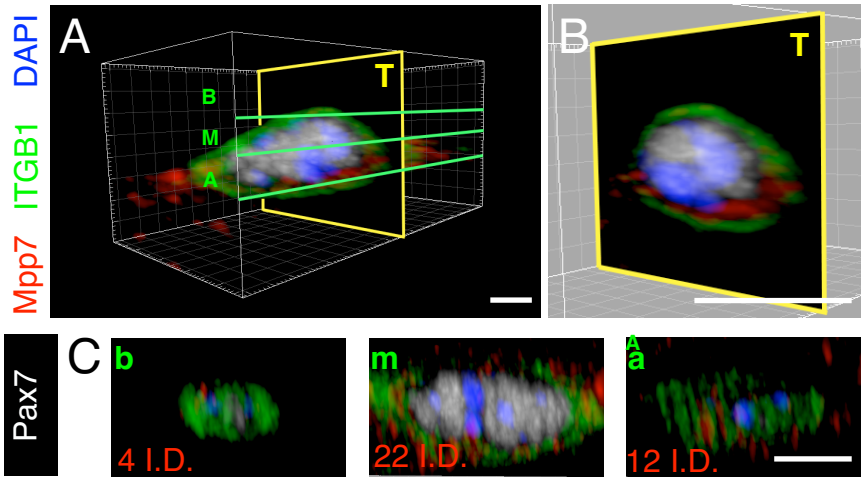
DAPI
ITGB1
Mpp7
A
B
M
A
T
B
T
Pax7
C
b
4 l.D.
m
22 l.D.
a
12 l.D.

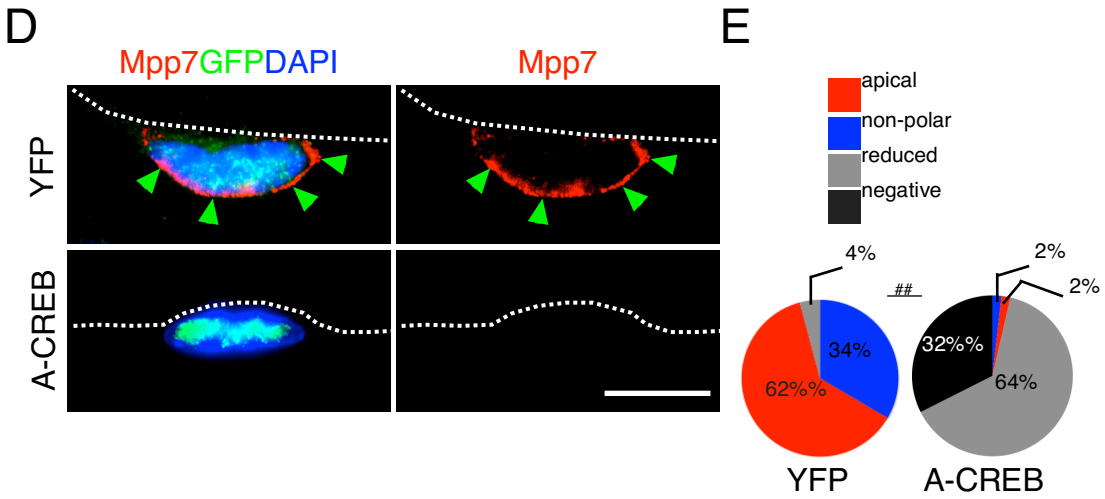
D
Mpp7GFPDAPI
Mpp7
YFP
A-CREB
E
apical
non-polar
reduced
negative
4%
##
2%
2%
34%
62%%
32%%
64%
YFP
A-CREB

Figure 25. Mpp7 is localized to the apical domain of SCs and reduced in $SCs_{A\text{-}CREB}$

(A) 3-dimensional (3-D) reconstruction of confocal images obtained from single myofiber-associated SCs. Letters mark b-basal, m-medial, a-apical planes parallel to the myofiber long axis and T-transverse plane orthogonal to the myofiber long axis. (B) Digital transverse slice obtained from 3-D reconstruction of SC. (C) Images rendered from basal (b), medial (m), and apical (a) planes delineated in (A). Mpp7 immunofluorescence I.D. shows Mpp7 is enriched in the medial and apical domains. (D) Immunofluorescence analysis of single myofiber-associated SCs shows reduced levels of Mpp7 in $SCs_{A\text{-}CREB}$. Green arrowheads mark apical domain. Dotted line marks basal lamina edge of myofiber. (E) Quantification of Mpp7 expression pattern in single myofiber-associated SCs. ##$p<0.01$, Chi-squared test. Scale bars 2 μm (A), 5 μm (B, D), 6 μm (C).

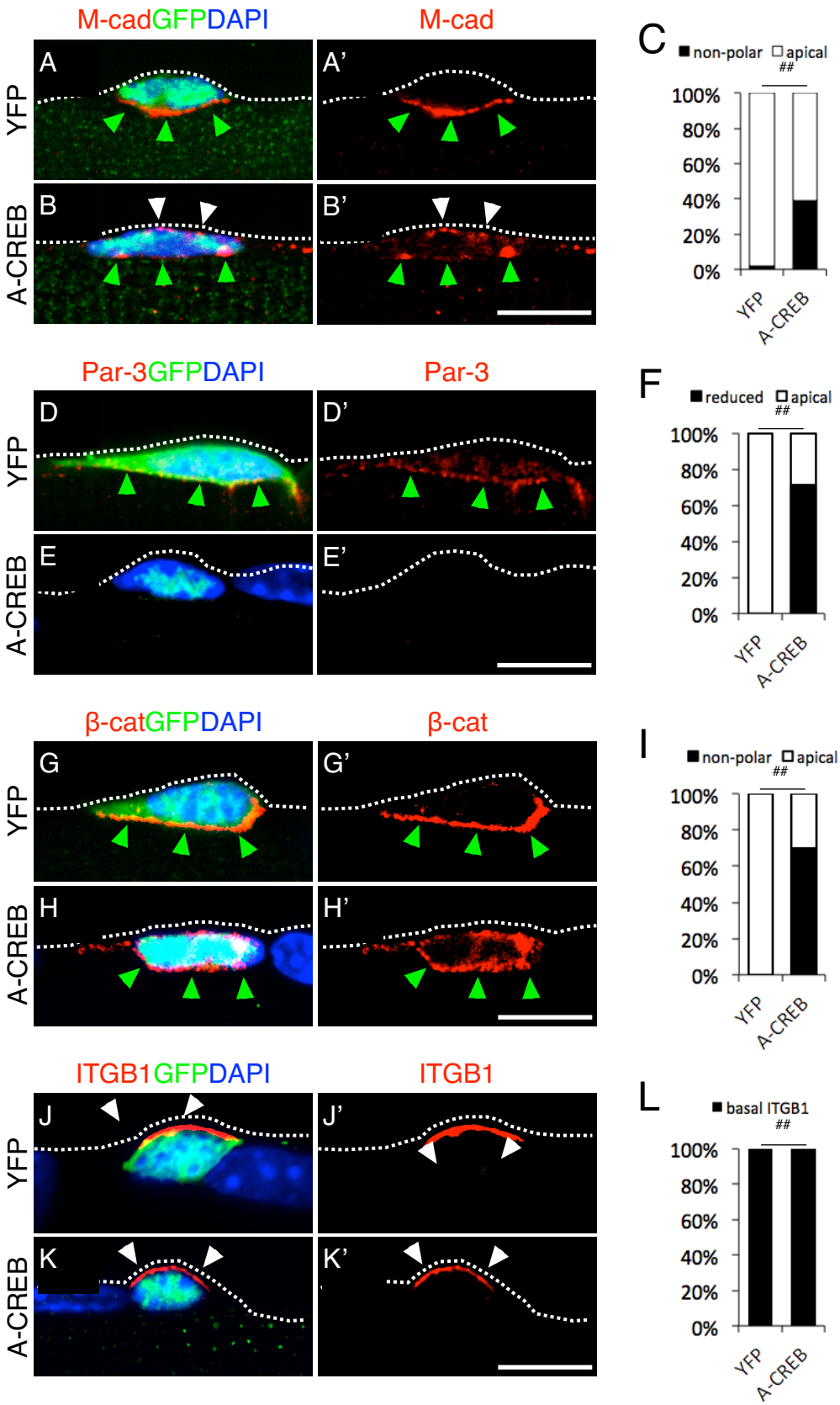
M-cadGFPDAPI
M-cad
A
A'
YFP
B
B'
A-CREB
C
non-polar
apical
##
100%
80%
60%
40%
20%
0%
YFP
A-CREB
Par-3GFPDAPI
Par-3
D
D'
YFP
E
E'
A-CREB
F
reduced
apical
##
100%
80%
60%
40%
20%
0%
YFP
A-CREB
β-catGFPDAPI
β-cat
G
G'
YFP
H
H'
A-CREB
I
non-polar
apical
##
100%
80%
60%
40%
20%
0%
YFP
A-CREB
ITGB1GFPDAPI
ITGB1
J
J'
YFP
K
K'
A-CREB
L
basal ITGB1
##
100%
80%
60%
40%
20%
0%
YFP
A-CREB

Figure 26. Apically localized proteins are disrupted in $SCs_{A\text{-}CREB}$ Single myofiber-associated SCs were isolated and immediately processed for immunofluorescence analysis. Loss of apically enriched M-cad (A,B), expression of Par-3 (D,E), and apically enriched β-cat (G,H) in $SCs_{A\text{-}CREB}$. Quantification of polarized M-cad (C), Par-3 (F), and β-cat (I) expression. Unperturbed basally polarized expression of ITGB1 (J,K) in $SCs_{A\text{-}CREB}$. (L) Quantification of polarized ITGB1 expression. N=3 mice/genotype, n≥50 cells/animal. ##p<0.01 Chi-squared test. Scale bars10 μm.

METHODS

Mice

See Chapters 2 and 3 for mice used.

Illumina cDNA sequencing (RNA-seq)

High quality (RIN>9) total RNA was isolated from FACS sorted cells using Arcturus Pico kit, catalog #KIT0204, Applied Biosystems. 70 ng of total RNA was then used as starting material for Ribozero rRNA depletion, catalog #RZH1086, Epicentre (Illumina). cDNA was generated from this rRNA depleted sample following Illumna TruSeq DNA sample prep (low input), Illumina.

Library read mapping

For RNA-seq, reads were aligned to mm9 UCSC version 7 mouse genome. Tuxedo protocol (Trapnell et al., 2012), Tophat and cufflinks, was followed to determine relative expression levels of genes. 2 biological replicates were used per experimental sample and control.

ChIP-PCR

Fragmented chromatin was obtained from $4x10^6$ myoblasts grown in growth media (20% fetal bovine serum, 5% horse serum, 1% chicken embryo extract, PENSTREP, 1% Glutamax, bFGF) using Covaris truChIP low cell chromatin shearing kit, catalog #010145, Covaris. Cells were fixed in 1% formaldehyde for 10 minutes and chromatin was sonicated using Covaris M22 Focused ultrasonicator, peak power 75, duty factor 5, cycles/burst 200, 6^oC using 30 second pulses at 2 minute intervals at 6W for 8 minutes of total sonication time to generate chromatin 200-1000bp in size. Antibodies used for IP:

anti-phospho-Ser133-CREB, catalog #9198 (87G3), Cell Signaling; anti-normal rabbit IgG, catalog #2729, Cell Signaling. Immunoprecipitated DNA was purified by QIAquick PCR Purification kit. Primers used to detect Mpp7 promoter motif 1: 5'- CAG CGT CTG GCT ATG TGC C-3', 5'- CCA GGC ATG ATA GCA CAT GG-3'; motif 2: 5'- TGC ACC TCC CAG CGA GAC-3', 5'- GCT CAG CAG GAT GAA CTA GC-3'; motif 3: 5'- GCT AGT TCA TCC TGC TGA GC-3', 5'- CAG TCC AAG CGC CAC TTA G-3', motif 4: 5'- GTG TAA CAA GGA AGT GTG TGA TG-3', 5'- CTT GCC TAA TAG GCA CAT GAC T-3'

Single fiber isolation

See Chapter 2 for methods used for obtaining single fibers.

Antibodies

Primary antibodies used were rabbit anti-Mpp7 (1:10), catalog #12983-1-AP, Proteintech; goat anti-Mpp7 (1:25), catalog #sc-163089, Santa Cruz; mouse anti-M-cadherin (1:250), catalog #81471, Santa Cruz; rabbit anti-Par-3 (1:250), catalog #07-330, Millipore; mouse anti-β-catenin IgG1 (1:100), catalog #RDI-BCATENIN, RDI. See Chapter 2,3 for additional antibodies used.

CHAPTER 7: MPP7 MEDIATES MYOBLAST PROLIFERATION AND SELF-RENEWAL

INTRODUCTION

Cellular quiescence and proliferation are regulated by polarity proteins in multiple stem cell systems (Florian and Geiger, 2010). The functional relevance of polarity during quiescence is unclear, however the importance of polarity during activation has been studied. The polarity protein Mark2 (Par1b) is basally localized in activated SCs and regulates asymmetric division (Dumont et al., 2015). The Scrib polarity protein, localized basolaterally in epithelia (Su et al., 2012), is critical for promoting myoblast proliferation and differentiation (Ono et al., 2015). Polarity proteins mediate SC divisions and cell fate through activation of signaling pathways. p38α/β MAPK pathway is activated by the core apical polarity complex components Par-3 and PKCλ during SC expansion to promote transit amplification *in vitro* (Troy et al., 2012). Given the requirement for polarity proteins during SC expansion, the significance of polarity during quiescence warrants further attention.

I found that Mpp7 polarity protein was the most highly down-regulated transcripts in $SCs_{A\text{-}CREB}$ (Table 2). This defect in polarity could be a secondary effect of another misregulated gene. In order to rule out this possibility, I tested the contribution of Mpp7 to the proliferation and self-renewal capacities of SCs.

RESULTS

Mpp7 expression rescues the proliferation and self-renewal defect of $SCs_{A\text{-}CREB}$

To test whether Mpp7 is a downstream mediator of CREB function in the SC, I introduced constructs for expressing Mpp7 together with bicistronic membrane-GFP (mGFP) or mGFP alone into $SCs_{A\text{-}CREB}$ on their myofibers; mGFP was used to follow transfected cells in conjunction with $SCs_{A\text{-}CREB}$ nGFP. Expression of Mpp7 increased $SCs_{A\text{-}CREB}$ proliferative cluster sizes and expanded both the $Pax7^{+}MyoD^{+}$ progenitor and $Pax7^{+}MyoD^{-}$ self-renewed fractions (Figure 27A-C). In parallel, I transfected the same constructs into unmarked wild-type SCs. Mpp7 expression did not alter proliferative cluster sizes, but rather increased the fractions of $Pax7^{+}MyoD^{+}$ progenitors and $Pax7^{+}MyoD^{-}$ self-renewed SCs (Figure 27A-C). Importantly, Mpp7 rescued the proliferative cluster size profiles, $Pax7^{+}MyoD^{+}$ fractions and $Pax7^{+}MyoD^{-}$ fractions of $SCs_{A\text{-}CREB}$ to levels equivalent to those in control SCs expressing mGFP alone (Figure 27). These data support Mpp7 is not only a target but also a functional mediator of CREB activity.

I next tested whether Mpp7 knockdown by siRNA is sufficient to cause an expansion defect in control YFP^{+} cells. I was not able to achieve successful siMpp7 knockdown in myofiber cultures, therefore I turned to SC-derived myoblasts, which also display high CREB activity (Figure 4A,B) and express *Mpp7* (Figure 25). As expected, A-CREB expression in SC-derived myoblasts showed compromised proliferation and increased differentiation (Figure 28). I tested 3 siRNAs against *Mpp7* transcripts and the 2 that were effective in reducing *Mpp7* expression (Figure 29) exhibited decreased EdU

incorporation and increased Mgn expression relative to scrambled control siRNA (Figure 30). All together, these data indicate that Mpp7 is a major downstream mediator of CREB function in SCs and myoblasts.

DISCUSSION

Polarity protein Mpp7 is highly downregulated (Figure 23) and apically localized proteins are also distributed aberrantly (Figure 26A-I) in $SCs_{A\text{-}CREB}$. Interestingly, Par-3, an activation promoting polarity protein, is absent or reduced in in $SCs_{A\text{-}CREB}$ (Figure 26D-F) suggesting that an overall defect in polarity may contribute to the lack of proliferation and self-renewal of $SCs_{A\text{-}CREB}$. I found that re-expressing Mpp7 alone is sufficient to restore the ability of $SCs_{A\text{-}CREB}$ to proliferate and self-renew (Figure 27). Interestingly, overexpression of Mpp7 in wild-type SCs also increased the proportion of self-renewing and progenitors populations (Figure 27) although proliferation did not change. The ability for Mpp7 to positively direct proliferation and self-renewal is a novel function for Mpp family of proteins and a novel role for a polarity protein in quiescent SCs. Given the high level of Mpp7 during quiescence and polarity defect of $SCs_{A\text{-}CREB}$, these data provide evidence that setting up a polarity during quiescence affects future potential for activation and self-renewal.

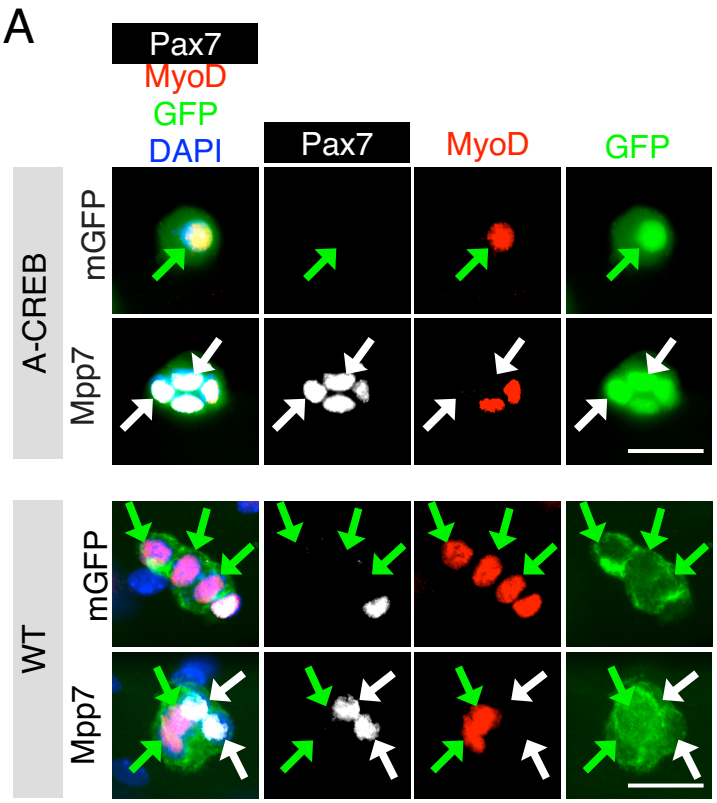
A
Pax7
MyoD
GFP
DAPI
Pax7
MyoD
GFP
A-CREB
mGFP
Mpp7
WT
mGFP
Mpp7

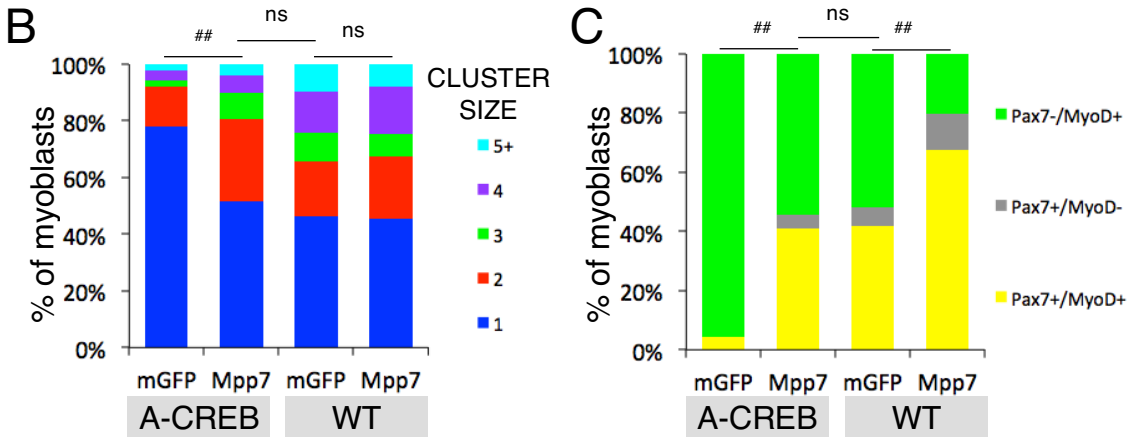
B
##
ns
ns
100%
80%
60%
40%
20%
0%
% of myoblasts
CLUSTER SIZE
5+
4
3
2
1
mGFP
Mpp7
mGFP
Mpp7
A-CREB
WT
C
##
ns
##
100%
80%
60%
40%
20%
0%
% of myoblasts
Pax7-/MyoD+
Pax7+/MyoD-
Pax7+/MyoD+
mGFP
Mpp7
mGFP
Mpp7
A-CREB
WT

Figure 27. Overexpression of Mpp7 in $SCs_{A\text{-}CREB}$ cells rescues proliferation defect and $Pax7^+$ cell population loss (A) EDL single fibers and associated SCs of A-CREB and CD1 mice were transfected with Mpp7::mGFP or mGFP and cultured in plating medium for a total of 4 days. Representative images of clonal clusters showing cluster size and $Pax7^-/MyoD^+$, $Pax7^+/MyoD^-$, or $Pax7^+/MyoD^+$ expression patterns. (B) Quantification of clonal cluster size after transfection with Mpp7::mGFP or mGFP. (C) Quantification of $Pax7^-/MyoD^+$, $Pax7^+/MyoD^-$, or $Pax7^+/MyoD^+$ expression patterns after transfection with Mpp7::mGFP or mGFP. ##$p<0.01$, Chi-squared test. Scale bars 25 μm.

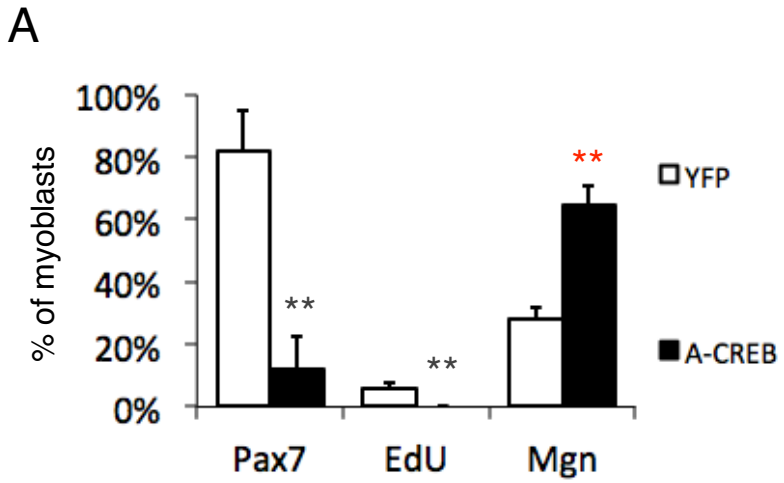

Figure 28. CREB inactivation in cultured myoblasts causes reduced proliferation and premature differentiation Primary myoblasts harvested from $Pax7^{CE/+}$;$Rosa26^{YFPYFP}$ and $Pax7^{CE/+}$;$Rosa26^{A\text{-}CREB/A\text{-}CREB}$ (TAM-) mice were cultured in growth medium for 1 passage and treated with 1μM 4-Hydroxytamoxifen for 24 hours. (A) Quantification of $Pax7^{+}$, EdU^{+} or Mgn^{+} lineage marked myoblasts 24 hours after 4-Hydroxytamoxifen treatment. **p<0.01, Student's t-test.

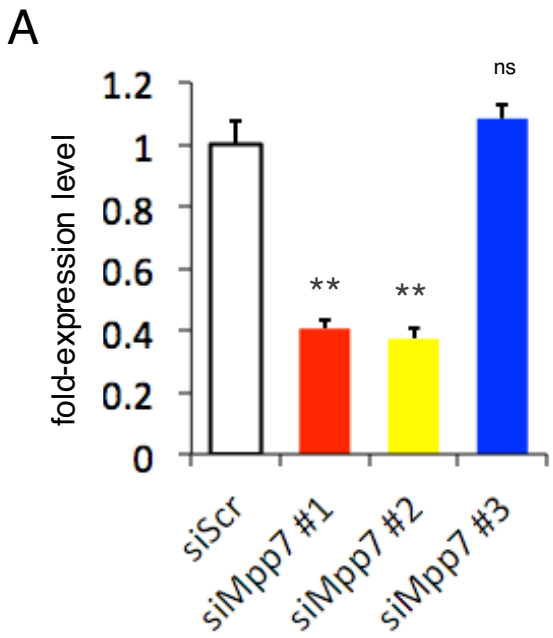

Figure 29. siRNA targeting *Mpp7* transcripts reduces *Mpp7* levels (A) 3 siRNAs targeting different regions of the *Mpp7* transcript were tested for ability to reduce *Mpp7* levels as detected by qRT-PCR. Data represented as mean +/- 1 standard deviation. **p<0.01, Student's t-test.

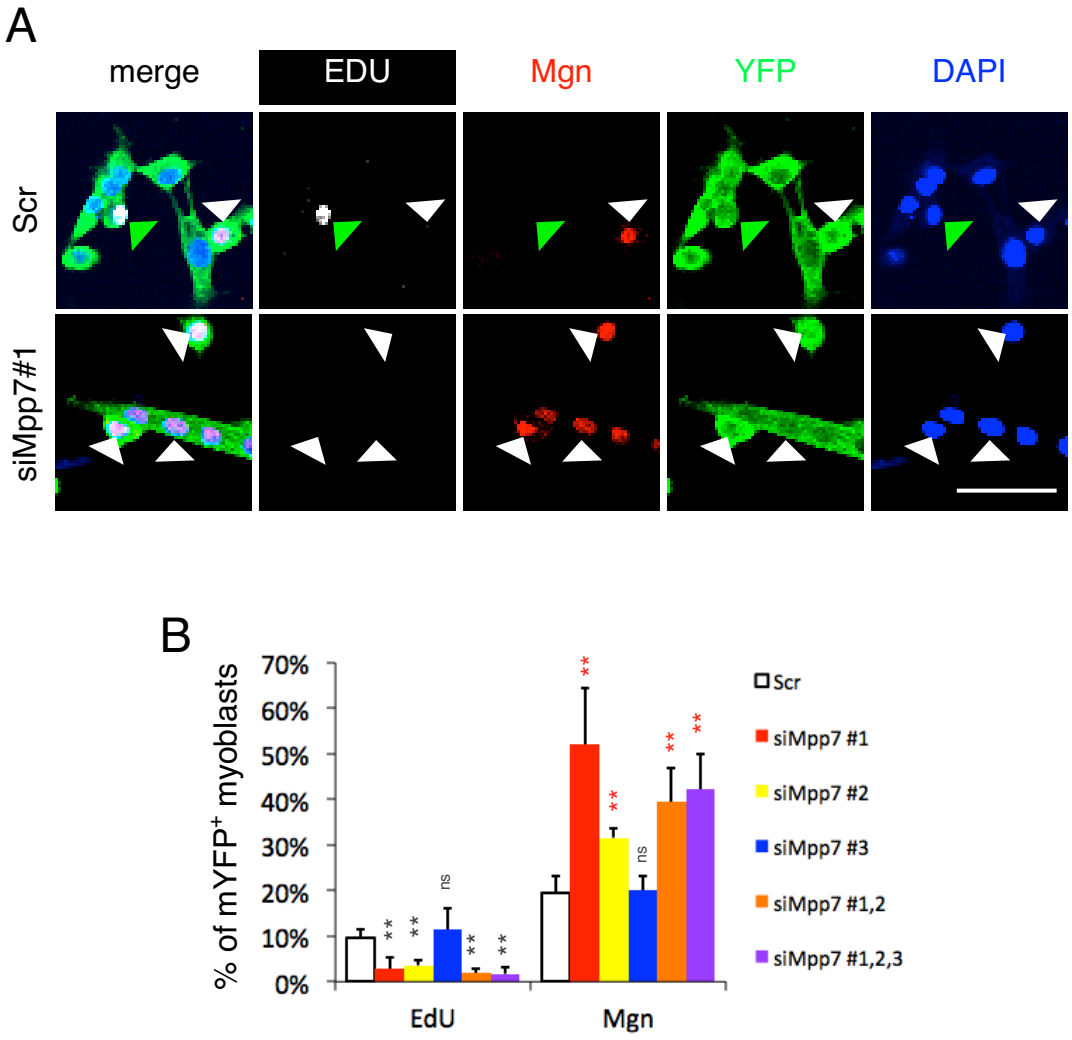

Figure 30. Knockdown of *Mpp7* transcripts leads to reduced proliferation and enhanced differentiation of cultured myoblasts TAM-treated YFP SCs were harvested and cultured in growth medium. Cell were transfected twice in 24 hour increments with indicated siMpp7 combinations. Analysis was performed 24 hours after last transfection. (A) Representative images of immunofluorescence detection of EdU and Mgn in siMpp7 and siScr (control) experiments. (B) Quantification of EdU incorporation and Mgn expression. Data represented as mean +/- 1 standard deviation. **p<0.01, Student's t-test.

METHODS

Mice

See Chapters 2 and 3 for mice used.

Single fiber isolation

See Chapter 2 for methods used for obtaining single fibers.

Plasmids

The backbone vector pMIGR1 (Pear et al., 1998) was modified to replace the GFP gene with EGFP-CAAX (membrane GFP, mGFP) to serve as a control. Human Mpp7 cDNA with a V5 C-terminal tag was cloned into the pMIGR1-mGFP to produce pMIGR1-V5Mpp7-IRES-mGFP. Each plasmid expresses membrane GFP as a reporter for transfection efficiency.

siRNAs

siRNAs targeting mouse *Mpp7* were purchased from Life Technologies, catalog #s: s93843 (#1), s93844 (#2),s93845 (#3), and resuspended to 20 μM working concentration. Silencer Select Negative Control siRNA, catalog #4390843, Life Technologies, was used as a control.

qPCR and primers

Total RNA was isolated from cells using Arcturus Pico kit, catalog #KIT0204, Applied Biosystems. cDNA was generated following standard methods using NEB M-MuLV Reverse Transcriptase, catalog #M0253S, New England BioLabs. Quantitect SYBR Green PCR Kit reagent, catalog #204141, Qiagen, was used in quantitative PCR reactions in a BioRad Thermocycler, catalog #CFX96 PCR, BioRad, for PCR product detection. *Mpp7* transcript was detecting using primers forward: 5'-AGG ATC GGC TTG CGA

CAT G-3' and reverse: 5'-ACA CGT CCC AGA GGA AGG TC-3'. *18S RNA* levels were determined using primers forward: 5'-GTA ACC CGT TGA ACC CCA TT-3' and reverse 5'-CCA TCC AAT CGG TAG TAG CG, as an internal control.

Single fiber transfection of plasmids

Single fibers were isolated as described in Chapter 2 and cultured in, growth media (20% fetal bovine serum, 5% horse serum, 1% chicken embryo extract, PENSTREP, 1% Glutamax, bFGF), for 8 hours on horse serum coated tissue culture dishes. Transfection solution was prepare at using TransfeX reagent, catalog#ACS-4005, ATCC, at DNA(ug):Transfex TransfeX reagent, at 1:2 ratio for 12 hours. Media was changed to plating media for the remainder of the culture for a total of 4 days after initial harvest.

Myoblast transfection of siRNAs

Plated myoblasts were cultured on matrigel coated tissue culture dishes and grown to 50% confluency prior to transfection. siRNAs were diluted in OPTIMEM and combined with Lipo 3000 reagent at 1:1 ratio following manufacture's protocol, catalog #L3000008, Life Technologies. Transfections were performed for 6 hours after which fresh plating media (10% horse serum, 0.5% chicken embryo extract, 1XPENSTREP, 1% Glutamax) was added to cells. 24 hours after the first transfection, a second transfection under the same conditions was performed. 24 hours after second transfection, myoblast were analyzed.

Antibodies

See Chapter 2 for antibodies used.

EdU treatment

EdU was added to tissue culture media at 10 μM final concentration for 2 hours prior to analysis.

EdU detection

See Chapter 3 for EdU detection methods.

CHAPTER 8: MPP7 PROMOTES PROLIFERATIONAND SELF-RENEWAL VIA AMOT-YAP

INTRODUCTION

The Hippo pathway effector YAP promotes myoblast proliferation and inhibits differentiation (Judson et al., 2012; Tremblay et al., 2014). Interestingly, polarized subcellular Angiomotin (AMOT) distribution differentially regulates Hippo signaling to direct YAP-dependent cell fate in pre-implantation embryos (Hirate et al., 2013; Leung and Zernicka-Goetz, 2013). YAP is repressed by core Hippo pathway kinases Mst1/2 and Lats1/2 YAP (Pan 2010), whereas it is either activated or repressed by AMOT family of proteins (consisting of AMOT, AMOTL1, and AMOTL2), depending on the cellular context (Chan et al., 2011; Yi et al., 2013; Zhao et al., 2011). Discriminating factors modulate AMOT activity and a seminal study identified Par-3, AMOTL1, AMOTL2, and tight junction associated Drosophila Stardust homologs, Mpp5 and Mpp7 to be AMOT binding partners (Wells et al., 2006). Whether Mpp7, and AMOT affect YAP activity in SCs in unknown. Moreover, the transcriptional regulation of polarity genes has not been investigated in SCs.

RESULTS

Mpp7 and AMOT regulate myoblast proliferation and YAP nuclear accumulation

I next sought to determine the mechanism by which how Mpp7 regulates proliferation. Among the Mpp7 protein interactions (Bohl et al., 2007; Stucke et al., 2007; Wells et al., 2006), an AMOT-containing complex (Wells et al., 2006) is of particular interest due to the critical role for AMOT in regulating Par-3 and YAP, both known proliferation regulators of SCs (Judson et al., 2012; Troy et al., 2012). Like Mpp7, AMOT is localized to the apical side of quiescent SCs (Figure 31A-E). By double labeling, I found overlapping signals between Mpp7 and AMOT (Figure 31D,E). Proximity ligation assay (PLA) confirmed this apical interaction between Mpp7 and AMOT (Figure 32). Furthermore, a portion of Mpp-AMOT and Mpp7-YAP PLA signals were localized to the SC nucleus of a portion of SCs (Figure 32,33,34), suggesting a possible role of AMOT and Mpp7 for YAP nuclear shuffling, previously observed in hepatocytes (Yi et al., 2013). Most $SCs_{A\text{-}CREB}$ displayed reduced AMOT (Figure 35) even though AMOT transcripts were not reduced (Figure 36), suggesting a translational or post-translational change. For the subset that exhibited a detectable level of AMOT, the expression pattern was almost exclusively non-polarize (Figure 35B). I next examined whether YAP also displayed aberrant expression. I found YAP accumulated in the nucleus in control quiescent SCs, but it was severely reduced in $SCs_{A\text{-}CREB}$ (Figure 37A,B). The lack of YAP target genes (Piccolo et al., 2014) in the $SCs_{A\text{-}CREB}$ down-regulated group (Table 2) suggests that YAP's transcriptional action is minimal in quiescent SCs, but becomes permitted after SC activation, i.e. after SC quiescence is lifted.

A constitutively active form of YAP, that can accumulate in the nucleus, enhanced proliferation and reduced differentiation of C2C12 and SC-derived myoblasts (Judson et al., 2012; Watt et al., 2010). To test whether Mpp7 and AMOT, as well as other potential regulators, play a role in YAP nuclear accumulation of myoblasts, I used an RNAi approach. After testing 3 different siRNAs per gene (Figure 38), I selected the siRNA with the most effective knockdown for the remainder of experiments. RNAi of *Mpp7*, *AMOT*, or AMOT family members *AMOT-L1* and *AMOT-L2*, each caused reduction of EdU^+ proliferating and Pax7 expressing cells, while increased Mgn^+ cells (Figure 39). Additionally, nuclear YAP was reduced (Figure 40). Confirming previous work, RNAi of YAP strongly reduced myoblast proliferation and $Pax7^+$ cells, while increased Mgn^+ cells (Figure 39). Furthermore, RNAi of Mpp7 caused down-regulation of canonical YAP downstream genes (Figure 41). To test the contribution of the Hippo pathway, I targeted Lats1 and Lats2, the immediate upstream kinase negative regulators of YAP. RNAi of *Lats1* and/or *Lats2* enhanced proliferation, nuclear YAP, and Pax7 expression without affecting Mgn expression (Figure 39,40). The similarities among *Mpp7*, *AMOT* family and *YAP* RNAi, and the biochemical data of Mpp7-AMOT family (Wells et al., 2006) and AMOT-YAP (Chan et al., 2011; Yi et al., 2013; Zhao et al., 2011) protein complexes led me to propose that they form a regulatory axis that promotes proliferation and dictates myogenic fates of myoblasts.

DISCUSSION

Here, I have shown that Mpp7 directs an AMOT-YAP axis to regulate SC proliferation and Pax7 expression. Previous studies showed that Mpp7 and AMOT family members interact in HEK293T cells (Wells et al., 2006) and consistently I found that Mpp7 interacts with AMOT in SCs (Figure 32,33,34). Based on previous studies of AMOT and YAP interactions, the effect of AMOT on YAP activity could be either positive or negative depending on cellular context (Chan et al., 2011; Yi et al., 2013; Zhao et al., 2011). My data provides evidence for the former, in which AMOT is a positive regulator of YAP (Figure 40). This is consistent with the idea that overexpression of AMOT family members in cell lines might have a negative effect on YAP whereas biologically relevant levels of AMOT positively regulate YAP (Yi et al., 2013). In summary these data show that Mpp7 is a positive regulator of AMOT in the SC to promote YAP signaling.

The mechanism by which AMOT regulates YAP has been controversial. The sequestering of YAP by AMOT in the cytoplasm has been suggested (Chan et al., 2011, 2013; Wang et al., 2011; Zhao et al., 2011) as well as enhancing YAP nuclear entry by AMOT to promote YAP downstream target gene activation (Yi et al., 2013). SCs show nuclear localization of Mpp7-YAP interactions, indicating that Mpp7 may also be involved in the nuclear transport of YAP. Based on my localization studies, Mpp7 is found both on the apical membrane as well as the nucleus, and one scenario for YAP regulation may be that Mpp7 can promote transport of YAP into the nucleus, or at least protect it from degradation, through cooperation with AMOT.

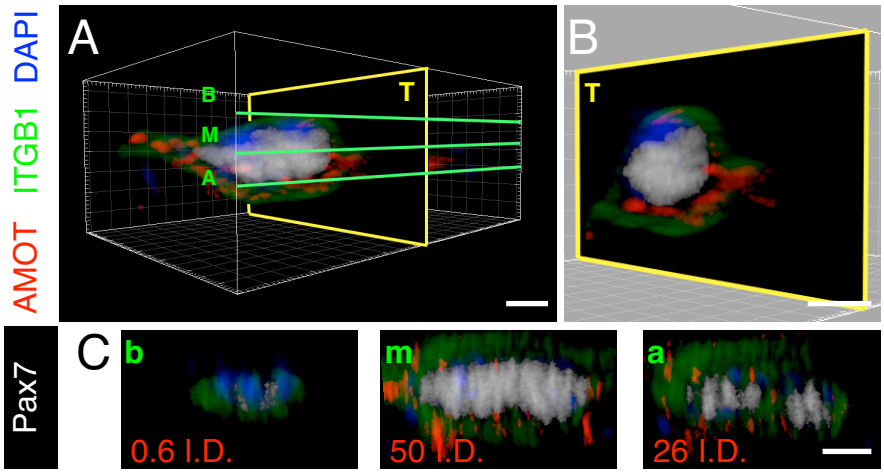
AMOT ITGB1 DAPI
A
B
T
M
A
B
T
Pax7
C
b
0.6 I.D.
m
50 I.D.
a
26 I.D.

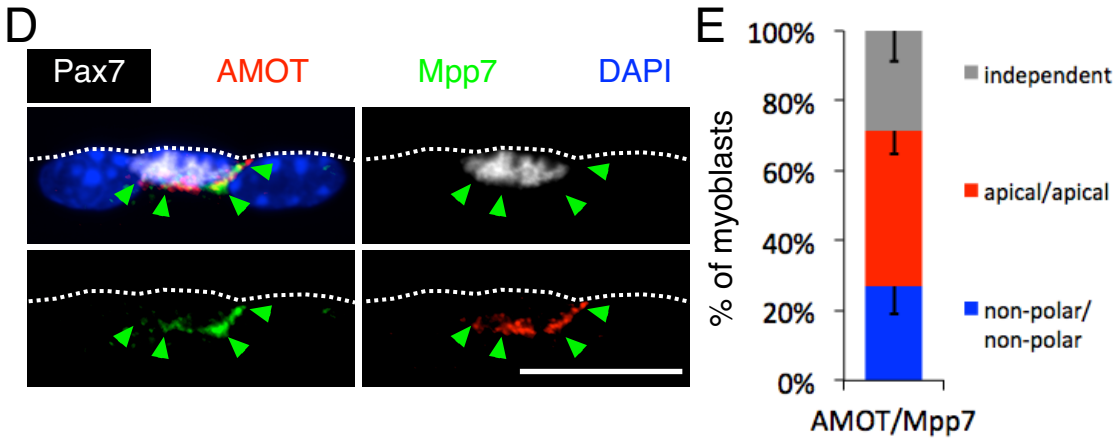
D
Pax7
AMOT
Mpp7
DAPI
E
100%
80%
60%
40%
20%
0%
% of myoblasts
AMOT/Mpp7
independent
apical/apical
non-polar/
non-polar

Figure 31. AMOT is localized to the apical domain of SCs (A) 3-dimensional (3-D) reconstruction of confocal images obtained from single myofiber-associated SCs. Letters mark b-basal, m-medial, a-apical planes parallel to the myofiber long axis and T-transverse plane orthogonal to the myofiber long axis. (B) Representative image of digital transverse slice of SCs obtained from 3-D reconstruction. (C) Images rendered from basal (b), medial (m), and apical (a) planes delineated in (A). AMOT immunofluorescence I.D. shows AMOT is enriched in the medial and apical domains. (D) Immunofluorescence analysis of AMOT and Mpp7 expression in single myofiber-associated SCs shows partial colocalization. Green arrowheads mark apical domain. Dotted line marks basal lamina edge of myofiber. (E) Quantification of AMOT/Mpp7 expression pattern in single myofiber-associated SCs. Scale bars 2 μm (A), 5 μm (B), 6 μm (C), 20 μm (D).

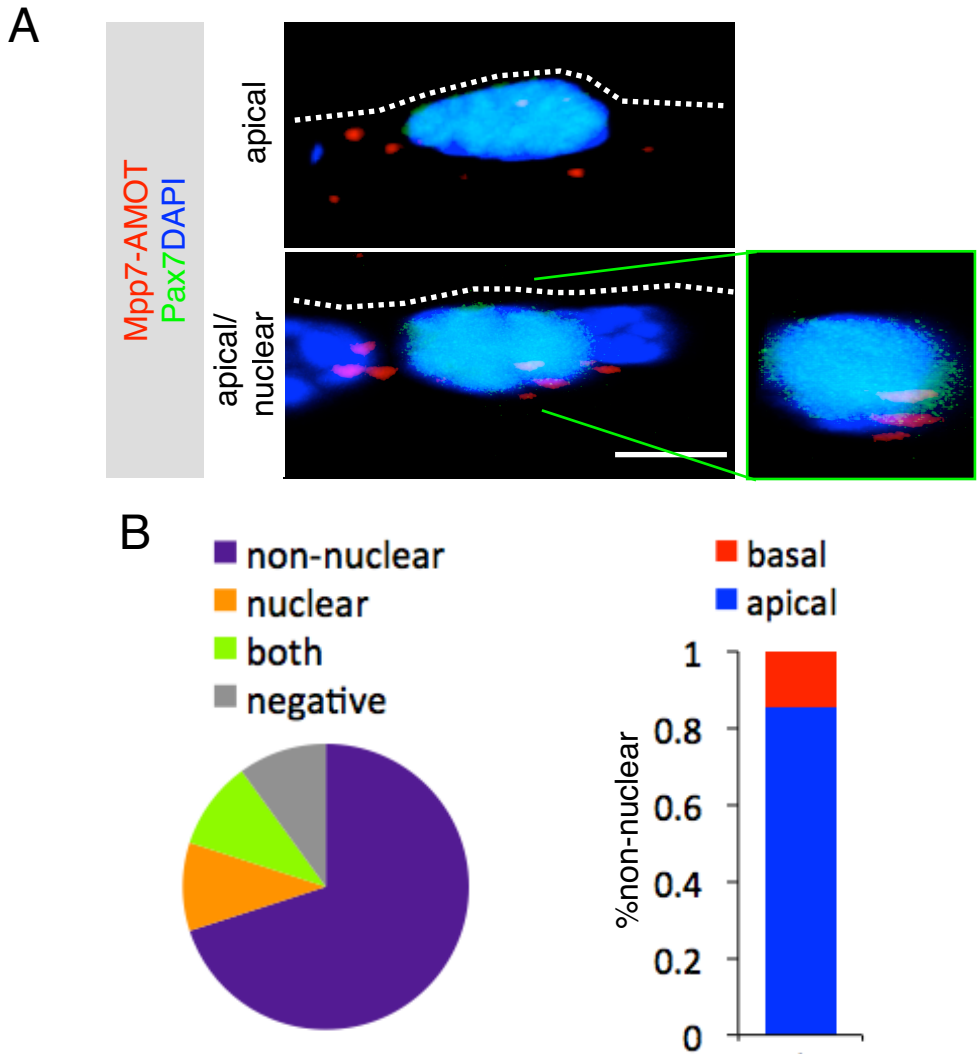

Figure 32. Direct binding between Mpp7 and AMOT proteins in SCs (A) Representative image of SCs after performing Proximity ligation assay (PLA) showing colocalization of Mpp7 and AMOT proteins within the apical domain (upper panel) and nuclear domain (lower panel) of SCs. Dotted line marks basal lamina edge of myofiber. Green lines indicate the region that is boxed to the right. Boxed region represents an orthogonal view, relative to the long axis of the myofiber, of the SC. (B) Quantification of sub-cellular localization of Mpp7-AMOT complexes in SCs. n=30 cells. Scale bar 5 μm.

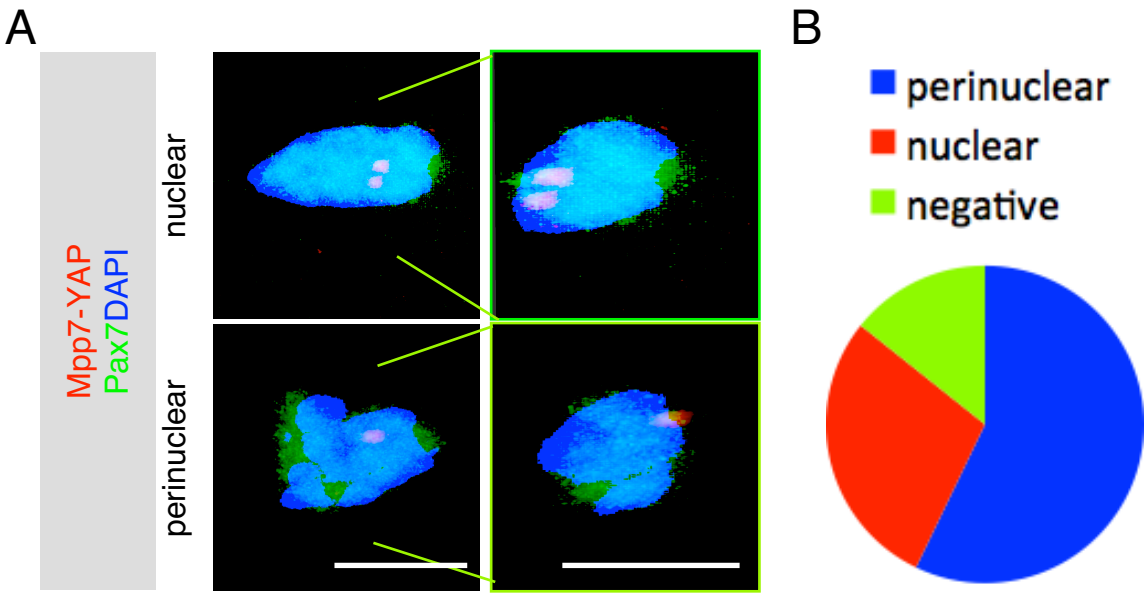

Figure 33. Direct binding between Mpp7 and YAP proteins in SCs (A) Proximity ligation assay (PLA) reveals colocalization of Mpp7 and YAP proteins within nuclear and perinuclear domains of SCs. Green lines indicate the region that is boxed to the right. Boxed region represents an orthogonal view, relative to the long axis of the myofiber, of the SC. (B) Quantification of sub-cellular localization of Mpp7-YAP complexes in SCs. n=30 cells. Scale bars 5 μm.

A

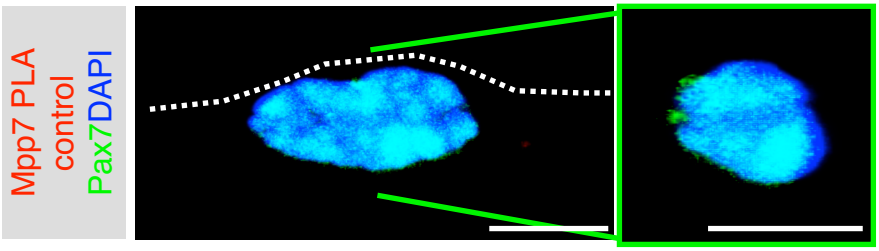

Figure 34. Proximity ligation assay control using single Mpp7 primary antibody recognition (A) Using Mpp7 antibody and omitting second antibody showed no PLA reaction in WT myofiber-associated SCs. Green lines indicate the region that is boxed to the right. Boxed region represents an orthogonal view, relative to the long axis of the myofiber, of the SC. n=30 cells. Scale bars 5 μm.

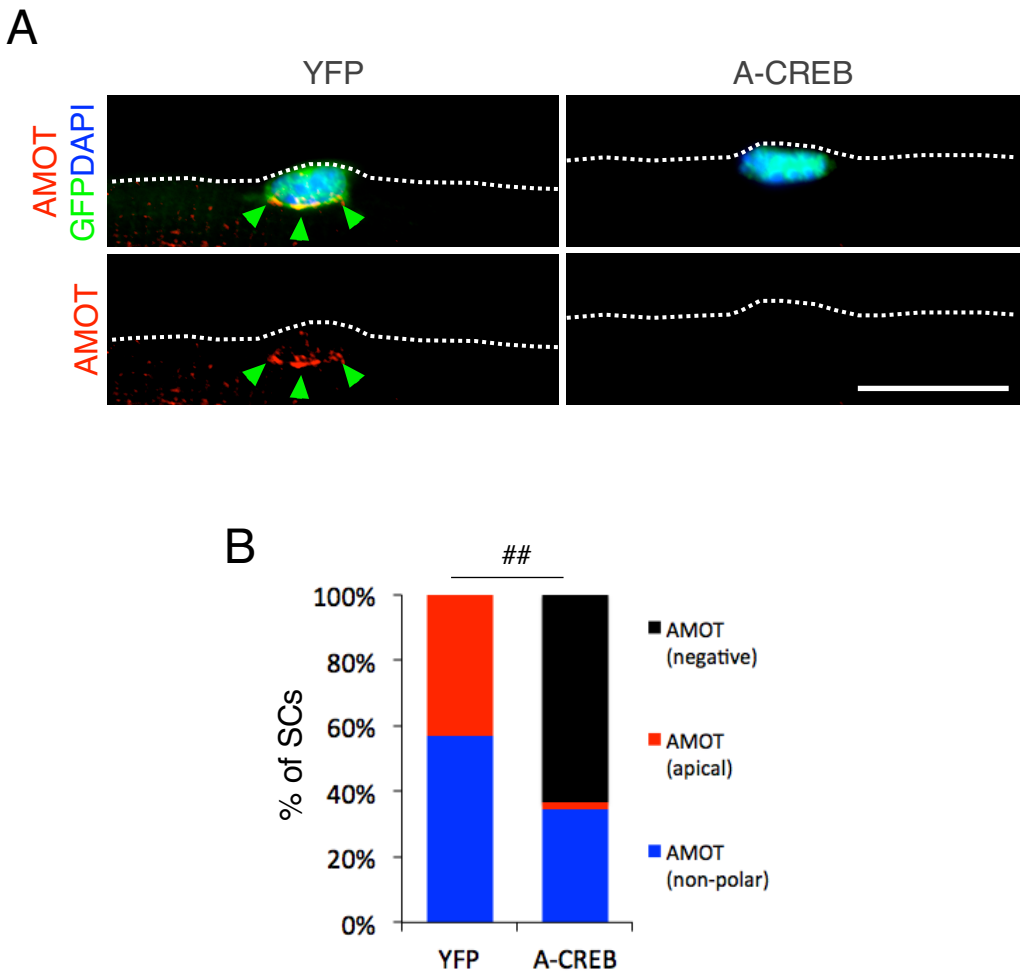

Figure 35. $SCs_{A\text{-}CREB}$ show reduced AMOT expression and AMOT apical localization (A) Immunofluorescence analysis of AMOT expression in single myofiber-associated SCs shows loss of apically localized AMOT expression in A-CREB SCs compared to YFP control. Green arrowheads mark apical domain. Dotted line marks basal lamina edge of myofiber. (B) Quantification of subcellular AMOT localization within YFP SCs or A-CREB SCs. ##$p<0.01$, Chi-squared test. Scale bar = 30 μm.

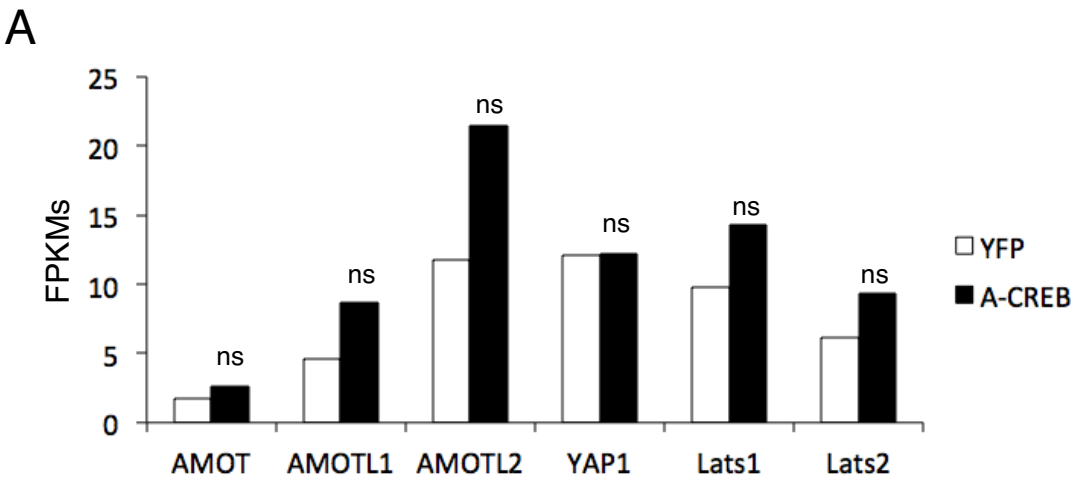

Figure 36. AMOT family and Hippo pathway transcripts are not significantly affected in $SCs_{A\text{-}CREB}$ (A) FPKM of select transcripts in SCs during quiescence. N=2 mice/genotype.

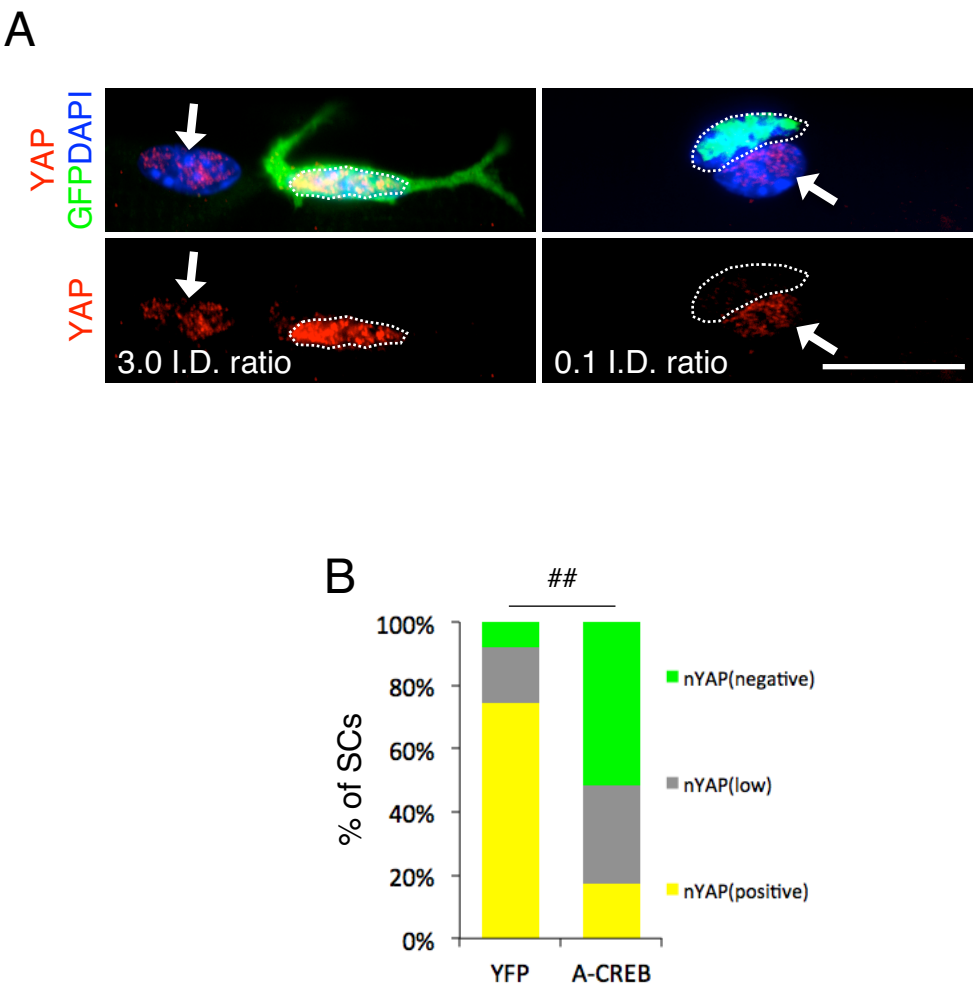

Figure 37. $SCs_{A\text{-}CREB}$ show reduced nuclear YAP localization (A) Immunofluorescence analysis of YAP expression in single myofiber-associated SCs shows loss of nuclear YAP in $SCs_{A\text{-}CREB}$ compared to YFP. White arrow marks myonuclei. Dotted line delineates SC nucleus. I.D. ratio calculated as SC nuclear YAP fluorescence integrated density as a fraction of average myonuclear fluorescence integrated density. (B) Quantification of nuclear YAP expression within YFP SCs or SCsA-CREB. ##$p<0.01$, Chi-squared test. Scale bar 30 μm.

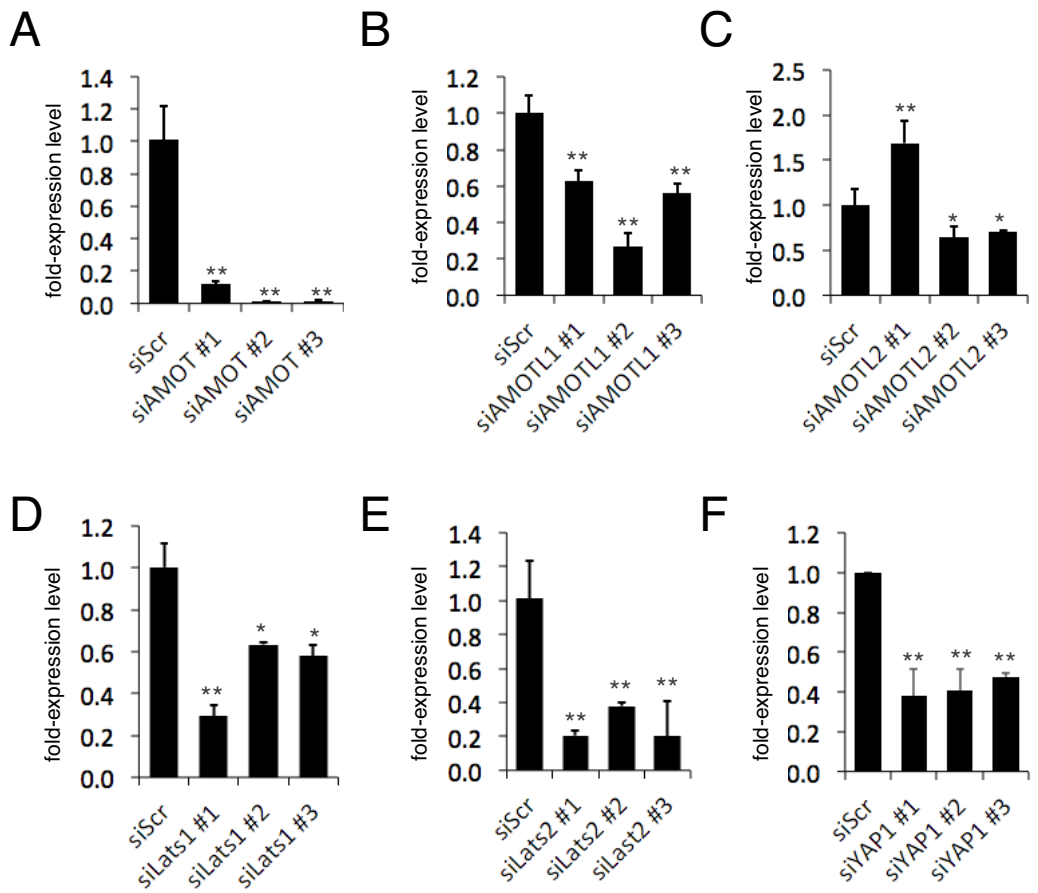

Figure 38. Efficiency of knockdown using siRNAs targeting AMOT family and Hippo pathway components WT SCs were harvested and cultured in growth medium. Cell were transfected twice in 24 hour increments with indicated siRNAs. Analysis was performed 24 hours after last transfection. Quantification of *AMOT* (A), *AMOTL1* (B), *AMOTL2* (C), *Lats1* (D), *Lats2* (E), and *YAP* (F) transcripts as fold change relative to control siScr by qRT-PCR. Data represented as mean +/- 1 standard deviation. *p<0.05, **p<0.01, Student's t-test.

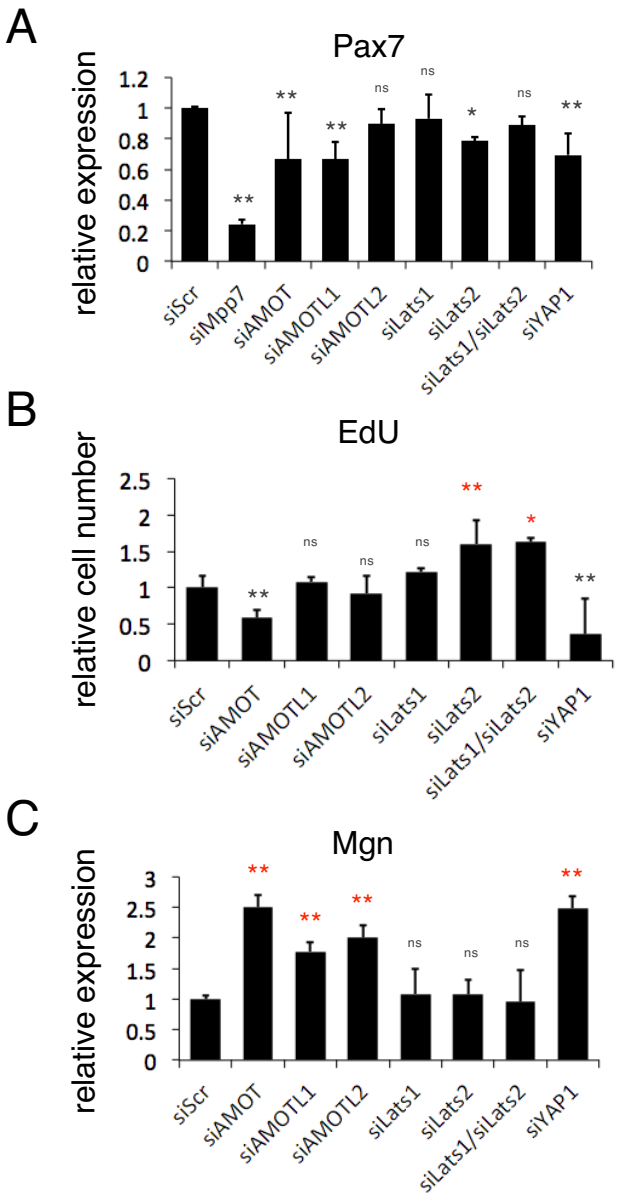

Figure 39. Mpp7 protein, AMOT family and Hippo pathway components contribute to myoblast proliferation and differentiation (A) TAM-treated YFP SCs were harvested and cultured in growth medium. Cell were transfected twice in 24 hour increments with indicated siRNAs. Analysis was performed 24 hours after last transfection. Quantification of Pax7 expression (A), EdU incorporation (B), and Mgn expression (C). Data represented as mean +/- 1 standard deviation. *p<0.05,**p<0.01, Student's t-test

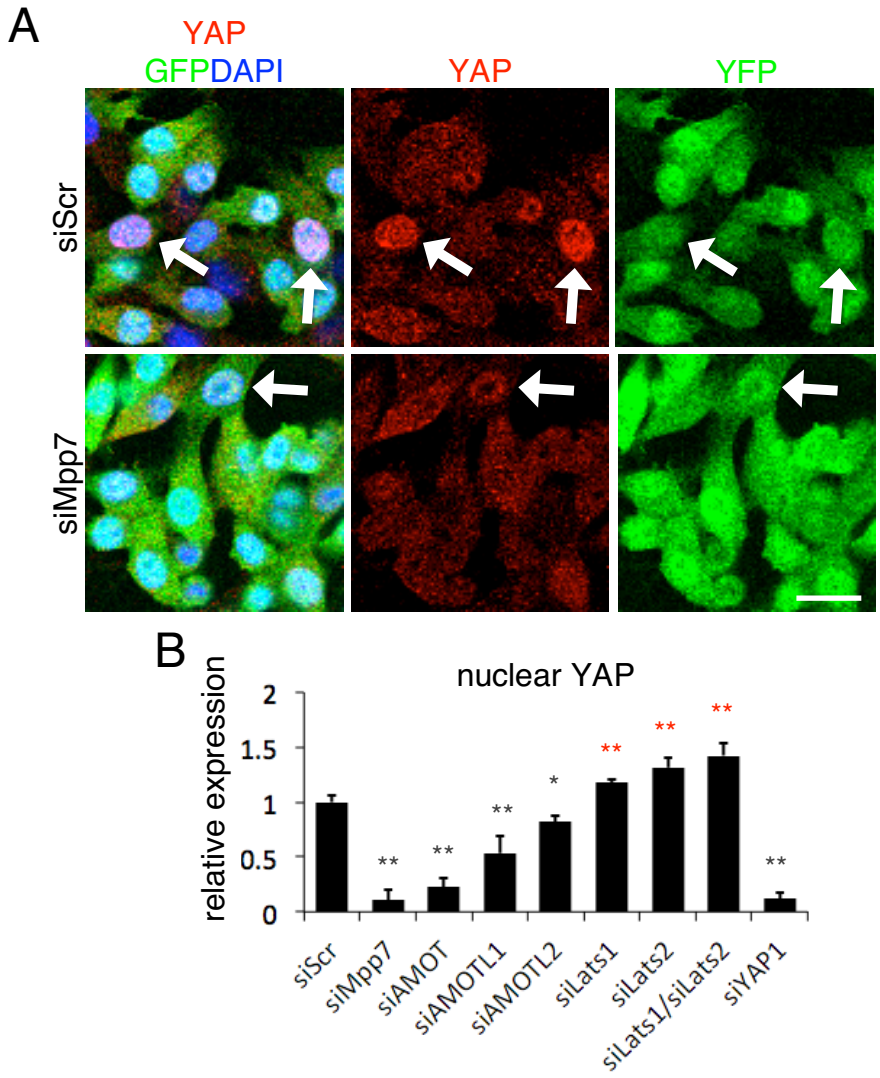

Figure 40. Nuclear accumulation of YAP depends on Mpp7 protein, AMOT family and Hippo pathway component levels in primary myoblasts TAM-treated YFP satellite cels were harvested and cultured in growth medium. Cell were transfected twice in 24 hour increments with indicated siRNAs. Analysis was performed 24 hours after last transfection. (A) Representative images of immunofluorescence detection of nuclear YAP in siMpp7 and siScr (control) experiments. (B) Quantification of nuclear YAP after transfection using indicated siRNA . Data represented as mean +/- 1 standard deviation. *p<0.05,**p<0.01, Student's t-test. Scale bar 20 μm.

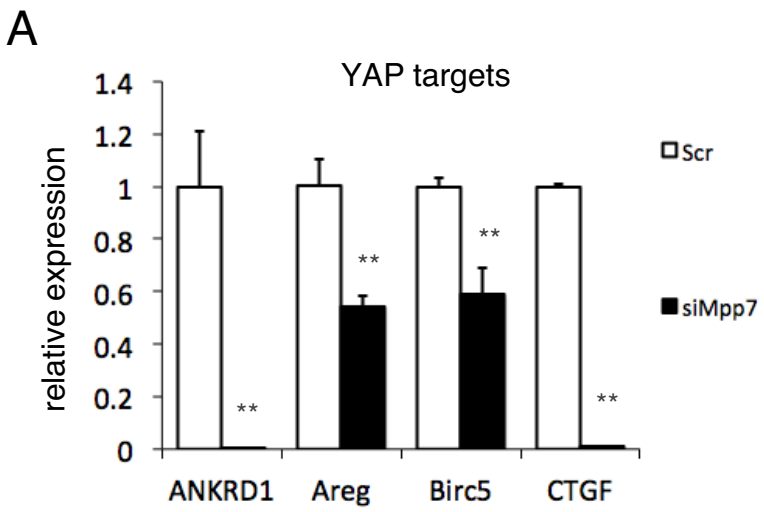

Figure 41. Knockdown of Mpp7 reduces YAP target gene expression (A) TAM-treated YFP SCs were harvested and cultured in growth medium. Cell were transfected twice in 24 hour increments with siMpp7. Analysis was performed 24 hours after last transfection. (A) Quantification of indicated transcripts by qRT-PCR after siRNA transfection. **p<0.01, Student's t-test.

A

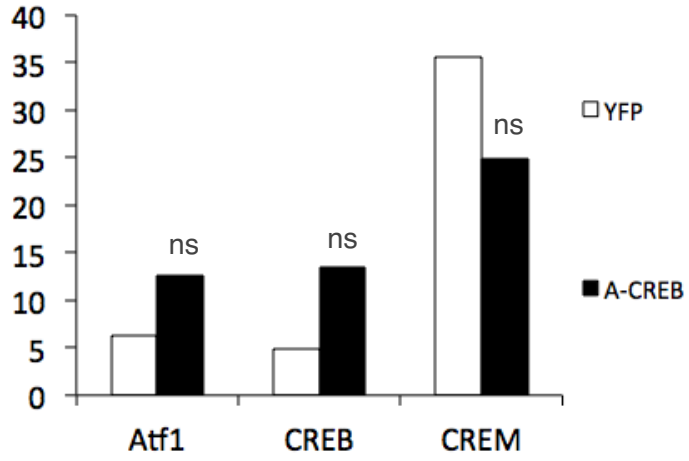

Figure 42. CREB family is expressed in SCs (A) FPKMs of CREB family members of FACS sorted quiescent SCs. N=2 mice/genotype.

METHODS

Mice

See Chapters 2 and 3 for mice used.

Single fiber isolation

See Chapter 2 for methods used for obtaining single fibers.

Antibodies

Primary antibodies use were rabbit anti-AMOT, catalog #sc-98803, Santa-Cruz; rabbit anti-YAP/TAZ, catalog #8418S, Cell Signaling. See Chapter 2,3, and 6 for additional antibodies used.

Proximity Ligation Assay (PLA)

Single fibers were obtained using the methods described in Chapter 2. Primary antibody application was performed as described in Chapter 2. PLA was performed per manufacture's protocol, Duolink In Situ Red Started Kit Goat/Rabbit, catalog #DUO92105, Sigma. In short, after primary antibody application, PLUS and MINUS PLA probes were added to samples and then a ligation reaction performed to join probe ends. Amplification of the probe linkers were performed in the presence of fluorescently labeled nucleotides for detection of protein-protein proximity. Secondary antibody application was performed as described in Chapter 2. Samples were mounted under coverslips using Duolink in situ fluorescence medium, provided in the kit. For the negative control reaction, only one primary antibody was used and the same protocol was performed as described above.

qPCR and primers

See Chapter 7 for methods for cDNA generation, qPCR, and primers for detecting *Mpp7* transcripts. *AMOT* transcript was detecting using primers forward: 5'- CCG CCA GAA TAC CCT TTC AAG -3' and reverse: 5'- CTC ATC AGT TGC CCC TCT GT -3'; *AMOTL1* transcript was detecting using primers forward: 5'- ATG TAG CCT CTG GAA GAG TGT -3' and reverse: 5'- TGA GTG AGG GTT TCC GTG GA -3'; *AMOTL2* transcript was detecting using primers forward: 5'- GGA GAA GAG TTG CCC ACC TAT -3' and reverse: 5'- TCG AAG AGC TTC ATC CTG TCG -3'; *YAP1* transcript was detecting using primers forward: 5'- ACC CTC GTT TTG CCA TGA AC -3' and reverse: 5'- TGT GCT GGG ATT GAT ATT CCG TA -3'; *Lats1* transcript was detecting using primers forward: 5'- AAA GCC AGA AGG GTA CAG ACA -3' and reverse: 5'- CCT CAG GGA TTC TCG GAT CTC -3'; *Lats2* transcript was detecting using primers forward: 5'- GGA CCC CAG GAA TGA GCA G -3' and reverse: 5'- CCC TCG TAG TTT GCA CCA CC -3'; *ANKRD1* transcript was detecting using primers forward: 5'- TAA TCG CTC ACA ATC TGT TGA CA -3' and reverse: 5'- GCC TCT CAC CTT CCG ACC T -3'; *Areg* transcript was detecting using primers forward: 5'- GCA GAT ACA TCG AGA ACC TGG -3' and reverse: 5'- CTG CAA TCT TGG ATA GGT CCT TG -3'; *Birc5* transcript was detecting using primers forward: 5'- CTG GGA ACC CGA TGA CAA C -3' and reverse: 5'- TGG CTC TCT GTC TGT CCA G -3'; *CTGF* transcript was detecting using primers forward: 5'- GGG CCT CTT CTG CGA TTT C -3' and reverse: 5'- ATC CAG GCA AGT GCA TTG GTA -3'. *18S RNA* transcript levels were used as internal controls. See Chapter 7 for *18S RNA* primers.

siRNAs

See Chapter 7 for siRNA targeting mouse *Mpp7*. The following siRNAs were purchased from Life Technologies targeting mouse *AMOT*, catalog #s: s77828 (#1),s77829 (#2), s77830 (#3); mouse *AMOTL1*, catalog #s: s93825(#1), s93826(#2), s93827(#3); mouse *Lats1*, catalog #s: s201588 (#1), s201589 (#2), s201590 (#3); mouse *Lats2*, catalog #s: s78350 (#1), s78351 (#2), s78352 (#3), mouse *YAP1*, catalog #s: s76159 (#1), s76160 (#2), s202423 (#3). siRNAs targeting mouse *AMOTL2* were purchased from Sigma, catalog #s: SASI_Mm02_00324945 (#1), SASI_Mm02_00324945 (#2), SASI_Mm02_00324945 (#3). All siRNAs were resuspended at a 20 μM working concentration.

EdU treatment

See Chapter 7 for methods on EdU application.

EdU detection

See Chapter 3 for methods on EdU detection.

CHAPTER 9: CONCLUSION

Here I provide evidence that CREB activity in quiescent SCs directs Mpp7 expression, which in turn maintains the protein level and/or localization of known (Par-3 and YAP) and new (AMOT) SC regulators. Given CREB activity, as well as Mpp7 and AMOT expression extend into the period of myoblast activation, CREB-Mpp7-AMOT forms a previously uncharacterized regulatory axis that endows quiescent SCs with the competence to initiate expansion and maintain proliferative capacity of SC-derived myoblasts.

Muscle regeneration requires CREB activity

I found that pCREB displays dynamic changes during myogenic progression, extending previous reports for CREB activity in myogenic progenitors and myoblasts (Chen et al., 2005; Stewart et al., 2011). Although crushed muscle extracts and bFGF could stimulate pCREB in myoblasts (Stewart et al., 2011), neither was included in our culture. High pCREB levels in SCs and myoblasts are thus induced by myofibers, serum factors, or cell-cell paracrine signals. As all three CREB members are expressed in the SC lineage (Figure 42) they likely all contribute to the pCREB signal of SCs and myoblasts (Figure 1,3,4).

Instead of inactivating the combined 6 alleles of this gene family, I used A-CREB to selectively inhibit their activity collectively (Ahn et al., 1998) in the SC and found that regeneration was severely compromised by CREB inhibition. My observation that CREB activity is required for SC proliferation and self-renewal extends the gain-of-function data that CREB-YP enhances myoblasts proliferation (Stewart et al., 2011). Additionally, the role of CREB in the SC and in a regeneration context had not previously been

studied. The requirement for CREB in the regeneration of myofibers (Figure 9,10) can be directly related to its role in proliferation. However the finding that CREB can direct self-renewal was a surprise. Not only did CREB affect the number of total $Pax7^+$ cells, which could represent both $Pax7^+$ progenitor and self-renewing population, CREB maintains the ability to selectively enhance $Pax7^+/MyoD^-$ self-renewing cells (Figure 12, 18). This is the first time CREB has been shown to direct SC cell fate.

Mpp7 mediates CREB activity

Using a comparative RNA-seq approach, I identified Mpp7 as a downstream target of CREB in SCs (Figure 23). This provided initial evidence that Mpp7 was mediating the effects of CREB inhibition. I validated this hypothesis by performing rescue experiments whereby re-expressing Mpp7 alone is sufficient to restore the ability of $SCs_{A\text{-}CREB}$ to proliferate and self-renew (Figure 27). Ectopic Mpp7 in control cells increases self-renewed SCs, but does not force myogenic expansion (Figure 27). One possibility is that the Mpp7-directed pathway is sufficient to drive self-renewal but it needs cooperation with additional signaling inputs for extra proliferative cycles and those inputs are limiting in culture. For example, HGF and FGF signaling are well known pathways for SC proliferation. Further exploration of the intersection and cooperation between Mpp7 and other SC proliferation regulators is needed.

CREB-Mpp7-AMOT axis endows quiescent SC the competence for expansion

Notably, the CREB-Mpp7-AMOT regulatory axis is established in quiescent SCs, while its inhibition seems to not affect Pax7 expression (Figure 6) or niche retention (Figure 7). Loss of Par-3, an apical determinant, likely causes the loss of apical restriction of M-cadherin/□-catenin. Knockdown of Par3 in myofiber-associated myoblasts results in

fewer proliferative myoblasts and fewer differentiated cells *in vitro* (Troy et al., 2012), This is in correspondence with the lack of proliferation in Mpp7 knockdowns, however they differ in that shPar-3 promotes the $Pax7^{+}$ cell fate (Troy et al., 2012) whereas Mpp7 knockdown promotes differentiation. Notably, because of the time for isolation and expression of shRNA, the nature of Par-3 loss during quiescence is unclear and should not be compared to Mpp7 loss in the $SCs_{A\text{-}CREB}$ model. As M-cadherin and β-catenin have not been shown to be important for SC quiescence, their loss or changes may indeed have little impact on quiescent $SCs_{A\text{-}CREB}$. In summary, the loss of Mpp7 in the SC differs from studies identifying quiescence molecules, and instead provides evidence for an apical polarity regulator that allows for and maintains proliferation after activation.

More intriguing is the CREB-Mpp7-AMOT axis for regulation of YAP in quiescent SCs. YAP is detected in the nucleus of quiescent SCs, however YAP-directed proliferation is not operational (Figure 7,37). Recent studies have established an alternative concept that retention of quiescence relies on the active suppression of activation rather than passive preservation. Through the activity of microRNAs, chromatin modifiers and cell surface receptors SCs preserve a mitotically inactive state (Boonsanay et al., 2016; Cheung et al., 2012; Crist et al., 2012; Yamaguchi et al., 2015). $SCs_{A\text{-}CREB}$ show defects in the apical domain during quiescence, however $SCs_{A\text{-}CREB}$ exhibits a distinct phenotype from these SCs with inactivated quiescence program. $SCs_{A\text{-}CREB}$ show no mitotic activity nor differentiation during quiescence and maintain Pax7 expression and position in the SC niche (Figure 7). $SCs_{A\text{-}CREB}$ manifests myogenic defects only after injury and isolation.

Given that YAP localizes to the SC nucleus during quiescence while its downstream targets are not significantly downregulated upon A-CREB expression (Table 2), YAP must be prevented from action. I envision that YAP or its DNA binding co-factors TEAD1 and TEAD3, the only family members of the TEAD family expressed during quiescence (Figure 42) are prevented from accessing their target genes by the quiescent facultative heterochromatin and/or from inhibitory co-factors. In either scenario, the CREB-Mpp7-AMOT axis promotes YAP nuclear entry, which primes SCs for activation upon injury stimulus and perpetuates proliferative potential during transit amplification of myoblasts.

Mpp7-AMOT complex acts as a molecular scaffold for Par-3 and YAP signaling

In epithelial cell lines, Mpp7 associates with Dlg1 or Crb3-Mpp5m the core adherence and tight junction signaling components, respectively, and regulates the function of tight junctions (Bohl et al., 2007; Stucke et al., 2007). Here I focused on a lesser-studied link between Mpp7 and AMOT. Proteomic analysis of AMOT binding partners revealed two complexes: one containing the core tight junction regulators Rich1, Crb3, PATJ, and Mpp5 (AMOT-tight junction complex), and the other, AMOT-L1, AMOT-L2, Mupp1, and Mpp7 (Mpp7-AMOT complex) (Wells et al., 2006). The same study established a physical association between AMOT and Par-3 and their role in maintenance of tight junctions, but the Mpp7-AMOT complex was not explored. In $SCs_{A\text{-}CREB}$, Mpp7, AMOT and Par-3 staining signals are greatly diminished (Figure 25,26,31). Because only *Mpp7*'s transcript level is reduced among them (Figure 23) the protein stability of AMOT and Par-3 appears to be Mpp7-dependent, or they are mutually inter-dependent.

All components of the Mpp7-AMOT complex, but not all of those in the AMOT-tight junction complex, are expressed in the quiescent SCs, (Figure 23, 36). AMOT, as well as AMOT-L1 and AMOT-L2, have been shown to bind YAP and its related protein TAZ (Chan et al., 2011; Zhao et al., 2011). Current models in cell culture systems position AMOT as a cytoplasmic and tight junction localized binding partner of YAP, which restricts its activity by retaining it from the nucleus (Chan et al., 2011; Wang et al., 2011; Zhao et al., 2011). However, AMOT has been proposed to act positively to regulate YAP activity *in vivo* (Yi et al., 2013). Interestingly, YAP/TAZ can act synergistically with Pax7 for enhancing induction of Pax3, Mitf, and Myf5 enhancer reporter constructs (Manderfield et al., 2014) suggesting AMOT-mediated YAP activity could be directly affecting the transcriptional activity of Pax7 to promote self-renewal of SCs. $SCs_{A\text{-}CREB}$ have concomitant loss of Mpp7, AMOT, and YAP levels. RNAi data indicate that Mpp7, AMOT, AMOT-L1 and AMOT-L2 all contribute to nuclear accumulation of YAP in myoblasts. Thus, the Mpp7-AMOT complex acts as a positive regulator of YAP for adult myogenic expansion. I propose that Mpp7-AMOT complex is an alternative scaffold for the conventional AMOT-tight junction signaling complex for YAP and acts in parallel yet coordinated fashion with Par-3 signaling to drive SC proliferation and self-renewal after activation.

CHAPTER 10: EXCERPT FROM: A SERIES OF CRE-ER(T2) DRIVERS FOR MANIPULATION OF THE SKELETAL MUSCLE LINEAGE

The following text and accompanying figure were published in:
Southard, S., Low, S., Li, L., Rozo, M., Harvey, T., Fan, C.-M. and Lepper, C. (2014), A series of Cre-ER^{T2} drivers for manipulation of the skeletal muscle lineage. Genesis, 52: 759–770. doi: 10.1002/dvg.22792

For the *Myod1*^{CE} allele, we did not observe cell marking by tmx at E8.75, but found cell marking in the lateral edge of inter-limb somites when tmx was administered at E975 (Fig. 3A). Given the perdurance of tmx of ~ 12 h in vivo (Nakamura *et al.,* 2006), this period overlaps with the earliest *Myod1* expression timing and pattern (Sassoon *et al.,* 1989). Progressively more facial and distal limb muscles were labeled at later stages (Fig. 3B-F). Eight to sixteen hours long X-gal reactions were needed to observe signals in these *Myod1*^{CE} embryos, likely reflecting that *Myod1*^{CE} marks mostly differentiating muscle cells that did not expand. Alternatively, lower levels of CE may be produced by *Myod1*^{CE} compared to *Pax3*^{CE} .The E13.75 to E15.25 treated embryos appeared to have less intense staining, likely due to lower substrate penetrance through the skin (Fig. 3E). Removal of skin from E14.75 to E16.25 treated embryos indeed increased staining signal (Fig. 3F). As E10.75 represents a time of robust labeling, we chose this time point for a longer term tracing to E16.25. These embryos showed staining of the trunk and body wall muscles as well as subcutaneous muscles (Fig. 3G). Although both fore and hind limb muscles were positive, the fore limb muscles showed a stronger staining, consistent with the more advanced developmental stage at E10.75 (the labeling time). The observation of strong staining after a 6-day chase suggests that minimally a fraction of myogenic progenitors at E10.75 were labeled by tamoxifen in the *Myod1*^{CE} embryos and subsequently amplified; thus, resulting in an expanded population of lineage-marked myogenic cells (in comparison to other *CE* alleles that did not display such a persistence, see below). This observation is consistent with the report that *Myod1*^{Cre} (constitutive *Cre* KI at the *Myod1* locus) directs lineage marking of muscle stem cells (Kanisicak *et al*., 2009). For adult muscles, we selected the cardiac and various hind limb muscles for

whole mount analyses. Although there was no staining of the heart (Fig. 3I), differential staining in different muscle groups was obvious, with the soleus (Fig. 3L) showing the lowest staining signal among gastrocnemius, plantaris, TA, and Extensor Digitorum Longus (EDL) muscles (Fig. 3J,K,M,N). Differential *Myod1* expression levels among adult limb muscles and fiber types have indeed been reported (Hughes *et al*., 1993, 1997). Cross section of the TA muscles showed a mosaic pattern of labeling intensity (Fig. 3O), likely reflecting differential levels of CE and/or frequency of reporter recombination in different myofibers.

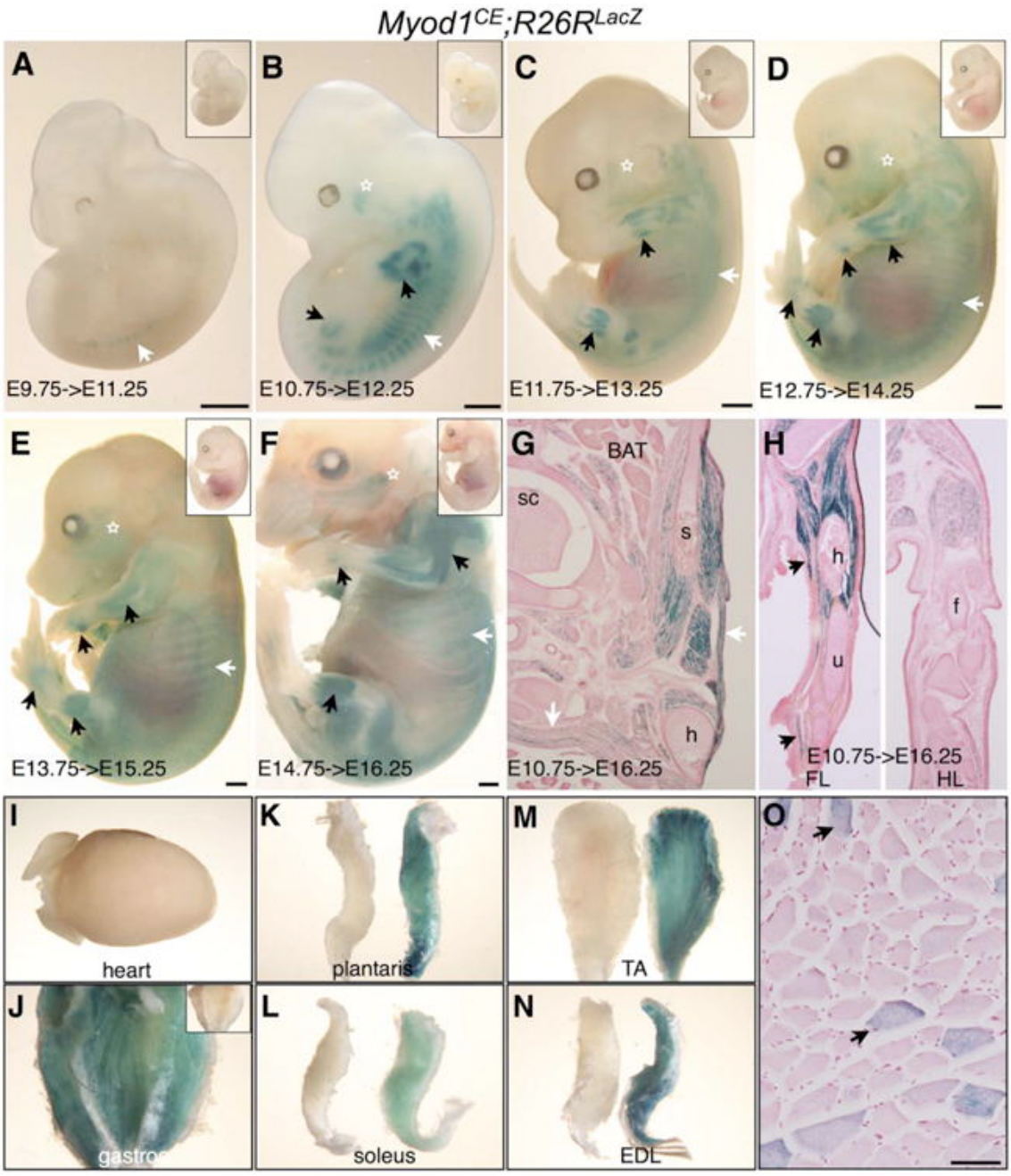
Myod1CE;R26RLacZ
A
B
C
D
E9.75->E11.25
E10.75->E12.25
E11.75->E13.25
E12.75->E14.25
E
F
G
H
BAT
sc
s
h
f
u
E13.75->E15.25
E14.75->E16.25
E10.75->E16.25
E10.75->E16.25
FL
HL
I
K
M
O
heart
plantaris
TA
J
L
N
soleus
EDL

Myod1^{CE} characterization. Time of tmx administration and embryo harvest is as in Figure 2. (A–F) Embryos (saggital view) were subjected to X-gal reactions (8–16 h); insets are control embryos; embryo in (F) was skinned. (G) Transverse section of the embryo at the brachial level, and (H) fore limb (FL, left) and hind limb (HL, right) levels (24 h reaction); sc, spinal cord; s, scapula; h, humerus; u, ulna; f, femur. (I–N) Adult muscles subjected to whole mount X-gal reactions (overnight); muscle names at bottom. Corresponding muscles from animals without tmx treatment (inset in J, and left muscles in K–M) were photographed side by side. (O) Cross section of TA muscles stained for X-gal (overnight) and Nuclear Fast Red. Open stars, facial muscles; arrows, limb muscles, white arrows, trunk muscles. Scale bars = 500 μm, except for in (O), 100 μm.

CHAPTER 11: EXCERPT FROM: MAKING SKELETAL MUSCLE FROM PROGENITOR AND STEM CELLS: DEVELOPMENT VERSUS REGENERATION

The following was published in:
Fan, C.-M., Li, L., Rozo, M. E., & Lepper, C. (2012). Making Skeletal Muscle from Progenitor and Stem Cells: Development versus Regeneration. Wiley Interdisciplinary Reviews. Developmental Biology, 1(3), 315–327.

Myogenic induction by Wnt proteins

In the embryo, the spinal cord and surface ectoderm surrounding the somite are necessary and sufficient for inducing myogenesis[17,61-63]. Several *Wnt* genes are expressed in these two tissues. Co-cultures of presomitic cells and cells producing selective Wnt proteins induce expression of *Pax3* and *Pax7*[64], as well as *Myf5* and *MyoD*[65,66]. In accordance, *Wnt1;Wnt3a* (both normally expressed in the dorsal spinal cord) double mutant embryos have reduced expression of *Pax3* and *Myf5* in the medial dermomyotome[67]. The myogenic inducing potential of Wnt genes expressed by the surface ectoderm has not been tested genetically. *In vitro* pharmacological studies suggest that Wnts activate the Gα - adenylyl cyclase - protein kinase A signaling cascade to phosphorylate the transcription factor CREB, which in turn activates myogenic genes. Consistently, both germ line inactivation of *Creb* and dominant negative *Creb* over-expression in the somite lead to severely reduced expression of *Pax3, Myf5*, and *MyoD in vivo*[66]. In addition, the PKC pathway, which can be activated via Gα signaling, has also been implicated in myogenic induction by modulating Pax3 activity and *MyoD* expression[68].

The canonical Wnt/β-catenin pathway also plays a role in myogenesis. Inactivation of *β-catenin* in presomitic mesoderm cells leads to disorganized somites due to segmentation defects[69], disallowing a firm conclusion about its role in the primary wave of myogenesis[70]. *En1-Cre* directed *β-catenin* inactivation in the central dermomyotome leads to an increase in the domain of myogenic cells at the expense of dermal cells, indicating an inhibitory role of *β-catenin* during the secondary wave of myogenesis[11]. By contrast, *β-catenin* inactivation by *Pax7-Cre* caused only a modest defect in muscle architecture, represented by a change in muscle fiber sub-type

distribution[70]. Since both *Pax7* and *En1* are expressed in the central dermoymtome, the discrepancies likely reflect different timing of expression and/or efficiency of Cre between the two alleles. Analysis of the role of *β-catenin* via gene inactivation is further complicated by an accompanying cell adhesion defect in mutant cells. Inactivation of *BCL9*, which regulates β-catenin's nuclear activity but not its adhesion function, should in principle eliminate this issue. Yet, conditional inactivation of *BCL9* by *Myf5-Cre*, causes no developmental defects[71]. The timing of *Myf5-Cre* activity and BCL9 protein perdurance may obscure a potential role of the canonical pathway in embryonic myogenesis.

The role of Wnt signaling in adult regenerative myogenesis is multifaceted (Fig. 3). A selective combination of Wnt5a, 5b, 7a, and 7b can convert muscle resident $CD45^+Sca1^+$ cells (i.e. the side-population cells) to express Pax7[72], suggesting that $CD45^+Sca1^+$ cells are a source of *de novo* $Pax7^+$ stem cells for muscle regeneration. Although these *Wnt* genes were originally reported to be up-regulated during regeneration[72], subsequent re-evaluation did not substantiate such claim[73]. Thus, the physiological significance of the side-population cells and whether their conversion to $Pax7^+$ cells occurs *in vivo* are not yet known. On the other hand, FGF6 and FGFR4 are expressed during the early phase of the regenerative response[73,74], and both *Fgf6* and *Fgfr4* mutants display compromised muscle regeneration[74,75], supporting the importance of FGF signaling pathway for proficient muscle repair.

For symmetric division of $Pax7^+$ muscle stem cells, Wnt7a has been shown to employ the planar cell polarity (PCP) pathway: *Wnt7a* gene delivery into muscles via electroporation causes increased muscle stem cell number, and consequently muscle

hypertrophy, and the PCP component Vangl-2 is a likely effector mediating this function[76]. Although β-catenin nuclear localization has been documented in cultured proliferating myoblasts, it may act in the transit amplifying progenitors rather than in the self-renewing stem cells[77]. β-catenin nuclear localization is also detected in differentiating myogenic cells[71]. Importantly, *BCL9* inactivation or pharmacological intervention of β-catenin activity *in vivo* caused delayed myogenic differentiation but did not disturb progenitor proliferation during regeneration, evidence that the canonical pathway participates in the differentiation step[71,78]. Wnt3a has also been shown to employ the canonical pathway to accelerate myocyte fusion using the *in vitro* C2C12 myoblast model[79]. As myocyte fusion immediately follows differentiation, separating Wnt/β-catenin functions in these two steps in unsynchronized populations of cells may prove to be difficult.

Lastly, Wnt/β-catenin pathway activation also induces muscle fibrosis and thus, is implicated in the decline of muscle function in aging. Gene delivery of *Wnt3a* via intramuscular eletroporation leads to fibrotic accumulation[76]. *In vitro*, recombinant Wnt3a causes direct conversion of myoblasts into fibroblasts[78]. Importantly, a β-catenin transcriptional reporter is activated in aging but not in young muscles after injury, and depletion of Wnt proteins via soluble Frz receptors can rejuvenize aged myoblasts to prevent fibrogenesis[71]. While Wnt acts locally to divert aging muscle stem cells to the fibrogenic fate, TGFβ1 has been reported to be a candidate systemic factor that may attenuate muscle stem cell activation[80,81] as serum levels of TGFβ1 increase in aging humans and mice[82]. Most of the above cited effects of Wnt and TGFβ1 in adult and aging

muscle regeneration are primarily based on *in vitro* culture or *in vivo overexpression*, pharmacology and RNAi studies; the genetic evidence remains to be obtained.

REFERENCES

Ahn, S., Olive, M., Aggarwal, S., Krylov, D., Ginty, D.D., and Vinson, C. (1998a). A dominant-negative inhibitor of CREB reveals that it is a general mediator of stimulus-dependent transcription of c-fos. Mol. Cell. Biol. *18*, 967–977.

Ahn, S., Olive, M., Aggarwal, S., Krylov, D., Ginty, D.D., and Vinson, C. (1998b). A dominant-negative inhibitor of CREB reveals that it is a general mediator of stimulus-dependent transcription of c-fos. Mol. Cell. Biol. *18*, 967–977.

Altarejos, J.Y., and Montminy, M. (2011). CREB and the CRTC co-activators: sensors for hormonal and metabolic signals. Nat. Rev. Mol. Cell Biol. *12*, 141–151.

Armstrong, R.B., Ogilvie, R.W., and Schwane, J.A. (1983). Eccentric exercise-induced injury to rat skeletal muscle. J. Appl. Physiol. *54*, 80–93.

Asakura, A., Seale, P., Girgis-Gabardo, A., and Rudnicki, M.A. (2002). Myogenic specification of side population cells in skeletal muscle. J. Cell Biol. *159*, 123–134.

Bachmann, A., Schneider, M., Theilenberg, E., Grawe, F., and Knust, E. (2001). Drosophila Stardust is a partner of Crumbs in the control of epithelial cell polarity. Nature *414*, 638–643.

Bader, D., Masaki, T., and Fischman, D.A. (1982). Immunochemical analysis of myosin heavy chain during avian myogenesis in vivo and in vitro. J. Cell Biol. *95*, 763–770.

Bannister, A.J., and Kouzarides, T. (1996). The CBP co-activator is a histone acetyltransferase. Nature *384*, 641–643.

Berdeaux, R., Goebel, N., Banaszynski, L., Takemori, H., Wandless, T., Shelton, G.D., and Montminy, M. (2007). SIK1 is a class II HDAC kinase that promotes survival of skeletal myocytes. Nat. Med. *13*, 597–603.

Bischoff, R. (1975). Regeneration of single skeletal muscle fibers in vitro. Anat. Rec. *182*, 215–235.

Bjornson, C.R.R., Cheung, T.H., Liu, L., Tripathi, P.V., Steeper, K.M., and Rando, T.A. (2012). Notch signaling is necessary to maintain quiescence in adult muscle stem cells. Stem Cells Dayt. Ohio *30*, 232–242.

Bohl, J., Brimer, N., Lyons, C., and Pol, S.B.V. (2007). The Stardust Family Protein MPP7 Forms a Tripartite Complex with LIN7 and DLG1 That Regulates the Stability and Localization of DLG1 to Cell Junctions. J. Biol. Chem. *282*, 9392–9400.

Boonsanay, V., Zhang, T., Georgieva, A., Kostin, S., Qi, H., Yuan, X., Zhou, Y., and Braun, T. (2016). Regulation of Skeletal Muscle Stem Cell Quiescence by Suv4-20h1-Dependent Facultative Heterochromatin Formation. Cell Stem Cell *18*, 229–242.

Brack, A.S., and Rando, T.A. (2012). Tissue-Specific Stem Cells: Lessons from the Skeletal Muscle Satellite Cell. Cell Stem Cell *10*, 504–514.

Cantini, M., Massimino, M.L., Rapizzi, E., Rossini, K., Catani, C., Dalla Libera, L., and Carraro, U. (1995). Human satellite cell proliferation in vitro is regulated by autocrine

secretion of IL-6 stimulated by a soluble factor(s) released by activated monocytes. Biochem. Biophys. Res. Commun. *216*, 49–53.

Chakravarthy, M.V., Davis, B.S., and Booth, F.W. (2000). IGF-I restores satellite cell proliferative potential in immobilized old skeletal muscle. J. Appl. Physiol. Bethesda Md 1985 *89*, 1365–1379.

Chan, S.W., Lim, C.J., Chong, Y.F., Pobbati, A.V., Huang, C., and Hong, W. (2011). Hippo Pathway-independent Restriction of TAZ and YAP by Angiomotin. J. Biol. Chem. *286*, 7018–7026.

Chan, S.W., Lim, C.J., Guo, F., Tan, I., Leung, T., and Hong, W. (2013). Actin-binding and cell proliferation activities of angiomotin family members are regulated by Hippo pathway-mediated phosphorylation. J. Biol. Chem. *288*, 37296–37307.

Chargé, S.B.P., and Rudnicki, M.A. (2004). Cellular and Molecular Regulation of Muscle Regeneration. Physiol. Rev. *84*, 209–238.

Chen, A.E., Ginty, D.D., and Fan, C.-M. (2005). Protein kinase A signalling via CREB controls myogenesis induced by Wnt proteins. Nature *433*, 317–322.

Cheung, T.H., Quach, N.L., Charville, G.W., Liu, L., Park, L., Edalati, A., Yoo, B., Hoang, P., and Rando, T.A. (2012). Maintenance of muscle stem-cell quiescence by microRNA-489. Nature *482*, 524–528.

Collins, C.A., Olsen, I., Zammit, P.S., Heslop, L., Petrie, A., Partridge, T.A., and Morgan, J.E. (2005). Stem cell function, self-renewal, and behavioral heterogeneity of cells from the adult muscle satellite cell niche. Cell *122*, 289–301.

Cornelison, D.D., and Wold, B.J. (1997). Single-cell analysis of regulatory gene expression in quiescent and activated mouse skeletal muscle satellite cells. Dev. Biol. *191*, 270–283.

Crist, C.G., Montarras, D., and Buckingham, M. (2012). Muscle satellite cells are primed for myogenesis but maintain quiescence with sequestration of Myf5 mRNA targeted by microRNA-31 in mRNP granules. Cell Stem Cell *11*, 118–126.

Davis, R.L., Weintraub, H., and Lassar, A.B. (1987). Expression of a single transfected cDNA converts fibroblasts to myoblasts. Cell *51*, 987–1000.

Day, K., Shefer, G., Richardson, J., Enikolopov, G., and Yablonkareuveni, Z. (2007). Nestin-GFP reporter expression defines the quiescent state of skeletal muscle satellite cells. Dev. Biol. *304*, 246–259.

Dellavalle, A., Sampaolesi, M., Tonlorenzi, R., Tagliafico, E., Sacchetti, B., Perani, L., Innocenzi, A., Galvez, B.G., Messina, G., Morosetti, R., et al. (2007). Pericytes of human skeletal muscle are myogenic precursors distinct from satellite cells. Nat. Cell Biol. *9*, 255–267.

Dumont, N.A., Wang, Y.X., von Maltzahn, J., Pasut, A., Bentzinger, C.F., Brun, C.E., and Rudnicki, M.A. (2015). Dystrophin expression in muscle stem cells regulates their polarity and asymmetric division. Nat. Med. *21*, 1455–1463.

Fan, C.M., and Tessier-Lavigne, M. (1994). Patterning of mammalian somites by surface ectoderm and notochord: evidence for sclerotome induction by a hedgehog homolog. Cell *79*, 1175–1186.

Fan, C.-M., Li, L., Rozo, M.E., and Lepper, C. (2012). Making Skeletal Muscle from Progenitor and Stem Cells: Development versus Regeneration. Wiley Interdiscip. Rev. Dev. Biol. *1*, 315–327.

Florian, M.C., and Geiger, H. (2010). Concise review: polarity in stem cells, disease, and aging. Stem Cells Dayt. Ohio *28*, 1623–1629.

Floss, T., Arnold, H.H., and Braun, T. (1997). A role for FGF-6 in skeletal muscle regeneration. Genes Dev. *11*, 2040–2051.

Gonzalez, G.A., and Montminy, M.R. (1989). Cyclic AMP stimulates somatostatin gene transcription by phosphorylation of CREB at serine 133. Cell *59*, 675–680.

Gopinath, S.D., Webb, A.E., Brunet, A., and Rando, T.A. (2014). FOXO3 promotes quiescence in adult muscle stem cells during the process of self-renewal. Stem Cell Rep. *2*, 414–426.

Gros, J., Manceau, M., Thomé, V., and Marcelle, C. (2005). A common somitic origin for embryonic muscle progenitors and satellite cells. Nature *435*, 954–958.

Gussoni, E., Soneoka, Y., Strickland, C.D., Buzney, E.A., Khan, M.K., Flint, A.F., Kunkel, L.M., and Mulligan, R.C. (1999). Dystrophin expression in the mdx mouse restored by stem cell transplantation. Nature *401*, 390–394.

Herzig, S., Long, F., Jhala, U.S., Hedrick, S., Quinn, R., Bauer, A., Rudolph, D., Schutz, G., Yoon, C., Puigserver, P., et al. (2001). CREB regulates hepatic gluconeogenesis through the coactivator PGC-1. Nature *413*, 179–183.

Hirate, Y., Hirahara, S., Inoue, K.-I., Suzuki, A., Alarcon, V.B., Akimoto, K., Hirai, T., Hara, T., Adachi, M., Chida, K., et al. (2013). Polarity-dependent distribution of angiomotin localizes Hippo signaling in preimplantation embryos. Curr. Biol. CB *23*, 1181–1194.

Hoffman, E.P., Brown, R.H., and Kunkel, L.M. (1987). Dystrophin: The protein product of the duchenne muscular dystrophy locus. Cell *51*, 919–928.

Huang, D.W., Sherman, B.T., and Lempicki, R.A. (2009a). Systematic and integrative analysis of large gene lists using DAVID bioinformatics resources. Nat. Protoc. *4*, 44–57.

Huang, D.W., Sherman, B.T., and Lempicki, R.A. (2009b). Bioinformatics enrichment tools: paths toward the comprehensive functional analysis of large gene lists. Nucleic Acids Res. *37*, 1–13.

Hutcheson, D.A., Zhao, J., Merrell, A., Haldar, M., and Kardon, G. (2009). Embryonic and fetal limb myogenic cells are derived from developmentally distinct progenitors and have different requirements for beta-catenin. Genes Dev. *23*, 997–1013.

Judson, R.N., Tremblay, A.M., Knopp, P., White, R.B., Urcia, R., De Bari, C., Zammit, P.S., Camargo, F.D., and Wackerhage, H. (2012). The Hippo pathway member Yap plays a key role in influencing fate decisions in muscle satellite cells. J. Cell Sci. *125*, 6009–6019.

Ke, N., Claassen, G., Yu, D.-H., Albers, A., Fan, W., Tan, P., Grifman, M., Hu, X., DeFife, K., Nguy, V., et al. (2004). Nuclear Hormone Receptor NR4A2 Is Involved in Cell Transformation and Apoptosis. Cancer Res. *64*, 8208–8212.

Keller, C., Hansen, M.S., Coffin, C.M., and Capecchi, M.R. (2004). Pax3:Fkhr interferes with embryonic Pax3 and Pax7 function: implications for alveolar rhabdomyosarcoma cell of origin. Genes Dev. *18*, 2608–2613.

Knudsen, K.A., Smith, L., and McElwee, S. (1989). Involvement of cell surface phosphatidylinositol-anchored glycoproteins in cell-cell adhesion of chick embryo myoblasts. J. Cell Biol. *109*, 1779–1786.

Konigsberg, U.R., Lipton, B.H., and Konigsberg, I.R. (1975). The regenerative response of single mature muscle fibers isolated in vitro. Dev. Biol. *45*, 260–275.

Kuang, S., Gillespie, M.A., and Rudnicki, M.A. (2008). Niche Regulation of Muscle Satellite Cell Self-Renewal and Differentiation. Cell Stem Cell *2*, 22–31.

LaBarge, M.A., and Blau, H.M. (2002). Biological progression from adult bone marrow to mononucleate muscle stem cell to multinucleate muscle fiber in response to injury. Cell *111*, 589–601.

Le, W., Xu, P., Jankovic, J., Jiang, H., Appel, S.H., Smith, R.G., and Vassilatis, D.K. (2003). Mutations in NR4A2 associated with familial Parkinson disease. Nat. Genet. *33*, 85–89.

Le Grand, F., Jones, A.E., Seale, V., Scimè, A., and Rudnicki, M.A. (2009). Wnt7a Activates the Planar Cell Polarity Pathway to Drive the Symmetric Expansion of Satellite Stem Cells. Cell Stem Cell *4*, 535–547.

Lepper, C., and Fan, C.-M. (2010). Inducible lineage tracing of Pax7-descendant cells reveals embryonic origin of adult satellite cells. Genes. N. Y. N 2000 *48*, 424–436.

Lepper, C., Partridge, T.A., and Fan, C.-M. (2011). An absolute requirement for Pax7-positive satellite cells in acute injury-induced skeletal muscle regeneration. Dev. Camb. Engl. *138*, 3639–3646.

Lesiak, A., Pelz, C., Ando, H., Zhu, M., Davare, M., Lambert, T.J., Hansen, K.F., Obrietan, K., Appleyard, S.M., Impey, S., et al. (2013). A Genome-Wide Screen of CREB Occupancy Identifies the RhoA Inhibitors Par6C and Rnd3 as Regulators of BDNF-Induced Synaptogenesis. PLoS ONE *8*, e64658.

Leung, C.Y., and Zernicka-Goetz, M. (2013). Angiomotin prevents pluripotent lineage differentiation in mouse embryos via Hippo pathway-dependent and -independent mechanisms. Nat. Commun. *4*.

Li, L., and Clevers, H. (2010). Coexistence of quiescent and active adult stem cells in mammals. Science *327*, 542–545.

Lopez, T.P., and Fan, C.-M. (2013). Dynamic CREB family activity drives segmentation and posterior polarity specification in mammalian somitogenesis. Proc. Natl. Acad. Sci. U. S. A. *110*, E2019–E2027.

Manderfield, L.J., Engleka, K.A., Aghajanian, H., Gupta, M., Yang, S., Li, L., Baggs, J.E., Hogenesch, J.B., Olson, E.N., and Epstein, J.A. (2014). Pax3 and hippo signaling coordinate melanocyte gene expression in neural crest. Cell Rep. *9*, 1885–1895.

Martianov, I., Choukrallah, M.-A., Krebs, A., Ye, T., Legras, S., Rijkers, E., Ijcken, W.V., Jost, B., Sassone-Corsi, P., and Davidson, I. (2010). Cell-specific occupancy of an extended repertoire of CREM and CREB binding loci in male germ cells. BMC Genomics *11*, 530.

Mauro, A. (1961). Satellite cell of skeletal muscle fibers. J. Biophys. Biochem. Cytol. *9*, 493–495.

Mayr, B., and Montminy, M. (2001). Transcriptional regulation by the phosphorylation-dependent factor CREB. Nat. Rev. Mol. Cell Biol. *2*, 599–609.

Mintz, B., and Baker, W.W. (1967). Normal mammalian muscle differentiation and gene control of isocitrate dehydrogenase synthesis. Proc. Natl. Acad. Sci. U. S. A. *58*, 592–598.

Mitchell, K.J., Pannérec, A., Cadot, B., Parlakian, A., Besson, V., Gomes, E.R., Marazzi, G., and Sassoon, D.A. (2010). Identification and characterization of a non-satellite cell muscle resident progenitor during postnatal development. Nat. Cell Biol. *12*, 257–266.

Montminy, M.R., and Bilezikjian, L.M. (1987). Binding of a nuclear protein to the cyclic-AMP response element of the somatostatin gene. Nature *328*, 175–178.

Montminy, M.R., Sevarino, K.A., Wagner, J.A., Mandel, G., and Goodman, R.H. (1986). Identification of a cyclic-AMP-responsive element within the rat somatostatin gene. Proc. Natl. Acad. Sci. U. S. A. *83*, 6682–6686.

Moss, F.P., and Leblond, C.P. (1970). Nature of dividing nuclei in skeletal muscle of growing rats. J. Cell Biol. *44*, 459–462.

Moss, F.P., and Leblond, C.P. (1971). Satellite cells as the source of nuclei in muscles of growing rats. Anat. Rec. *170*, 421–435.

Mourikis, P., Sambasivan, R., Castel, D., Rocheteau, P., Bizzarro, V., and Tajbakhsh, S. (2012). A critical requirement for notch signaling in maintenance of the quiescent skeletal muscle stem cell state. Stem Cells Dayt. Ohio *30*, 243–252.

Murphy, M.M., Lawson, J.A., Mathew, S.J., Hutcheson, D.A., and Kardon, G. (2011). Satellite cells, connective tissue fibroblasts and their interactions are crucial for muscle regeneration. Dev. Camb. Engl. *138*, 3625–3637.

Nakajima, T., Uchida, C., Anderson, S.F., Lee, C.-G., Hurwitz, J., Parvin, J.D., and Montminy, M. (1997). RNA Helicase A Mediates Association of CBP with RNA Polymerase II. Cell *90*, 1107–1112.

Ogryzko, V.V., Schiltz, R.L., Russanova, V., Howard, B.H., and Nakatani, Y. (1996). The transcriptional coactivators p300 and CBP are histone acetyltransferases. Cell *87*, 953–959.

Ono, Y., Urata, Y., Goto, S., Nakagawa, S., Humbert, P.O., Li, T.-S., and Zammit, P.S. (2015). Muscle Stem Cell Fate Is Controlled by the Cell-Polarity Protein Scrib. Cell Rep. *10*, 1135–1148.

Pear, W.S., Miller, J.P., Xu, L., Pui, J.C., Soffer, B., Quackenbush, R.C., Pendergast, A.M., Bronson, R., Aster, J.C., Scott, M.L., et al. (1998). Efficient and rapid induction of a chronic myelogenous leukemia-like myeloproliferative disease in mice receiving P210 bcr/abl-transduced bone marrow. Blood *92*, 3780–3792.

Piccolo, S., Dupont, S., and Cordenonsi, M. (2014). The Biology of YAP/TAZ: Hippo Signaling and Beyond. Physiol. Rev. *94*, 1287–1312.

Polesskaya, A., Seale, P., and Rudnicki, M.A. (2003). Wnt signaling induces the myogenic specification of resident CD45+ adult stem cells during muscle regeneration. Cell *113*, 841–852.

Relaix, F., Rocancourt, D., Mansouri, A., and Buckingham, M. (2005). A Pax3/Pax7-dependent population of skeletal muscle progenitor cells. Nature *435*, 948–953.

Reznik, M. (1969). Thymidine-3H uptake by satellite cells of regenerating skeletal muscle. J. Cell Biol. *40*, 568–571.

Rhodes, S.J., and Konieczny, S.F. (1989). Identification of MRF4: a new member of the muscle regulatory factor gene family. Genes Dev. *3*, 2050–2061.

Riccio, A., Ahn, S., Davenport, C.M., Blendy, J.A., and Ginty, D.D. (1999). Mediation by a CREB family transcription factor of NGF-dependent survival of sympathetic neurons. Science *286*, 2358–2361.

Robertson, T.A., Papadimitriou, J.M., and Grounds, M.D. (1993). Fusion of myogenic cells to the newly sealed region of damaged myofibres in skeletal muscle regeneration. Neuropathol. Appl. Neurobiol. *19*, 350–358.

Ruffell, D., Mourkioti, F., Gambardella, A., Kirstetter, P., Lopez, R.G., Rosenthal, N., and Nerlov, C. (2009). A CREB-C/EBPbeta cascade induces M2 macrophage-specific gene expression and promotes muscle injury repair. Proc. Natl. Acad. Sci. U. S. A. *106*, 17475–17480.

Sacco, A., Doyonnas, R., Kraft, P., Vitorovic, S., and Blau, H.M. (2008). Self-renewal and expansion of single transplanted muscle stem cells. Nature *456*, 502–506.

Sambasivan, R., Yao, R., Kissenpfennig, A., Van Wittenberghe, L., Paldi, A., Gayraud-Morel, B., Guenou, H., Malissen, B., Tajbakhsh, S., and Galy, A. (2011). Pax7-expressing satellite cells are indispensable for adult skeletal muscle regeneration. Dev. Camb. Engl. *138*, 3647–3656.

Schultz, E., Gibson, M.C., and Champion, T. (1978). Satellite cells are mitotically quiescent in mature mouse muscle: an EM and radioautographic study. J. Exp. Zool. *206*, 451–456.

Seale, P., Sabourin, L.A., Girgis-Gabardo, A., Mansouri, A., Gruss, P., and Rudnicki, M.A. (2000). Pax7 is required for the specification of myogenic satellite cells. Cell *102*, 777–786.

Shea, K.L., Xiang, W., LaPorta, V.S., Licht, J.D., Keller, C., Basson, M.A., and Brack, A.S. (2010). Sprouty1 regulates reversible quiescence of a self-renewing adult muscle stem cell pool during regeneration. Cell Stem Cell *6*, 117–129.

Shinin, V., Gayraud-Morel, B., Gomès, D., and Tajbakhsh, S. (2006). Asymmetric division and cosegregation of template DNA strands in adult muscle satellite cells. Nat. Cell Biol. *8*, 677–682.

Short, J.M., Wynshaw-Boris, A., Short, H.P., and Hanson, R.W. (1986). Characterization of the phosphoenolpyruvate carboxykinase (GTP) promoter-regulatory region. II. Identification of cAMP and glucocorticoid regulatory domains. J. Biol. Chem. *261*, 9721–9726.

Singh, M.A.F., Ding, W., Manfredi, T.J., Solares, G.S., O'Neill, E.F., Clements, K.M., Ryan, N.D., Kehayias, J.J., Fielding, R.A., and Evans, W.J. (1999). Insulin-like growth factor I in skeletal muscle after weight-lifting exercise in frail elders. Am. J. Physiol. - Endocrinol. Metab. *277*, E135–E143.

Snow, M.H. (1978). An autoradiographic study of satellite cell differentiation into regenerating myotubes following transplantation of muscles in young rats. Cell Tissue Res. *186*, 535–540.

Stewart, R., Flechner, L., Montminy, M., and Berdeaux, R. (2011). CREB Is Activated by Muscle Injury and Promotes Muscle Regeneration. PLoS ONE *6*, e24714.

Stucke, V.M., Timmerman, E., Vandekerckhove, J., Gevaert, K., and Hall, A. (2007). The MAGUK protein MPP7 binds to the polarity protein hDlg1 and facilitates epithelial tight junction formation. Mol. Biol. Cell *18*, 1744–1755.

Su, W.-H., Mruk, D.D., Wong, E.W.P., Lui, W.-Y., and Cheng, C.Y. (2012). Polarity protein complex Scribble/Lgl/Dlg and epithelial cell barriers. Adv. Exp. Med. Biol. *763*, 149–170.

Tatsumi, R., Anderson, J.E., Nevoret, C.J., Halevy, O., and Allen, R.E. (1998). HGF/SF is present in normal adult skeletal muscle and is capable of activating satellite cells. Dev. Biol. *194*, 114–128.

Trapnell, C., Roberts, A., Goff, L., Pertea, G., Kim, D., Kelley, D.R., Pimentel, H., Salzberg, S.L., Rinn, J.L., and Pachter, L. (2012). Differential gene and transcript expression analysis of RNA-seq experiments with TopHat and Cufflinks. Nat. Protoc. *7*, 562–578.

Tremblay, A.M., Missiaglia, E., Galli, G.G., Hettmer, S., Urcia, R., Carrara, M., Judson, R.N., Thway, K., Nadal, G., Selfe, J.L., et al. (2014). The Hippo Transducer YAP1 Transforms Activated Satellite Cells and Is a Potent Effector of Embryonal Rhabdomyosarcoma Formation. Cancer Cell *26*, 273–287.

Troy, A., Cadwallader, A.B., Fedorov, Y., Tyner, K., Tanaka, K.K., and Olwin, B.B. (2012). Coordination of Satellite Cell Activation and Self-Renewal by Par-Complex-Dependent Asymmetric Activation of p38α/β MAPK. Cell Stem Cell *11*, 541–553.

Urciuolo, A., Quarta, M., Morbidoni, V., Gattazzo, F., Molon, S., Grumati, P., Montemurro, F., Tedesco, F.S., Blaauw, B., Cossu, G., et al. (2013). Collagen VI regulates satellite cell self-renewal and muscle regeneration. Nat. Commun. *4*, 1964.

Wang, W., Huang, J., and Chen, J. (2011). Angiomotin-like proteins associate with and negatively regulate YAP1. J. Biol. Chem. *286*, 4364–4370.

Watt, K.I., Judson, R., Medlow, P., Reid, K., Kurth, T.B., Burniston, J.G., Ratkevicius, A., Bari, C.D., and Wackerhage, H. (2010). Yap is a novel regulator of C2C12 myogenesis. Biochem. Biophys. Res. Commun. *393*, 619–624.

Webster, M.T., Manor, U., Lippincott-Schwartz, J., and Fan, C.-M. (2016). Intravital Imaging Reveals Ghost Fibers as Architectural Units Guiding Myogenic Progenitors during Regeneration. Cell Stem Cell *18*, 243–252.

Weissman, I.L. (2000). Stem cells: units of development, units of regeneration, and units in evolution. Cell *100*, 157–168.

Wells, C.D., Fawcett, J.P., Traweger, A., Yamanaka, Y., Goudreault, M., Elder, K., Kulkarni, S., Gish, G., Virag, C., Lim, C., et al. (2006). A Rich1/Amot Complex Regulates the Cdc42 GTPase and Apical-Polarity Proteins in Epithelial Cells. Cell *125*, 535–548.

Wen, Y., Bi, P., Liu, W., Asakura, A., Keller, C., and Kuang, S. (2012). Constitutive Notch activation upregulates Pax7 and promotes the self-renewal of skeletal muscle satellite cells. Mol. Cell. Biol. *32*, 2300–2311.

Wright, W.E., Sassoon, D.A., and Lin, V.K. (1989). Myogenin, a factor regulating myogenesis, has a domain homologous to MyoD. Cell *56*, 607–617.

Yaffe, D., and Feldman, M. (1965). THE FORMATION OF HYBRID MULTINUCLEATED MUSCLE FIBERS FROM MYOBLASTS OF DIFFERENT GENETIC ORIGIN. Dev. Biol. *11*, 300–317.

Yamaguchi, M., Watanabe, Y., Ohtani, T., Uezumi, A., Mikami, N., Nakamura, M., Sato, T., Ikawa, M., Hoshino, M., Tsuchida, K., et al. (2015). Calcitonin Receptor Signaling Inhibits Muscle Stem Cells from Escaping the Quiescent State and the Niche. Cell Rep. *13*, 302–314.

Yi, C., Shen, Z., Stemmer-Rachamimov, A., Dawany, N., Troutman, S., Showe, L.C., Liu, Q., Shimono, A., Sudol, M., Holmgren, L., et al. (2013). The p130 Isoform of Angiomotin Is Required for Yap-Mediated Hepatic Epithelial Cell Proliferation and Tumorigenesis. Sci. Signal. *6*, ra77–ra77.

Zammit, P.S., Heslop, L., Hudon, V., Rosenblatt, J.D., Tajbakhsh, S., Buckingham, M.E., Beauchamp, J.R., and Partridge, T.A. (2002). Kinetics of myoblast proliferation show that resident satellite cells are competent to fully regenerate skeletal muscle fibers. Exp. Cell Res. *281*, 39–49.

Zammit, P.S., Golding, J.P., Nagata, Y., Hudon, V., Partridge, T.A., and Beauchamp, J.R. (2004). Muscle satellite cells adopt divergent fates: a mechanism for self-renewal? J. Cell Biol. *166*, 347–357.

Zhang, X., Odom, D.T., Koo, S.-H., Conkright, M.D., Canettieri, G., Best, J., Chen, H., Jenner, R., Herbolsheimer, E., Jacobsen, E., et al. (2005). Genome-wide analysis of cAMP-response element binding protein occupancy, phosphorylation, and target gene activation in human tissues. Proc. Natl. Acad. Sci. U. S. A. *102*, 4459–4464.

Zhao, B., Li, L., Lu, Q., Wang, L.H., Liu, C.-Y., Lei, Q., and Guan, K.-L. (2011). Angiomotin is a novel Hippo pathway component that inhibits YAP oncoprotein. Genes Dev. *25*, 51–63.

CURRICULUM VITAE

3520 San Martin Dr.
Baltimore, MD 21218
Cell Phone: (510) 219-0743
Email: li@ciwemb.edu

Birth
September 22, 1981 in San Francisco, CA, U.S.A.

Education

Ph.D. Candidate	Cell, Molecular, Developmental Biology, and Biophysics Department Johns Hopkins University July 2009 to current
M.S.	Biology Department San Francisco State University June 2009
B.S.	Molecular and Cell Biology Department University of California, Berkeley December 2003

Teaching Experience

2014	Baltimore Polytechnic Institute, Course on PCR
2012	Baltimore Talent Development High School, Biology teaching session
2010	Graduate Teaching Assistant, Developmental Biology
2010	Graduate Teaching Assistant, Genetics
2007-2009	Graduate Teaching Associate, Introduction to Biology
2008	SEPAL, Expanding Your Horizons (EYH)

Appointments

2006-2007	Research Associate, United States Department of Agriculture, Albany, CA
2004-2006	Laboratory Assistant, United States Department of Agriculture, Albany, CA
2001-2004	Laboratory Assistant, University of California, Berkeley, Berkeley, CA

Publications

2014	Southard S, Low SH, Li L, Rozo M, Harvey T, Fan CM, Lepper C. A Series of Cre-ERT2 Drivers for Manipulation of the Skeletal Muscle Lineage. Genesis, Aug;52(8):759-70
2014	Galli L, Szabo LA, Li L, Htaik YM, Onguka O, Burrus LW. Concentration-dependent effects of WNTLESS on WNT1/3A signaling. Developmental Dynamics, 2014 Sep;243(9):1095-105

2014 Galli LM, Munji RN, Chapman SC, Easton A, Li L, Onguka O, Ramahi JS, Suriben R, Szabo LA, Teng C, Tran B, Hannoush RN, Burrus LW. Frizzled10 mediates WNT1 and WNT3A signaling in the dorsal spinal cord of the developing chick embryo. Developmental Dynamics 243(6):833-43.

2012 Fan CM, Li L, Rozo ME, Lepper C. Making skeletal muscle from progenitor and stem cells: development versus regeneration. Wiley Interdisciplinary Reviews: Developmental Biology (3):315-27

2005 Curry JD, Li L, Schlissel MS. Quantification of Jkappa signal end breaks in developing B cells by blunt-end linker ligation and qPCR. Journal of Immunological Methods 296(1-2):19-30.

Awards

2008 Gloria Spencer Women's Association Scholarship
2008 Nelson Scholarship
2008 Maxwell Scholarship
2009 Graduate Student Project Showcase Award